OBJECT-ORIENTED METHOD FOR POST-EVENT LANDSLIDE MAPPING: THE UTILITY OF TEXTURE

Melanie Tramaine Marian Harris
March, 2010

Object-Oriented Method for Post-Event Landslide Mapping: the Utility of Texture

by

Melanie Tramaine Marian Harris

Thesis submitted to the International Institute for Geo-information Science and Earth Observation in partial fulfilment of the requirements for the degree of Master of Science in Geo-information Science and Earth Observation, Specialisation: Geo-Hazards

Thesis Assessment Board

Chairman: Prof. Victor Jetten
External Examiner : Dr. E.A. Addink
First Supervisor : Dr. Norman Kerle
Second Supervisor : Dr. Cees van Westen

Observer : Dr. Tom Loran

INTERNATIONAL INSTITUTE FOR GEO-INFORMATION SCIENCE AND EARTH OBSERVATION
ENSCHEDE, THE NETHERLANDS

Disclaimer

This document describes work undertaken as part of a programme of study at the International Institute for Geo-information Science and Earth Observation. All views and opinions expressed therein remain the sole responsibility of the author, and do not necessarily represent those of the institute.

Abstract

In the immediate aftermath of an event, the most pressing issue is how to collect and disseminate accurate information to aid disaster managers in organising rescue, emergency and damage assessment operations in the field. Post-event hazard information is important and it needs to be produced as quickly and as accurately as possible; therefore, inventories need to be generated rapidly from available satellite imagery and other data. Object-oriented analysis (OOA) has been proven useful for identifying landslides, however, a gap in knowledge surrounding the utility and systematic application of texture measures for landslide detection. Thus this research sought to evaluate and assess the utility of object-based texture analysis for identifying landslides. To do this a series of tests were set up to compare actual values of pixel vs. object-based texture calculations, determine how a single texture value is arrived at for each object, examine the factors affecting texture calculations (band, scale factor, directionality) and determine which texture measure is most useful for landslide mapping. Finally, an object-based procedure was developed and applied in a test site (Wenchuan County, Sichuan Province, China) to test what was learnt in the evaluation of object-based texture. The results show that texture cannot be used in isolation to distinguish landslides from its false positives such as bare ground and settlement areas. If however it is used in conjunction with spectral and morphological data identification and ultimately classification results can be enhanced.

Keywords: GLCM Texture, OOA, landslides

Acknowledgements

I would first like to thank the Almighty God for His guidance throughout my tenure here at ITC, especially during the thesis phase. Without Him this work would not have been possible.

I would like to express my sincerest gratitude to my first supervisor Dr. Norman Kerle for his guidance and support. I would also like to thank the AES programme director Drs. Tom Loran for his assistance in facilitating the completion of this thesis. To my second supervisor, your assistance in the latter part of this research was no doubt most welcome and appreciated.

A significant portion of this work would not have been possible without the data and advice given by Tolga Gorum. He was always willing to offer his assistance wherever possible and for this I am grateful.

To Tapas Martha, your advice in the early phase of this research helped to give me a good start and though you were far away throughout the rest of the process you still offered help via email.

I take this opportunity also to thank my family for all their prayers and blessings whilst I was away. Though far in distance, I never felt far from their love and support. This work is especially dedicated to my mother Ms. Ava Candida Harris who has been a constant source of inspiration to me throughout every aspect of my holistic development. Much love to my father, whose confidence in me knows no bounds. Finally, to all my friends, new and old, both home and abroad, I thank you for enhancing my experience with encouraging words, laughter and a bit of a push whenever I needed it.

Best wishes to you all!

Melanie T.M. Harris

15.03.2010

Table of contents

List of figures

List of tables

1. Introduction

Disaster risk management poses a significant challenge to both developed and developing nations across the world. Governments have realised that the ad hoc and reactive approach of collecting data only in the aftermath of a hazard event is not enough for sustainable disaster risk management. Even before the launch of the International Decade for Natural Disaster Reduction in the 1990s and its successor, the International Strategy for Disaster Reduction, a number of approaches (scientific, economic, social, and technological) for managing disasters have been explored. One such approach is the use of geo-information technologies for the collection, storage, analysis, visualization, dissemination and communication of raw data and derived information throughout each phase of the disaster cycle (Figure 1-1). In the Editor's note for "Geo-information for Disaster Management", the point is made that geo-information is the crucial component for effective disaster management and its multiple dimensions must be thoroughly understood and utilised (Rodriguez et al. 2009).

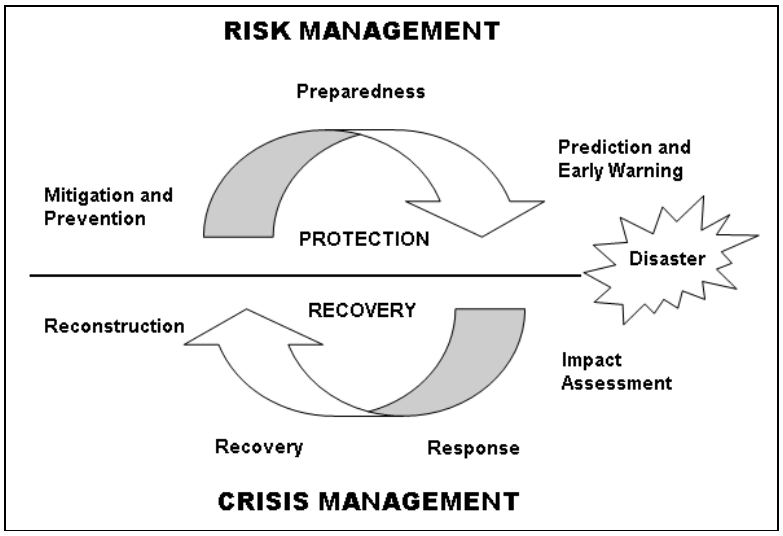

Figure 1-1 Disaster Risk Management Cycle

1.1. Background

Globally, natural hazards have far reaching implications on societies and their economies. In 2008, a total of 354 natural disasters were recorded globally with 234,584 people being killed, another 214.3 million people affected and losses amounting to approximately US$190.3 billion being incurred (Rodriguez et al. 2009). Whilst the number of occurrences of disasters and the number of people affected in 2008 remained below the average recorded for the period 2000-2007 (397 and 231.2 million, respectively), the monetary losses were more than double the average of the same period (US$91.6 billion). These figures however, represent direct economic losses and do not take into

account secondary economic losses which accumulate for an extended period following an event and often go unreported, such as, the loss of production due to a diminished workforce.

In terms of worldwide natural disaster importance (frequency, number of people killed and affected and economic losses), landslides rank third (Zillman 1999). Landslide activity occurs in all mountainous regions of the world causing widespread destruction and resulting in substantial human and economic losses. A global landslide hotspot study identified amongst others North-Western USA and Canada, the European Alps, Southern China, Nepal, India, Japan, Indonesia Honduras and Colombia as having a medium to high, high and very high landslide hazard (Nadim and Kjekstad 2009). Petley (2009) reported that there were 406 fatal landslide events in 2008 resulting in a total of 32,526 deaths. These numbers are dominated by the Sichuan earthquake (12th May, 2008), which triggered numerous landslides that killed approximately 29,000 people, according to Chinese authorities. Ignoring the bias of this single event, the remaining 405 fatal landslide events with 3526 deaths was still higher than the 394 fatal landslide events and 3017 deaths recorded for 2007 (Petley and Rosser 2007). There are many estimates for economic losses as a result of landslides in literature (Table 1-1). These figures may differ from reality because of the tendency for agencies collecting data to attribute the losses from landslides to the triggering event, such as tropical storms or earthquakes, and not address them as individual events.

Table 1-1: Estimated Economic losses as a result of landslides *(combined sources)*

COUNTRIES	ESTIMATED LOSSES (US$)	SOURCE
Italy, Austria, Switzerland and France	1-5 billion	Kjekstad and Highland (2009)
United States	3.2 billion	Schuster and Highland (2001)
Canada	1 billion	
Venezuela	62 million	
Japan	1.5 billion	Sidle and Ochiai (2006)
Korea	60 million	
India	1.3 billion	
Nepal	19.6 million	
China	0.5 billion	

Mass movement, also known as landslides, is the term given to the outward and downward movement of natural (rock, soil, debris) and artificial (mine waste) slope-forming materials by gravitational forces (Sidle and Ochiai 2006). These movements may be triggered by prolonged or heavy precipitation and earthquakes; however, the underlying cause of instability is a combination of factors which act together to either increase the shear stress of the slope or reduce its shear strength (Varnes 1978). Mass movements are classified according to various criteria such as the type of movement, material involved, rate of movement, water content and state of activity. Landslides can also cause other hazards such as the damming of watercourses, dam outburst floods and tsunamis (Marui and Nadim 2009). However, landslides are also significant natural geomorphic agents necessary for shaping our environment. Geertsema *et al.* (2009) refer to landslides as disturbance agents which are necessary for ecosystem cycling. They are essential for maintaining drainage-basin sediment budgets and they contribute to increased habitat diversity by changing site, soil and vegetation (Geertsema et al. 2009).

The effect of climate change on the occurrence of landslides also needs be considered. Most climate models predict an increase in the number and severity of meteorological events such as short, high-intensity rainfall events, changes of hydrological cycles and more extreme weather. Slope studies show that the soil water balance is of utmost importance in determining slope stability, therefore, more water signals a potential increase in the number of landslides. Additionally, potential global warming resulting in deglacierization and permafrost thaw have also led to increased mass movement in mountain areas (Clague 2009). Population increases in less developed countries have led to bad settlement practices, such as deforesting hillslopes to build squatter settlements. Even where properly planned settlements are constructed, the cutting of slopes for building roads destabilises the slope. This creates a state of disequilibrium in the slope system, thereby increasing the likelihood of slope failure. These issues contribute to an overall increase in the risk associated with landslides. Thus, in order to effectively protect their growing populations and infrastructural investments and do so in a sustainable manner, many governments have sought to develop risk management systems for landslides.

1.2. Justification

Risk management involves the identification and monitoring of hazard and risk, the estimation and evaluation of risk and options for reducing risk (Crozier and Glade 2005). Hazard and risk identification feed into the overall concept of risk estimation whereby risk is calculated as a function the hazard, the vulnerability, the elements at risk, and also the capacity of the community or society:

$$Risk = \frac{Hazard \times Vu\ln erability \times ElementsatRisk}{Capacity}$$

Where, in terms of landslides, hazard is the probability of occurrence of landslides of a certain size/volume reaching a particular distance downslope given a triggering event of a certain magnitude in a given area; elements at risk are the valued assets at risk; vulnerability is the amount of damage expected from landslides of a given magnitude expressed on a scale from 0 to 1; and, capacity is the ability of the society to cope with or recover from the event (van Westen 2009). In order to assess the landslide hazard it is necessary to first determine the spatial characteristics (location, extent, distribution), magnitude and frequency of potentially damaging landslides in an area. In order to do this, a detailed landslide inventory needs to be completed. Experts agree that the landslide inventory is the first and most logical step in any landslide hazard assessment (Wieczorek 1984; Soeters and van Westen 1996; Guzzetti et al. 1999). Inventory mapping is also required as the first step for all other methods of landslide hazard assessment (statistical, heuristic, probabilistic and deterministic) as they are the input and validation sets for these methods (van Westen 2007; Hervás and Bobrowsky 2009).

Traditionally, landslide inventory maps were compiled using a combination of analog aerial photo-interpretation techniques with detailed field investigations (1978; Varnes 1984; Brabb and Harrod 1989; Turner and Schuster 1996). This is not always ideal as aerial photos are rarely current, a problem especially in tropical countries where rapid vegetation regeneration masks evidence of

landsliding, and flight missions are expensive, especially considering their small spatial coverage. Aerial photo-interpretation in itself is quite subjective, no two experts will ever come up with identical inventories, and thus the experience and skill of the interpreter is also a concern (Rib and Liang 1978; Soeters and van Westen 1996; Guzzetti et al. 2000).

In the immediate aftermath of an event, the most pressing issue is how to collect and disseminate accurate information to aid disaster managers in organising rescue, emergency and damage assessment operations in the field. Field surveys take time to plan and weeks or months to execute depending on the availability of trained personnel. And even with proper planning, many areas may be too vast, unsafe and/or inaccessible even with the right equipment. Field surveys are also expensive; training, maintaining and equipping field teams cost a great deal. Post-event hazard information is important and it needs to be produced as quickly and as accurately as possible; therefore, if inventories can be generated rapidly from available satellite imagery, it would be very helpful.

1.3. Problem Statement

(Semi-)automatic landslide mapping based on image data, a developmental step following visual interpretation that has been applied for decades to aerial photos, has traditionally been done using pixel-based methods, such as change detection (Cheng et al. 2004; Nichol and Wong 2005), image thresholding (Rosin and Hervás 2005), supervised classification with NDVI (Yang and Hsu 2006) and NDVI with Principal Component Analysis (PCA) (Forsythe and Wheate 2003; Nikolakopoulos et al. 2005). Those, however, focus entirely on statistical image analysis, ignoring altogether the concept of relationships at the spatial unit level and how this changes with scale. Additionally, the spectral characteristics of landslides in an image are often non-unique; bare rock, mines and dirt roads also share the same spectral signatures. These false positives greatly limit the accuracy of per-pixel landslide analysis. There are also hybrid approaches (those that are not pure pixel- or object-based) such as signal processing techniques (Fourier and wavelet analyses) that have been applied to landslide mapping with some success (Booth et al. 2009). Object-oriented analysis (OOA) is a knowledge-based technique comprising image segmentation and classification which allows for the inclusion of information such as shape and texture and also field observations as a thematic layer. When considered with the neighbourhood concept and how relations may change at different scales, OOA greatly aids classification. The usefulness of OOA for identifying landslides has been demonstrated by various studies (Barlow et al. 2003; Martin and Franklin 2005). These however, focussed mainly on spectral characteristics, shape and size relations to detect landslides. This was improved on by Barlow and Franklin (Barlow et al. 2006) with the integration of elevation data to aid classification. Attempts were also made to incorporate textural parameters (Haralick's GLCM) into the classification scheme (Barlow et al. 2006; Moine et al. 2009), but these were trial and error approaches which failed to establish clear linkages with the landslide phenomena. Finally, work done by Martha et al. (2009) successfully integrated spectral and morphological analyses to classify 5 different types of landslides. There is a gap in knowledge surrounding the utility and systematic application of texture measures for landslide detection. Thus, the intention of this research is to determine how far texture can be applied as a diagnostic feature for identifying a landslide and then translate the texture features into quantitative measures which can be applied in an automated object oriented analysis context.

1.4. Main Objective, Sub-Objectives and Research Questions

1.4.1. Main Objective

To examine the utility of texture measures for identifying landslide features using object-oriented analysis.

1.4.2. Sub-Objectives and Research Questions

1 To evaluate the relationship between landslide features and different texture measures.
   a. Can texture be used to distinguish landslides from other features in the landscape?
   b. Understand how texture is calculated in an object-based environment; what influences the selection of parameters?
   c. Which texture measures are useful and why?
   d. Can texture measures be applied explicitly in identifying landslides?
   e. Can texture be used to merge over-segmented landslides?

2 To develop an OOA procedure to test the applicability of texture for detecting landslides.
   - How can the texture measures identified in objective 1 be combined in an OOA-based procedure to identify landslides (inclusive of morphometric and spectral data)?

3 To assess the accuracy of the OOA-based landslide detection at a specific test site.
   a. Do automatic identification results match the manually delineated inventory data?
      - How do the inventories compare in a ROC analysis?
      - How do the inventories compare in visual assessment?
   b. What data quality issues can we expect from the input data used?

2. Literature Review

In order to adequately prepare for, mitigate against and recover from a disaster, end users need to gain sufficient knowledge of the nature and extent of potential hazards which they may face. They need to understand *what* the characteristics of the hazard are, *when* to expect an event, *how long* the event may last and *how* to respond. In terms of the landslide hazard, such analysis begins with a landslide inventory. This review examines the development of landslide inventory mapping from the basic analog photo-interpretation to the more advanced semi-automatic and automatic interpretation of satellite imagery and elevation information by pixel and non-pixel based approaches. It also looks at the progress of the application of texture measures in both a pixel-based and object-based context and digital elevation models (DEMs) and their derivatives to landslide mapping.

2.1. Landslide Inventory Mapping

An inventory map shows the spatial distribution of mass movements in an area represented as points or polygons depending on the purpose of the investigation (Soeters and van Westen 1996). They can be compiled through different methods, including historical surveys, field surveys, visual image interpretation of remotely sensed imagery, semi automatic and automatic interpretation of imagery and digital elevation information and dating methods (Guzzetti et al. 2000; van Westen 2007). Inventories also contain essential classification information such as the type, state of activity, dimensions of landslides and slide anatomy (Appendix 1- Landslide Inventory Form). Different types of mass movements pose different hazards depending on rate of movement and the material involved (Wieczorek 1984). For example, hazard of inundation is posed by debris flows, hazard of impact by rockfalls, rotational and translational slides and hazard of shearing and ground distortion by earthflows and creep. It is equally important to know the slide anatomy i.e., the scarp, zone of depletion and zone of accumulation (see **Error! Reference source not found.**). In the scarp area, the hazards posed by loss of support and differential settlement or tilting are significant. With regards to the depletion and accumulation zones, they can be combined and used to determine the run-out potential of a slide. This has direct bearing on the assessment of potential loss of life, property and interruption of lifelines in the downslope area. It can also be used to aid emergency planning of evacuation routes, placement of lifelines and location of shelters. Depth classification, which is useful for informing engineering mitigation works for example, deciding whether grading or excavation is more feasible in protecting against reactivation, is also significant (Varnes 1974; Wieczorek 1984).

Traditionally, landslide inventory maps were compiled using a combination of visual assessment of stereo analog aerial photographs with detailed field investigations (Rib and Liang 1978; Varnes 1984; Brabb and Harrod 1989; Turner and Schuster 1996). This is not always ideal as aerial photos are rarely current, a problem especially in tropical countries where rapid vegetation regeneration masks evidence of landsliding, flight missions are expensive and photo-interpretation and subsequent GIS database construction takes time (Table 2-1). This table, for example, shows that to create a 1:100,000 scale inventory, it took 2 photo-interpreters 9 months and a GIS specialist an additional 2 months to complete the database. To get a more detailed inventory (1:10,000), 3 photo-interpreters took 28 months and 4 GIS specialists spent another 20 months to complete the database.

Aerial photo-interpretation in itself is quite subjective, no two experts will ever come up with identical inventories, and thus the experience and skill of the interpreter is also a concern (Rib and Liang 1978; Soeters and van Westen 1996; Guzzetti et al. 2000). However, visual assessment is not all haphazard as there are some guidelines (visual clues) that experts use in interpretation. Various authors have compiled lists of photographic characteristics which highlight some diagnostic landslide features (Rib and Liang 1978; Dikau and European Commission. 1996; Soeters and van Westen 1996). Features such as shape, concavities and convexities present in the slope, tension cracks and dimensions of the slide (morphometry), state of vegetation and drainage elements (ponding and diversions), and even the presence of anthropogenic elements for example, retaining walls. Even though these guidelines exist, the final map produced is the result of an individual's perception of what he/she sees in the stereo image in accordance with their expert knowledge on the landsliding process, hence why visual assessment is considered subjective.

Table 2-1 Characteristics of 3 inventory maps *(adapted from Galli et al. (2008))*

CHARACTERISTICS		MAP A	MAP B	MAP C
Type of Inventory		Reconnaissance	Geomorphological	Multi-temporal
Date of Inventory	*Year*	1987-88	1999-2001	2002 (updated 03-04)
Area extent	*km²*	8456	8456	78.89
Sets of aerial photographs		1	2(+1)	5
Scale of aerial photographs		1:33,000	1:33,000; 1:13,000 (1:73,000)	1:13,000 to 1:33,000
Scale of final published map		1:100,000	1:10,000	1:10,000
Time taken for photo-interpretation	*Month*	9	28	5
Team for photo-interpretation	*Interpreters*	2	3	2
Rate of photo-interpretation	*km²/interpreter/month*	470	101	8
Time taken for GIS database construction	*Month*	2	20	1
Team for GIS database construction	*GIS Specialist*	1	4	1

Chacón *et al.* (2006) in their review, have traced some early attempts at landslide mapping beginning in the 1960s with works by Záruba and Mencl (1961; 1969). The review goes on to map the development of landslide hazard, susceptibility and risk mapping, citing many significant developments in this field. The launch of the LANDSAT and SKYLAB satellites missions in the early 1970s provided researchers with the opportunity to use medium resolution data for landslide susceptibility mapping (Rib and Liang 1978). For the next 30 years, improvements in sensor variety and capacity considered, medium resolution satellite data were used extensively in landslide mapping studies, especially at national and regional scales. With the advent of very high resolution optical sensors with stereoscopic capabilities (IKONOS, QuickBird, CARTOSAT) and advances in digital image analysis techniques, landslide inventory mapping too has evolved (van Westen 2004). Visual interpretation with satellite imagery allows for faster revisits, improved coverage and quicker acquisition of data over large areas and with greater detail (van Westen et al. 2006; Martha et al. *"In press"*). The 2nd IGOS Geohazards Theme Report (2007) suggests that these

high resolution images and elevation datasets are the state-of-the-art in landslide mapping and is the best to use for a holistic landslide hazard assessment. Whilst visual assessment of such data can be done, it is not the most efficient method for such digital data and as such various automated and semi-automated techniques have been developed.

2.1.1. Pixel-based Inventory Mapping

A substantial body of literature exists on automated and semi-automated post-event landslide mapping using pixel-based methods, such as unsupervised and supervised classification, change detection with image fusion and artificial neural networks (ANN). In their study on the utility of manual classification of Landsat ETM+ imagery for landslide detection, Petley *et al*. (2002) obtained unsatisfactory results. The classification only identified 67 out of 388 landslides in the study area; the remaining 75% were not detected due to coarse spatial and spectral resolution and shadowed slopes. Borghuis *et al.* (2007) attained 63% classification accuracy when their automated (unsupervised classification) results were compared to that of manual mapping. Change detection and image fusion were used by Nichol and Wong (2005) to identify accurately 70% of landslides in an area in Hong Kong. Cheng *et al*. (2004) proved that change detection based on spectral ratioing and image differencing was useful in detecting fresh, un-vegetated landslides. Similarly, Hervás *et al.* (2003) demonstrated that change detection and thresholding techniques could also be used to identify landslides. However, these methods all rely heavily on spectral characteristics to identify a landslide, which raises some issues. First, per-pixel classification places pixels in a class according to where they fall in the spectral feature space; this ignores its spatial association, where it falls in relation to its neighbours (Liu et al. 2006). Such contextual analysis is a main tool used in visual analysis by experts (Blaschke et al. 2004). Second, the spectral signature of landslides is typically not diagnostic; it is shared with many other features present in the landscape, such as roads, bare rock or river banks. Finally, the use of automated pixel-based procedures to delineate landslides often results in smaller feature areas in comparison to manually detected landslides (Borghuis et al. 2007). Another point is that even though these studies were somewhat successful in identifying landslides, classification into different landslide types was beyond the scope of the researchers.

Aspects of morphology, vegetation and drainage present diagnostic features of landslides which cannot be detected from analysis of spectral signatures only as is done in pixel-based methods. Thus, in order to use the same diagnostic features that experts use in visual interpretation we need to integrate morphometric data derived from digital elevation models (DEMs), contextual information for example, the presence of anthropogenic features such as retaining walls through spatial association and spectral signature information, all on one platform (Table 2-2).

2.1.2. Object-based Inventory Mapping

OOA is a knowledge-based technique comprising image segmentation and classification. Its power lies in its ability to integrate spectral, morphometric and thematic data (Table 2-2), and using these to mirror the process of visual assessment (using the 7 image interpretation keys: colour, shape, tone/shade, size, site and association), thereby, attaining a more thorough image classification.

Table 2-2 Two types of remotely sensed information classification patterns *(adapted from Liu et al. (2006))*

PIXEL-BASED CLASSIFICATION PATTERN	$Pixel + FeatureSet\begin{Bmatrix} DNValue \\ Texture \end{Bmatrix} + Classifier$
OBJECT-BASED CLASSIFICATION PATTERN	$Object + Featureset\begin{Bmatrix} DNValue \\ Texture \\ Shape \\ SpatialAss\ ociation \end{Bmatrix} + Classifier$

The concept of knowledge-based techniques for OOA originated in the 1970s and has developed substantially since then, as is shown in the reviews of Baltsavias (2004) and Liu *et al.* (2006). OOA involves firstly the segmentation of the image, followed by analysis of the segments, and their subsequent classification. In OOA, these segments or image-objects are essentially the smallest units of analysis in the image. They are defined by Blaschke et al. (2004) citing from Hay et al. (2001) as *"basic entities, located within an image that are perceptually generated from H-res pixel groups, where each pixel group is composed of similar digital values, and possesses an intrinsic size, shape, and geographic relationship with the real-world scene component it models"*. Image segmentation is the process by which a digital image is broken down into regions which are spatially cohesive, i.e, *"spatially continuous, disjoint and homogenous regions"* (Blaschke et al. 2004). These regions are essentially discrete objects which ideally, should hold some significance for subsequent analysis. However, more often than not, these units are spectrally uniform but may hold little similarity to actual features in reality.

Whilst OOA has been used extensively in medical imaging and life sciences, its application in earth sciences and, more specifically, landslide related studies is limited. Barlow *et al.* (2003) demonstrated that the combination of NDVI, DEM-derived slope and aspect data and shape criteria were effective in identifying landslide scars; however, the spatial resolution of the Landsat TM greatly restricted the size of slides that could be identified (only slides >1ha could be identified) and the shape criteria were too stringent for classification of complex slides. Martin and Franklin (2005) improved the resolution issue by applying data fusion to the Landsat TM data and added the element of classification based on dominant materials (soil vs. bedrock), but applied a similar analysis technique as used by Barlow et al. (2003). Spatial resolution again appeared as a limiting factor to the analysis especially as it regarded texture measures. The use of high resolution data (greater spatial detail) in subsequent studies by Barlow *et al.* (2006) and Moine *et al.* (2009) enabled the application of texture measures calculated using grey level co-occurrence matrix (GLCM) after Haralick *et al.* (1973) to distinguish between landslide types. However, very little was said about how these texture measures were applied and in what context they were used. A recent study by Martha *et al.* (*"In press"*) saw the development of a more robust procedure for classifying multiple landslide types using shape and DEM derivatives of slope, terrain curvature, hillshade and flow direction. The results of this research showed 76.4% recognition of landslides surveyed in the study area but, more significantly, it showed that 5 different landslide types could be distinguished automatically (69.1% classification accuracies). This paper is the first to successfully synthesize diagnostic features used by experts in visual analysis of landslides and produce an automated OOA-based procedure for the recognition and classification of landslides.

From the above, we can see that there is still much to do in terms of object-based landslide research. Firstly, none of these authors have yet explored the possibility of identifying landslides explicitly (without

having to first eliminate false positives) from imagery. They all acknowledge that fresh landslides present a clear disturbance on the landscape therefore, it is logical to assume that we should be able to automatically identify and extract these as objects of interest from the imagery. Secondly, landslides have to be over-segmented in order to capture their complex and irregular forms, shapes and sizes (Martha et al. *In Press*). However, for significant and meaningful analysis to be done, i.e, in order to apply features such as length-width ratios and curvature, the multiple segments making up a landslide need to be merged into a single landslide object. Martha *et al.* (*In Press*) achieved this reconstitution of over-segmented landslides through a series of convoluted steps which cannot easily be reproduced in another study. Thus, even with all their successes, they identified this issue as one that needs to be addressed in a separate study. Pixel-based landslide-texture analyses have shown that the distortion caused on the surface by a landslide is a unique feature that can be easily enhanced and extracted using textural analysis. If the texture values within the landslide are more similar to each other than they are to their surrounding areas therein, a boundary can be forged between the landslide and the rest of the landscape (see Section 2.2.2).

2.1.3. Image Segmentation

Image segmentation is the process by which a digital image is broken down into regions or objects wherein there is homogeneity of the pixel values. These regions are essentially discrete objects which should ideally define the boundary of the feature of interest; such spatial contiguity is an explicit goal of segmentation. Various segmentation techniques exist for example, thresholding, clustering, density slicing, edge-based segmentation, split-and-merge and region growing. In the Definiens software environment where this research analysis was carried out, multiple segmentation algorithms can be applied to attain reasonable classified outputs. No single segmentation routine can adequately produce single segments outlining each landslide due in a large part to feature size variability. Thus various segmentation algorithms were applied at different points in the analysis (see chapters 4 and 5). Initial segmentation however, was done using the multi-resolution algorithm, a process controlled by scale, colour, shape, smoothness and compactness criteria (Figure 2-1).

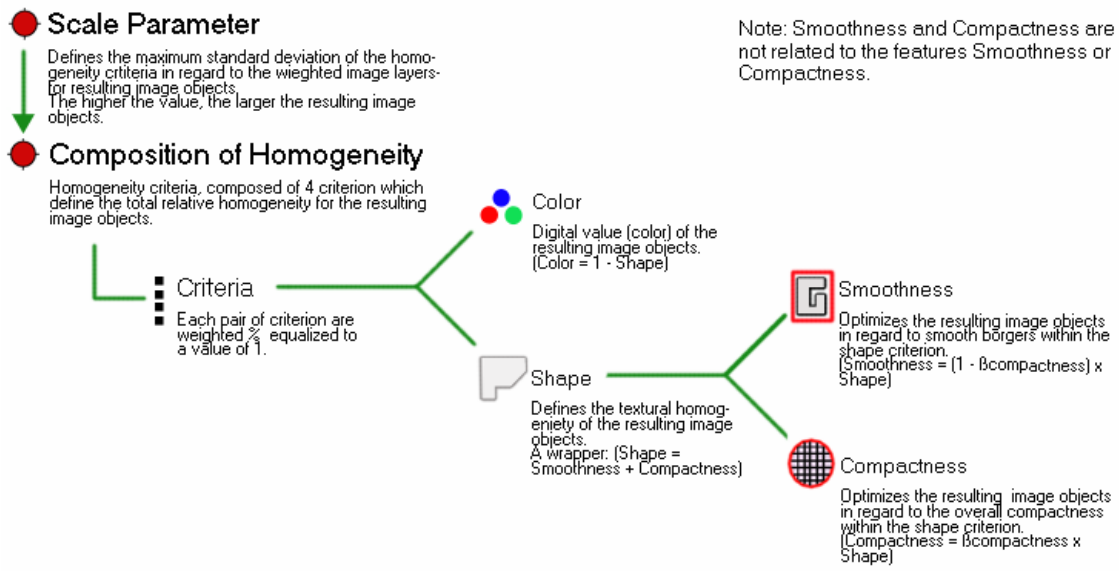

Figure 2-1 Multiresolution segmentation concept flow diagram. *(source Defeniens 7 Reference Book)*

2.2. Texture

Haralick (1979) defines texture in this way: *"Image texture is described by the number and types of its primitives and the spatial organisation or layout of its primitives. The spatial organization may be random, may have a pairwise dependence of one primitive on a neighbouring primitive, or may have a dependence of a primitive at a time. The dependence may be structural, probabilistic or functional."* Berberoglu and Curran (2004) simplify this and describe texture as a *"measure of the spatial variation of digital image spectral brightness or digital number (DN)."* Texture describes the smoothness or roughness of an image scene and is determined by the *frequency* and *distribution* of pixels in the scene. In texturally rough images there is high pixel variation, i.e., pixel values change abruptly over short distances, for example, roads and buildings in an urban centre. In contrast, smooth images have pixel values that vary gradually over large distances for example, large water bodies and fields (Whitworth et al. 2005). In terms of image objects, texture can provide important information about their arrangement and spatial relationships within the image (i.e, Contextual relationships) and also within an object (i.e. inherent textures), see Section 2.2.1. Table 2-3 below outlines the main texture techniques used in the analysis of remotely sensed imagery.

Table 2-3 Major texture analysis techniques used in remote sensing *(adapted from Berberoglu and Curran (2004))*

TEXTURE MEASURES IN REMOTE SENSING	ADVANTAGES	DISADVANTAGES	REFERENCES
First Order Statistics Standard deviation, Variance.	• Simple to calculate • Indicates Local variance	• No directionality (isotropy, anisotropy) • Does not consider relation between different pixels • Sensitive to noise	Forest mapping (Arai 1993) Local variance at different spatial resolutions (Woodcock and Strahler 1987)
Second Order Statistics Co-occurrence matrix Contrast, Angular second moment, Correlation, Entropy, Dissimilarity, Homogeneity, Sum average, Sum variance, Sum entropy, Difference variance, Difference entropy, Information measures of correlation, maximum correlation coefficient	• Describe relation between different pixels (regionalised variables) • Sensitive to directionality • Insensitive to noise • Does not over-emphasize field boundaries	• Computationally intensive • Similarity among the statistics derived from co-occurrence matrix	Introduction (Haralick et al. 1973) Vegetation classification (Dikshit 1996) Land cover mapping (Marceau et al. 1990) Forest regeneration (Luckman et al. 1997)
Geostatistics Variogram, Correlogram, Covariance function, General relative variogram, Rodogram, madogram, Pairwise relative variogram	• Provides different scene measures (sill, range, nugget) • Sensitive to directionality • Insensitive to noise • Robust • Mathematically simple • Underlying assumptions not rigid • Requires mean to be weakly stationary • Easy to interpret	• Computationally intensive • Large dataset required to fit a variogram model • One 'unusual' DN value causes misquantification of all surrounding pixels	An introduction (Atkinson and Lewis 2000) Lithological discrimination (Chica-Olmo and Abarca-Hernández 2000)
Fractals	• Utilises multi-spatial resolution data • Can quantify roughness • Computationally not intensive • Uses spatial units larger than pixels	• Some methods for assessing fractal dimension result in lumped values rather than spatial pattern • Noise has severe effect on this assessment.	Introduction (Ait-Kheddache and Rajala 1988)

The grey level co-occurrence matrix (GLCM) (Haralick et al. 1973; Haralick 1979) is widely used for computing second order texture measures in remote sensing (Narasimha Rao et al. 2002). The matrix statistically describes the relationship between neighbouring pixels. It records the number of pixels with a grey level *i* which are separated from pixels with a grey level *j* by a certain distance and in a particular direction. Haralick et al. (1973) using these matrices, defined fourteen features for quantifying texture in images. Hall-Beyer (2007) grouped some of these texture features into three main categories; 1) contrast, 2) orderliness and 3) descriptive statistics. Table 2-4 describes these three groups and the texture measures which are a part of each.

Table 2-4 Description of GLCM texture features from combined sources (Haralick et al. 1973; Baraldi and Parmiggiani 1995; Narasimha Rao et al. 2002; Definiens 2007; Hall-Beyer 2007)

TEXTURE GROUP	GLCM TEXTURE PARAMETERS	DESCRIPTION
CONTRAST: *uses weights related to distance from the diagonal. Contrast along the diagonal is zero and it increases away from the diagonal*	Contrast $\sum_{i,j=0}^{N-1} P_{i,j}\left(i-j\right)^2$	• measures the amount of local variation in the image • if *i* and *j* are equal, the cell is on the diagonal and (i-j)=0; in other words, it represents pixels that are the same as their neighbour, so the weight is 0. • values increase exponentially with distance from the diagonal; therefore if the difference between *i* and *j* is *1*, contrast is small, and the weight= 1. If *i* and *j* differ by 2, weight = 4 and so on. • High contrast values indicate high coarse textures. • *N.B: Contrast can be <1, therefore, if put into an 8-bit or 16 bit integer channel, the value would become 0.*
	Dissimilarity $\sum_{i,j=0}^{N-1} P_{i,j}\left\|i-j\right\|$	• Describes the heterogeneity of the grey levels • Similar to contrast but values increase linearly (0, 1, 2,3 etc.) with distance from diagonal • High values indicate coarse textures
	Homogeneity $\sum_{i,j=0}^{N-1} P_{i,j}\frac{P_{i,j}}{1+\left(i-j\right)^2}$	• a.k.a *Inverse Difference Moment*, weights values by the *inverse* of the Contrast weight • it assumes *larger* values for *smaller* differences in pixel pair grey tone therefore, weights *decrease* exponentially away from the diagonal. • Homogeneity increases where there is less contrast.
ORDERLINESS: *is a measure of how regular (orderly) the pixel values are. It is a weighted average related to the number of times a given pixel pair occurs. If the weight increases with commonness, then the texture measure increases with orderliness. But if it decreases with commonness, the measure increase with disorder.*	Angular Second Moment (ASM) $\sum_{i,j=0}^{N-1} P_{i,j}^{\,2}$	• measures the textural uniformity (pixel pair repetition) • High values of ASM occur when the grey level distribution is very orderly
	Entropy $\sum_{i,j=0}^{N-1} P_{i,j}\left(-\ln P_{i,j}\right)$ *N.B. Because ln(0) is undefined, it is assumed that 0 * ln(0) = 0.*	• Measures the disorder of an image. If the image is texturally not uniform, values are low which imply that entropy is large. • By definition, the sum of $P_{i,j}$ = 0, therefore, the maximum value of ENT is 0.5 and is reached when all probabilities are equal. When this occurs, there is a random distribution of DN values, thus maximum "chaos" or entropy.
DESCRIPTIVE STATISTICS: *these are statistics derived from or expressed in terms of the GLC matrix. It is like calculating the regular statistic but it includes combination with a certain neighbour pixel value.*	Mean $\mu_i = \sum_{i,j=0}^{N-1} i\left(P_{i,j}\right)$ $\mu_j = \sum_{i,j=0}^{N-1} j\left(P_{i,j}\right)$	• Indicator of the distribution of grey levels with respect to the central position. In Definiens, since the GLCM is symmetrical, each pixel is counted both as a reference and a neighbour, thus both values are identical. • P_{ij} value is the probability value from the GLCM, i.e. how many times that reference value occurs in a specific combination with a neighbour pixel.
	Standard Deviation $\sigma_i^2 = \sum_{i,j=0}^{N-1} P_{i,j}\left(i-\mu_i\right)^2$ $\sigma_j^2 = \sum_{i,j=0}^{N-1} P_{i,j}\left(j-\mu_j\right)^2$	• GLCM variance deals specifically with the dispersion around the mean of *combinations* of reference and neighbour pixels. • In Definiens, since the GLCM is symmetrical, variance calculated using *i* or *j* gives the same result. • Generally, coarse textured features are associated with higher standard deviations.
	Correlation $\sum_{i,j=0}^{N-1} P_{i,j}\left[\frac{\left(i-\mu_i\right)\left(j-\mu_j\right)}{\sqrt{\left(\sigma_i^2\right)\left(\sigma_j^2\right)}}\right]$	• measures the linear dependency of grey levels on those of neighbouring pixels. • Relation to actual calculated values is quite clear; 0 is uncorrelated, 1 is perfectly correlated • *N.B. When an image area is completely uniform, the GLCM variance is 0, as a result, the denominator of the correlation equation becomes 0, and correlation becomes undefined.*

P_{ij} is the normalized co-occurrence matrix, N is the number of rows or columns, σ_i and σ_j are the standard deviation of row i and column j, μ_i and μ_j are the mean of row i and column j.

2.2.1. Texture in Definiens

Definiens recognises two types of textural relations; i) **Contextual**: which denotes those features that express the *relationship of objects* to each other at different levels eg. *Layer value texture based on sub-objects*, and ii) **Inherent**: which refers to the features essential to the *pixels* in an image eg. *Texture after Haralick.* This research focusses more on the synthesis of the inherent texture features.

Contextual texture features are based on the analysis of sub-objects which is controlled by determining the feature distance (level) for analysis. Table 2-5 below shows the contextual texture features that can be applied in Defienens. For a more detailed look at the algorithms used and a better understanding of the feature, refer to the *Definiens 7 Reference Book* .

Table 2-5 Contextual texture features in Definiens, adapted from Definiens 7 Reference Book

CONTEXTUAL TEXTURE GROUP	TEXTURE FEATURE	DESCRIPTION
LAYER VALUE TEXTURE BASED ON SUB-OBJECTS: *features refer to the spectral information given by the image layers.*	Mean of sub-objects: stddev.	Standard deviation of the different layer mean values of the sub-objects.
	Average mean difference to neighbors of subobjects	The contrast inside an image object expressed by the average mean difference of all its subobjects for a specific layer.
SHAPE TEXTURE BASED ON SUB-OBJECTS: *features refer to the structure of the sub-objects. They depend on an accurate segmentation of the image as the sub-objects need to be as meaningful as possible.*	Area of subobjects: mean	Mean value of the areas of the sub-objects.
	Area of subobjects: stddev.	Standard deviation of the areas of the sub-objects.
	Density of subobjects: mean	Mean value calculated from the densities of the subobjects.
	Density of subobjects: stddev.	Standard deviation calculated from the densities of the subobjects.
	Asymmetry of subobjects: mean	Mean value of the asymmetries of the subobjects.
	Asymmetry of subobjects: stddev.	Standard deviation of the asymmetries of the sub-objects.
	Direction of subobjects: mean	Mean value of the directions of the sub-objects.
	Direction of subobjects: stddev.	Standard deviation of the directions of the sub-objects.

Balaguer *et al.* (*In Press*) describe how the GLCM texture is implemented in an object-oriented context: for each object, a matrix (GLCM) is calculated based on the co-occurrences of the pixel values separated by a one pixel distance inside the polygon (object). To allow for directional invariance all four orientations (see Figure 2-2) are summed prior to the texture calculation, but each direction can also be considered separately.

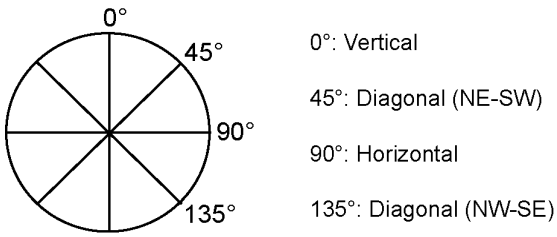

Figure 2-2 GLCM Directionality

Directionality governs how the neighboring pixel calculation is done and it depends on the feature angle:

- 0 deg.= (x;y-1) and (x;y+1)
- 45 deg.= (x-1,y+1) and (x+1,y-1)
- 90 deg.= (x-1;y) and (x+1;y)
- 135 deg.= (x-1,y-1) and (x+1,y+1)
- All dir. = all neighbor pixels described above

To ensure that there are no border effects in the computed value for the image object, pixels on the immediate border of the object are also considered when constructing the matrix (. Which pixels would be dependent on the directional relationship being considered. Finally, only one value of the texture feature is computed for the object.

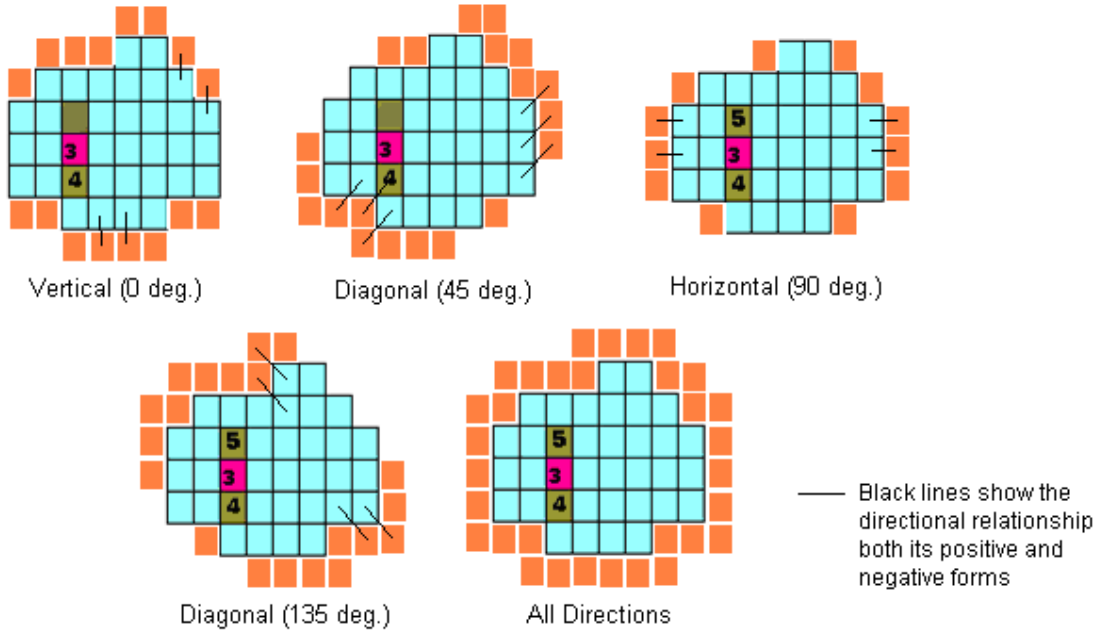

Figure 2-3 Pixels (orange) adjacent to the object border which are considered in the compilation of the GLC Matrix based on the Directionality applied.

For each GLCM, normalization is done according to the following formula (Definiens 2007):

Equation 1

$$P_{i,j} = \frac{V_{i,j}}{\sum_{i,j=0}^{N-1} V_{i,j}}$$

Where:

i *: the row number*
j *: the column number*
$\boldsymbol{V}_{i,j}$ *: the value in the cell* ***i,j*** *of the matrix*
$\boldsymbol{P}_{i,j}$ *: the normalized value in the cell* ***i,j***
N *: the number of rows or columns*

The result is a symmetrical GLCM where elements along the diagonal represent pixel pairs that have no grey level difference (Figure 2-4; orange dots and line) and the same values occur in cells on opposite sides of the diagonal. For example, the value in cell 3,2 would be the same as the value in cell 2,3. Grey level difference increases linearly with distance from the diagonal therefore, cells one cell away from the diagonal represent pixel pairs have one grey level difference, two cells away- two grey levels difference, and so on (Definiens 2007) (Figure 2-4).

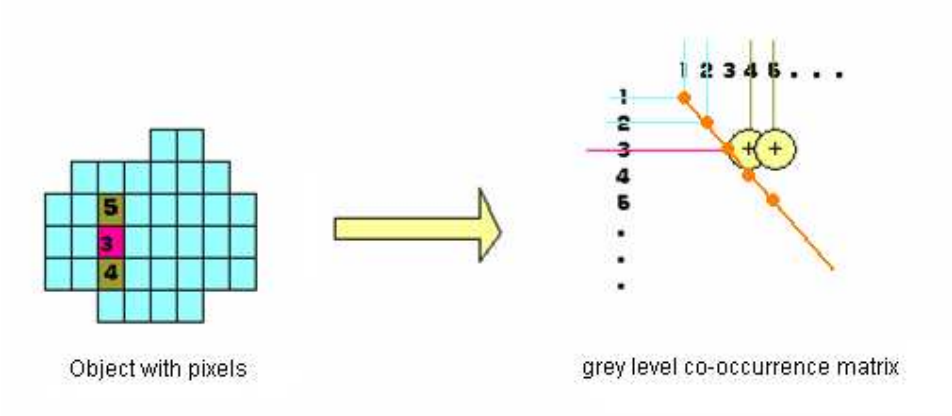

Figure 2-4 Object-based GLCM *(Source: adapted from Definiens 7 Reference book (2007))*

Calculation of the Haralick texture is very computationally intensive as a matrix is built for each object in the image. This poses a challenge for users as increasingly larger images are being used for analysis. Therefore, Definiens 7 presents two alternatives for GLCM texture calculation based on the bit range of the input image data; regular and quick 8/11. Texture calculations in Definiens are not dependant on image data bit-depth; however, if data with a higher dynamic range than 8-bit are used, before the GLCM is computed, they first have to be converted to 8-bit (*see Definiens 7 Reference Book (2007)*) then the regular version can be applied. Quick 8/11 is an optimized version of the texture calculations that is designed for 8-bit and 11-bit data. It is recommended that 8-bit data are used for the best texture results. Finally, the output value range for all the GLCM texture calculations in Definiens is 0 to 90.

2.2.2. Applications of GLCM Texture in Remote Sensing Studies

GLCM texture has been used successfully for identifying homogenous areas and thereby detecting the boundaries between them in forestry studies (Luckman et al. 1997; Wulder et al. 1998; Tuominen and Pekkarinen 2005; Kayitakire et al. 2006) and land use/ land cover classification (Marceau et al. 1990; Gong et al. 1992; Pacifici et al. 2009). These studies all applied GLCM texture via per-pixel analysis using moving windows of varying sizes. Through the research of these and other authors, much is understood about the relationship between the feature being investigated and GLCM texture measure variables such as scale, window size, kernel size and directionality. The same cannot be said however, for GLCM texture analysis applied in an object oriented context, for which only a small body of literature exists. Many studies actually calculate per-pixel texture images and then bring these into the object-based environment for segmentation and further analysis. On the other hand, very little published work exists on studies using derived texture parameters extracted from image segments created in an object-oriented environment.

GLCM texture with an object oriented approach has been applied effectively so far in some vegetation studies (Kamagata et al. 2008; Ozdemir et al. 2008). Kamagata *et al.* (2008) in their study, evaluated 3 methods for vegetation classification; pixel-based, object-based with spectral features only and object-based with texture added. These researchers found that the highest accuracies (65-95%) came from the object-based classification when texture features were added. Moreover, the authors noted that the texture features were especially helpful in distinguishing between vegetation types that were bundled in a complex mosaic pattern. Ozdemir *et al.* (2008) also used object-based texture calculations to determine the relationship between the imagery-derived texture features and ground-based derived indices (Gini coefficient and Shannon Index) for mapping tree size diversity. This study chose to examine the contrast group of texture measures and found that there was high correlation between the texture measures (especially GLCM Homogeneity) and the Gini coefficient but weak correlation between the measures and the Shannon Index.

Work done by Laliberte and Rango (2008) examined the effect of segmentation scale on texture measures and correlation between them using 5-cm resolution true-colour aerial photography. Pixel-based work has already established that texture is sensitive to scale and they found that in the object-based environment too, an appropriate scale (depends on the feature of interest) must be selected for meaning and effective analysis. Their work also showed that in order to reduce computation time and increase classification accuracy one should choose uncorrelated texture variables. This is in keeping with the recommendation by Hall-Beyer (2007) that in order not to end up using highly correlated variables in analysis, it is wise to use texture measures from different groups (see

Table 2-4). In terms of scale, they found that if image objects are too small, then texture values become insignificant and texture is no longer a useful feature for classification. In general, classification accuracies increased with segmentation scale, with significant increases occurring after scale 40. Entropy was found to be the most stable texture measure at all scales and entropy, contrast and mean were found to be highly uncorrelated at segmentation scales 40 and above where accuracies were highest.

GLCM Texture in Landslide Mapping

Landslides cause significant distortion of the ground surface thereby creating diagnostic disturbance features that, through the use of high-resolution imagery, can be enhanced and extracted by textural analysis (Mason et al. 1995; Eyers et al. 1998; Mason et al. 1998; Whitworth et al. 2002; 2005; 2006; Carr and Rathje 2008; Fernández et al. 2008). Early work by Mason *et al.* (1995; 1998) showed that the use of simple filters, such as centrally weighted texture gradient filters, could be applied to create a boundary between areas of different digital texture whilst forcing values within the area to average out and thereby reduce topographic variation. Eyers *et al.* (1998) also found that applying simple texture features could reveal characteristic landslide features. These authors were of the view that statistical measures such as GLCM after Haralick *et al.* (1973) were too complex and often gave results that were hard to understand and interpret. Subsequent work explored this view through examination of the potential of GLCM measures for identifying clearly, landslide features.

Hervas and Rosin (1996) applied GLCM texture derivatives to landslides in south-east Spain and found that they allowed for good discrimination between rough and smooth surfaces. They then used a ‘texture spectrum’ method to separate areas of slope instability from those false positives that were texturally similar. Whitworth *et al.* (2002; 2005; 2006) tested a range of texture filters (mean, variance and GLCM entropy) to determine which best highlighted active landslide areas and found that the GLCM texture feature (entropy) best discriminated landslides in Airborne Thematic Mapper (ATM) imagery. In the texture image, areas of very low texture were associated with agriculture fields and pastures (zones of stability); areas of very high texture and image variation were characteristic for dense woodland and hedgerow systems; and, areas of intermediate texture represented zones of instability on escarpment slopes (Whitworth et al. 2005; 2006). The results of this texture analysis were incorporated into a classification scheme which successfully identified landslides with an overall accuracy of 83%. Fernandez *et al.* (2008) did similar work in southern Spain and also found GLCM entropy to be most useful for highlighting zones of movement. In particular, the GLCM entropy values revealed rock slides very well whilst the values for rockfalls and debris flows were lower. Carr and Rathje (2008) tested 5 GLCM texture measures using different kernel sizes for computation all with the aim of finding which would best allow for separability between classes. They found that the texture measures greatly improved separability of the landslide and muddy water classes and slightly improved separability between the landslide and landslide debris and agriculture classes. These studies all implemented texture through per-pixel analysis with varying degrees of success.

With the use of OOA having been proven to improve classifications in general and the successful application of texture analysis in pixel-based landslide mapping, combining the both techniques for landslide mapping should significantly improve landslide detection accuracies. Martin and Franklin (2005) applied texture analysis as part of a larger classification scheme to identify scars of soil- and bedrock-dominated landslides. The exact measures used and how they were implemented were not discussed; however, it was mentioned that the resolution of the imagery used was a limiting factor to the analysis. GLCM homogeneity, dissimilarity, mean and variance applied to the panchromatic band were used by Barlow *et al.* (2006) to help distinguish between landslide types. They found that the textural properties were very useful for distinguishing the debris slide class from other classes, achieving 90% specific classification accuracy for that class. The overall accuracy for all mass movements was 77%. Once again however, which texture measure, why it was used or how it was implemented, was not discussed. Moine *et al.* (2009) used GLCM contrast, entropy, mean and correlation as quantitative representations of the qualitative landslide indicators-cracks, ridges and surface disturbance. They used membership functions with varying value ranges for the texture measures and other criteria to apply a classification. The best results came from classification schemes using spectral, shape and neighbourhood criteria. When texture criteria was used, results were not good thus leading the authors to conclude that texture was not a good indicator to be used for extracting landslides in very high resolution aerial images. Martha *et al.* (*In Press*) applied texture analysis in a different way. Rather than using texture for identifying landslides directly, it was used to identify and eliminate false positives. Generally however, these studies fail to comprehesively evaluate the potential of object-based texture analysis for landslide mapping. Even though pixel-based studies have proven that texture, especially GLCM entropy, significantly aids landslide identification, similar results have not been found for the object-based case.

From all of the above then we have learnt that for the best classification results only one texture measure from each texture group should be used, in order to avoid highly correlated variables in analysis (Hall-Beyer 2007; Laliberte and Rango 2008). The segmentation scale chosen needs to be meaningful not only because useful texture depends on it, but also because landslide objects differ in size; we need them all to be captured, in some cases as a single object but in most as a combination of multiple objects. Entropy has been identified as the most useful for landslide identification in pixel-based analysis (Whitworth et al. 2002; 2005; 2006; Fernández et al. 2008) and as the most stable texture feature at multiple scales (Laliberte and Rango 2008), this claim will be tested for its applicability in an object-based environment. In terms of object-based landslide detection two uses for texture are evaluated *(see Figure 2-5)*:

i. Boundary detection, and
ii. Reconstitution of over-segmented slides.

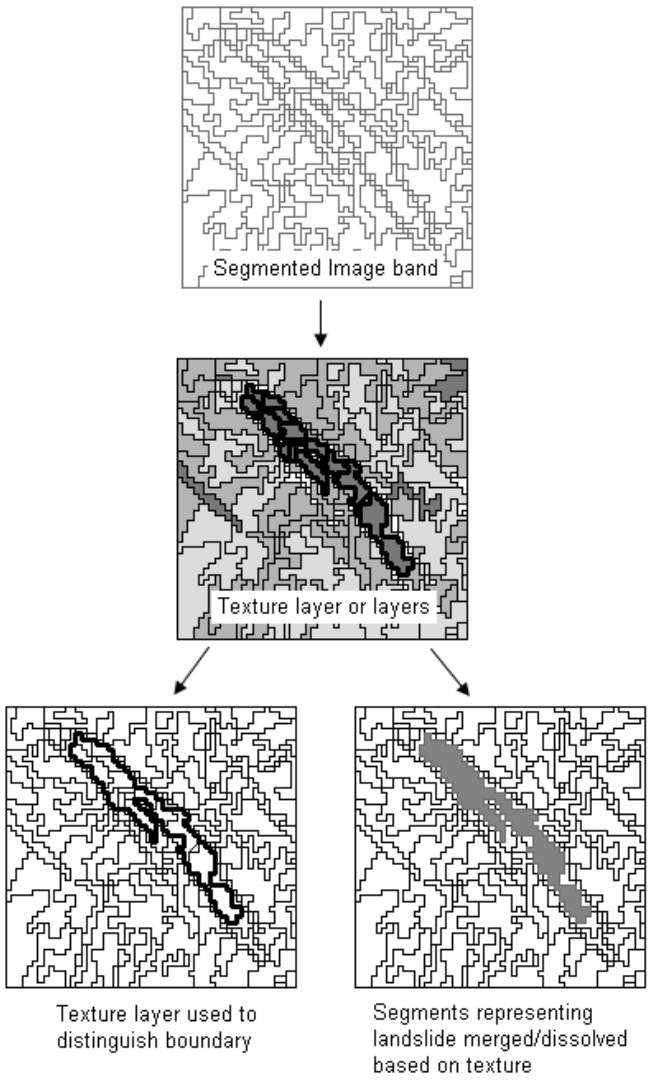

Figure 2-5 Intended use of texture for object-based landslide detection

Definiens has over 28 texture measures available for analysis and quite often the user can become daunted at the propect of having to go through all of these to make a decision on which they should apply for their purpose. In fact, much of the work done using these textures are still largely trial and error- the user keeps applying multiple textures until one works or they just give up. Thus, this research was designed to act as a guide for texture use by addressing unanswered questions, such as how variables such as object size, directionality and image band affect object-based texture analysis for landslide mapping, which object-based GLCM texture measures best represent landslide textures, whether or not landslides can be identified explicitly using object-based texture analysis and, how texture characterization can be incorporated implicitly into an automated routine for landslide detection.

2.3. DEM and its Derivatives

Elevation data has been applied to landslide studies for decades. Early photo-interpreters used aerial stereo pairs to view the landscape in 2.5D and thereby complete their analysis. Currently, digital elevation datasets are available from automatic stereoplotting of aerial photos or satellite data, digitized contour maps, ground surveys, LiDAR and RADAR. Digital elevation models (DEMs) have been applied in various capacities to landslide research such as, large-scale susceptibility mapping, change detection/DEM height differencing, mass propagation modeling, detection and classification. Many authors generally hold the view that landslides are strongly controlled by surface form/topography and as such, they try to devise a precise relationship between individual topographic attributes and mass movement processes. A significant body of research exists as it regards the application of digital elevation data to landslide studies, some of these contributions are referred to below:

1. *Identification and Classification*: Pike (1988), Singhroy *et al.* (1998), Barlow *et al.*(2003), Forsythe and Wheate (2003), Haugerud *et al.* (2003), Hervás *et al.* (2003), McKean and Roering (2004), Martin and Franklin (2005), Barlow *et al.* (2006), Glenn et al. (2006), Yang and Hsu (2006), Van Den Eeckhaut (2007), Barlow and Franklin (2008), Booth *et al.* (2009)
2. *Monitoring*: Van Westen and Getahun (2003), Canuti *et al.* (2004), Cheng et al. (2004), Singhroy and Molch (2004), Singhroy (2009)
3. *Susceptibility (Hazard and Risk) Mapping*: Shikada (1997), Mason *et al.* (1998), Pack *et al.* (1998), Singhroy (2000), Pike *et al.* (2001), Lineback Gritzner *et al.* (2001), Catani *et al.* (2005), Miliaresis *et al.* (2005), Schulz (2007), Castellanos and Van Westen (2008), Kawabata and Bandibas (2009)
4. *Propagation and Terrain Models*: Pike (1988), Hungr (1995), Iverson *et al.* (1998), Brunsden (1999), Huggel *et al.* (2003).
5. *Volume assessment* : Kerle (2002), Martha *et al.* (2010)

Moore et al. (1991) identified altitude, slope gradient, slope length, aspect and curvatures as the most relevant to the study of landslides. With respect to automated landslide mapping, these and other derivatives (hydrological) have been applied in varying capacities to aid landslide detection and classification by type. For example, recent work by Martha *et al.* (*In Press*) applied the use of some hydrological derivatives namely, flow direction and drainage lines and order, were used to eliminate landslide false positives. These previous works have proved the usefulness of DEMs and their derivatives for landslide identification.

2.4. Chapter Summary

This review has taken an in-depth look at landslide inventory mapping, from its traditional methods to current state-of-the art methods. It covered the devolpment of pixel-based methods and identified their shortcomings, such as the lack of contextual considerations and the inability of spectral characteristics to be the sole diagnostic property of landslides, thus leading to the rise of object-based methods. Landslide inventory mapping using OOA was shown to be in its infant stages and some gaps in the

knowledge, such as how best to reconstitute over-segmented landslides, were identified and taken on as part of the research for this study. Texture analysis and its applicability to landslide mapping were also reviewed and the reseacher sought to determine whether the findings of this object-based texture for landslides study would match those found in pixel-based studies. The review on object-based texture for landslide mapping also showed that there are many aspects and applications that have yet to be explored and this lead to the compilation of possible points for research in this area (see Recommendations). Finally, a review of the application of DEMs and their derivatives to landslide identification and classification showed that much has been done already and varying combinations of derivatives have been proven useful for identification.

In the next chapter, the research tools applied in this study inclusive of the case study area, the major diagnostic morphologic, vegetation and drainage features of landslides and their photographic characteristics and the data used are explained. This study aims to use the diagnostic features for detecting landslides by translating them into quantitative indicators (textural, spectral and morphological) which can be applied in an OOA context.

3. Research Tools and Methodology

This chapter begins by describing the case study area used both for evaluating the applicability of GLCM texture measures for landslide identification and for the subsequent development and testing of an automated procedure in which these textures are applied. The specifics of the event triggering the landslides are briefly discussed and a short description of the main types of slides found in the area is given. Keeping the focus on the slides prevalent in the study area, an overview of the major diagnostic morphologic, vegetation and drainage features of landslides and their photographic characteristics is presented. In the next sub-section, an outline of the data used, the processing steps applied to the datasets and the products derived from them is provided. The segmentation technique applied in Definiens 7 is also described in brief. Finally, a synopsis of the approach used to identify and classify the landslides is outlined.

3.1. Case Study Area

The area in which the proposed methodology will be applied is located in the eastern margin of the Tibetan plateau in the Sichuan Province of China (Figure 3-1). It has an average annual rainfall of 1,000 mm and an average annual temperature of 16.5°C. This area is very seismically active as a result of the convergence of the Indian Ocean Plate and Eurasian Plate which causes uplift of the Qinghai-Tibet plateau. Strong earthquakes are prevalent in this area and, in addition to the intense seasonal rainfall, contribute to the occurrence of numerous large and small landslides.

On May 12, 2008, an earthquake of magnitude 7.9 on the Richter scale with a focal depth of 19.0 km occurred at the eastern margin of the Tibetan plateau (white dot, Figure 3-1). Approximately 45.6 million people were affected and economic losses totalled US$85 billion; 68 858 people were killed and another 18 618 were reported missing (Rodriguez et al. 2009).

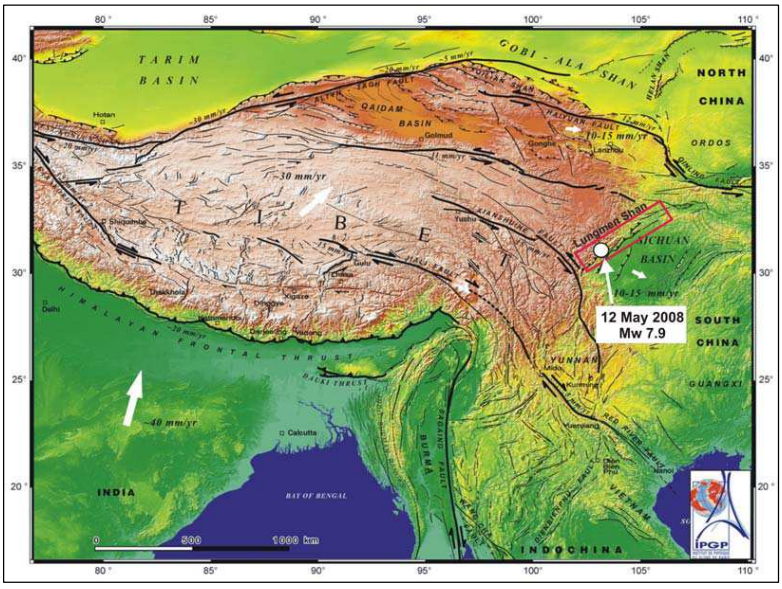

Figure 3-1 Geologic setting of the Qinghai-Tibet plateau in Southern China. White dot shows the location of the epicentre of the May 12, 2008 Sichuan earthquake. *(Source: T. Gorum; original from CIT, Tectonics Observatory Division)*

Approximately 15% of the deaths were attributed to landslides which also severely hampered rescue and relief operations (Wang et al. 2009). Post-earthquake investigations by experts from the Ministry of Land and Resources of China revealed approximately 15,000 sites with rockfalls, debris avalanches and debris flows triggered by the earthquake (Yin et al. 2009).

For the purposes of this research, the Wenchuan County was selected as the site where the procedure developed was tested. The extent of the study area was defined as the full extent of one Ikonos scene (Figure 3-2). The Min River, a tributary of the Yangtze River, flows through this region. The elevation ranges between 1273m and 3617m and a high relative relief is characteristic of the area. The area is also has an active fault running through it. The Wenchuan-Maoxian fault system however, did not rupture during the May 2008 earthquake event. Despite this, numerous landslides were triggered. According to Yin *et al.* (2009), 473 landslides were identified in the area: 342 new landslides and 131 pre-existing landslides. This study does not make a distinction between pre-existing and new landslides.

The Wenchuan County offers a significant challenge for automatic detection using the object-oriented approach especially because many slides in the area have complex forms with multiple individual source areas often merging to form one or more bodies, as can be seen in Figure 3-2. The automatic identification and classification procedure was developed for a small subset in the South-western corner of the Ikonos image and then tested with the remainder of the image.

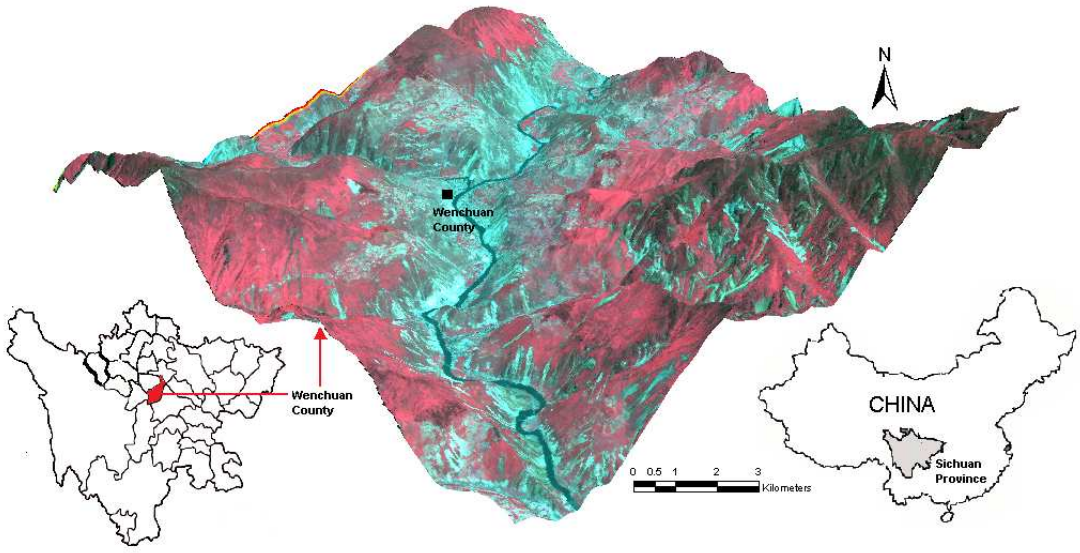

Figure 3-2 Location map of the case study area (Ikonos scene, 3D perspective)

Ongoing PhD research by Tolga Gorum (ESA Department, ITC) has produced a detailed landslide inventory for an area of approximately 120 km² in the Wenchuan County. This inventory was compiled through visual interpretation of satellite imagery combined with a detailed field campaign. The part coinciding with the extent of the Ikonos scene will be used to validate the results of the automated object-oriented procedure developed in this research.

3.1.1. Landslide Characterization

"Rock falls, disrupted rock slides, and disrupted slides of earth and debris are the most abundant types of earthquake-induced landslides, whereas earth flows, debris flows, and avalanches of rock, earth, or debris typically transport material the farthest. Because of their abundance or long distances of transport, these landslides generally have the greatest effects on the landscape during and after earthquakes"

-(Keefer 1999)

The three types of landslide discussed are done so in light of their prevalence in the study area, frequency of occurrence in earthquake situations and overall significance to landslide risk management. Using descriptions from *The Landslide Handbook* (Highland and Bobrowsky 2008), a brief statement of the failure mechanism involved in the movement along with a field photograph (*courtesy Tolga Gorum, PhD. Student*) is given below.

A. Rockfall: Material is detached from a steep slope and free falls, bounces or rolls downslope, dislodging and gathering additional material. As seen in the photo, material size can vary from large blocks to small rocks and cobbles. Material finally comes to a rest when the slope flattens, sometimes forming a triangular talus or scree deposit (depending on the amount of material involved). If the mass blocks an active channel, a landslide dam is created.

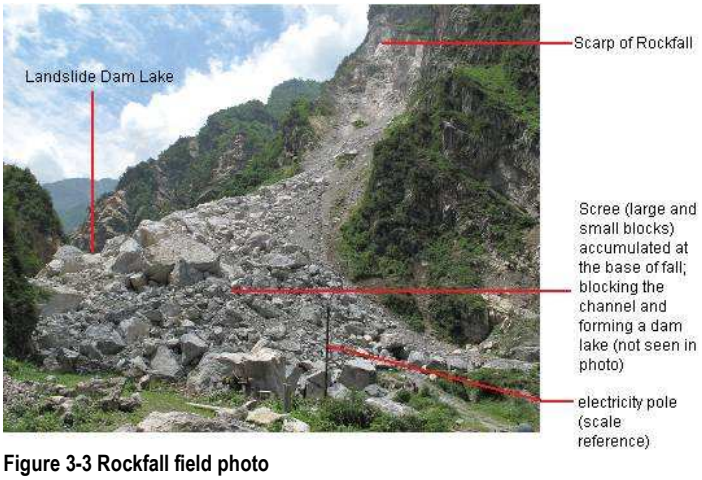

Figure 3-3 Rockfall field photo

B. Debris Slide: ranges from slide to flow based on the water content (*slide* being dry and *flow* being water saturated). It is a spatially continuous, relatively shallow, rapid mass movement of dry, unconsolidated rock and soil material. Scouring of additional material can also occur along its path. These movements (≥ 35 miles or 56 km per hour) are characterised with a long and narrow run-out,

Figure 3-4 Debris Slide field photo

which in this study area is concentrated along first and second order drainage lines. Debris accumulates at the base of the slope forming a triangular, cone-like structure called a *debris fan*.

C. Debris Avalanche: Fragmented debris is transported downslope in a large, very rapid, open-slope (unconfined) movement. These large, fast moving (100m per second) masses can transport massive blocks several kilometres from the source.

Figure 3-5 Debris avalanche field photo

Quite often, slope movements may involve a combination of one or more of the basic types of mass movements. This can occur as one large mass movement with different failure types occurring in various parts of the mass or as one movement with different but consecutive stages of development. For example, in this photo, it is believed that the upper row of slides occurred first and their run-outs triggered the slides on the lower slope. This final type is herein referred to as a *landslide complex*. Due to its jumbled appearance, it poses a challenge for automatic detection of the individual movements comprising the entire mass.

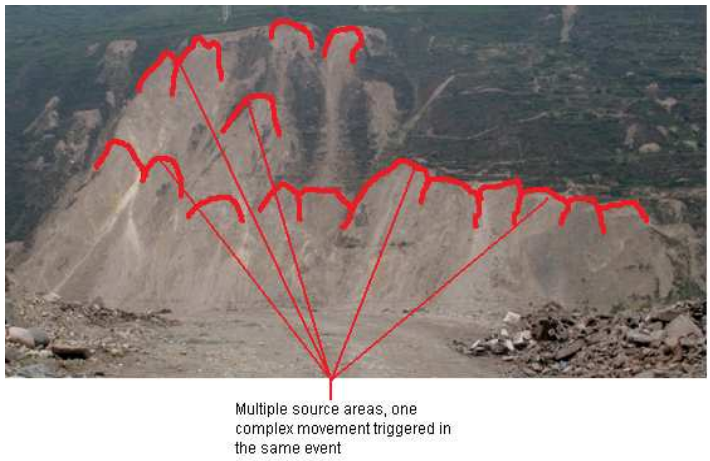

Figure 3-6 Landslide complex field photo

3.1.2. Landslide Diagnostic and Photographic Characteristics

It is important to know and understand the image characteristics used in the visual interpretation of landslides as these are just as important for guiding the sequence of automatic detection. These diagnostic and photographic characteristics have been discussed in detail by various authors (Rib and Liang 1978; Dikau and European Commission. 1996; Soeters and van Westen 1996; Highland and Bobrowsky 2008) and are mostly a synthesis of qualitative expert knowledge. Table 3-1 outlines these characteristics as per the major landslide types found in the study area.

Table 3-1 Landslide diagnostic and photographic characteristics by anatomy *(adapted from (Rib and Liang 1978; Dikau and European Commission. 1996; Soeters and van Westen 1996))*

LANDSLIDE ANATOMY	FEATURES			
	DIAGNOSTIC	PHOTOGRAPHIC		
		MORPHOLOGICAL	VEGETATION	DRAINAGE
ROCKFALL				
Main Scarp	Almost vertical, irregular, bare and fresh Has joint or faulting shears in rock Has spalling on surface if debris or soil	Jointed rock wall, > 50 degrees	Bare	
Body	Irregular surface of jumbled rock sloping away from scarp Wedge shaped hollows are typical		Linear scars in vegetation present along fall path	
	Irregular debris/ talus/ scree slope May have rounded outline Broad curved transverse ridge if slide is large Debris in valley floors, valley dams	Scree slopes 20-30 degrees	Low density on active scree slopes	
DEBRIS SLIDES/FLOWS (depending on water content)				
Main Scarp	Serrated or V-shaped/ funnel shaped upper part Large amounts of concavities or one major scar	Moderate to steep slopes	Bare	
Body	Long and narrow Commonly striated Exhibits vague flow structures	Very high D/L ratio	Bare	Flow lines follow drainage patterns
	Spreads laterally in lobes If dry, may have a very steep front about 1 meter high Depositional levees or flat desolate plains possible	Gentle slopes Steep front, if dry	Bare	Original streams blocked or deflected
DEBRIS AVALANCHE				
Main Scarp	Relatively small shallow niches on steep slopes	Steep slopes >35°	Bare or some 2° vegetation	
Body	Clear linear path, often absent after a few days as it can be quickly eroded by streams	Moderate D/L ratio	Bare or some 2° vegetation	Shallow linear gully can originate here
		Gentle slopes, if present	Bare	Original streams generally wash away material

The above information is translated into quantitative criteria in Definiens (shape, texture and contextual features) and used along with spectral characteristics to automatically detect landslides.

3.2. Data used & Processing

Two basic data sets, elevation and satellite imagery, were used to derive a number of products to be applied in an OOA-based procedure to identify landslides. Table 3-2 shows the overview of the data used in this study.

Table 3-2 Data used in analysis

LAYER	RESOLUTION	USE/PRODUCT
IKONOS	4m Multispectral	Spectral Analysis
	1m panchromatic	Textural Analysis
Topographic Contour	20m interval	DEM- 10m & 40m
Landslide Inventory- Visual Analysis		Accuracy Assessment
Point Location of Scarps- Visual Analysis	*Source: Aster*	Accuracy Assessment

3.2.1. DEM Generation & Derivative calculation

Topographic contours with a 20 meter interval were used to interpolate a continuous elevation dataset for the study area. Interpolation was done using the "Topo to Raster" tool found in the 3D Analyst toolbox in ArcGIS. Industry standards suggest that the best possible resolution for a contour interpolated DEM is 2 to 3 times the contour interval. To ensure that the resulting DEM was hydrologically correct, the "Drainage Enforcement" option was set to 'Enforce', thereby allowing the algorithm to eliminate all sink (spurious and real) that it encountered. The resulting DEM was very coarse (40m res.). To ease computation in Definiens a 10m res. DEM was created from the same contour data, smaller cell size but same coarse elevation data.

Table 3-3 shows the derivatives applied in this study. Most were created using automatic functions in ArcGIS then incorporated as layers in the Definiens software environment for subsequent analysis.

Table 3-3 DEM derivatives and their relevance to landslide identification and classification as per Martha et al.

TERRAIN ATTRIBUTE	DESCRIPTION	SIGNIFICANCE TO LANDSLIDE/ FALSE POSITIVE ELIMINATION
Altitude	Height above mean sea level or local reference	Climate, vegetation, potential energy determination, material volumes, vegetation and soil patterns
Slope	Gradient; computes the maximum rate of change in z-value from each cell to its neighbours.	Source areas on moderate to steep slopes
Hillshade	This function determines illumination values for each cell	Useful for eliminating shadows from analysis *(In ArcGIS, option to model shadows by applying sun elevation angle and azimuth at the time of image acquisition to the DEM)*
Relief	Maximum elevation change within an area	Landslides generally have a high internal relief
Plan Curvature	Curvature of the surface perpendicular to the slope direction	Influences convergence and divergence of flow.
Profile Curvature	Curvature of the surface in the direction of slop	Affects the acceleration and decelereation of flow thus influencing erosion and deposition. Useful for identifying the break in slope at which transportation ends and deposition begins
D-Inf Flow Direction	Direction of steepest descent from each cell	Features such as roads and terraces that run perpendicular to the flow direction can be eliminated from analysis
Ridge lines		Contextual analysis- closeness of an object to the ridge line identifies it as a scarp area.
Drainage lines Order		1st and 2nd order seasonal channels transport medium for debris flows/avalanches

3.2.2. Satellite Data

Availability of high resolution data such as Ikonos, has enabled the development of faster and more sophisticated landslide analysis techniques. Gao (Gao 2009) gives an overview of the satellite and its specifications. For this study, one cloud-free scene acquired on 23 May 2008 was used (all pre-processing was completed by PhD student Tolga Gorum prior to the start of this research).

Table 3-4 Ikonos spectral specifications

BAND	WAVELENGTH REGION (μm)	RESOLUTION (M)
1 (blue)	0.45-0.52	4
2 (green)	0.52-0.60	4
3 (red)	0.63-0.69	4
4 (near-IR)	0.76-0.90	4
PAN	0.45-0.90	1

Spectral characterization of landslides was done using the multispectral data and the red band was used to calculate landslide textural indices.

3.3. Methodology

As the aim of this research is to develop a working understanding of object-based texture the methodology that was developed is based on a comprehensive analysis of the concepts involved. In the Literature review the view of different authors that landslides have a distinct surface expression that can be identified with texture was given. However, even before this can be tested considerations of the data and the objectives of the analysis need to be understood. Thus, this research endeavours to provide a guide to choosing from the myriad of texture measures available to the user. The concepts outlined here can be applied to the identification of fresh landslides using texture in any object-oriented based program.

The methodology applied in this research is two-fold:

Phase 1. Evaluation of object-based texture analysis
Phase 2. Application of texture and DEM derivatives for landslide identification and anatomical classification

3.3.1. Phase 1

The idea here is to develop a working understanding of how GLCM texture is calculated within an object, what variables affect this calculation and how best they can be adjusted to fit the user's purpose, in this case for landslide identification. Figure 3-7 is a conceptual diagram of the approach to the understanding of object-based texture analysis. It shows that there first needs to be an analysis of the calculations, then address the parameters (what to choose and when), and finally determine which measure or measures best describe the feature of interest.

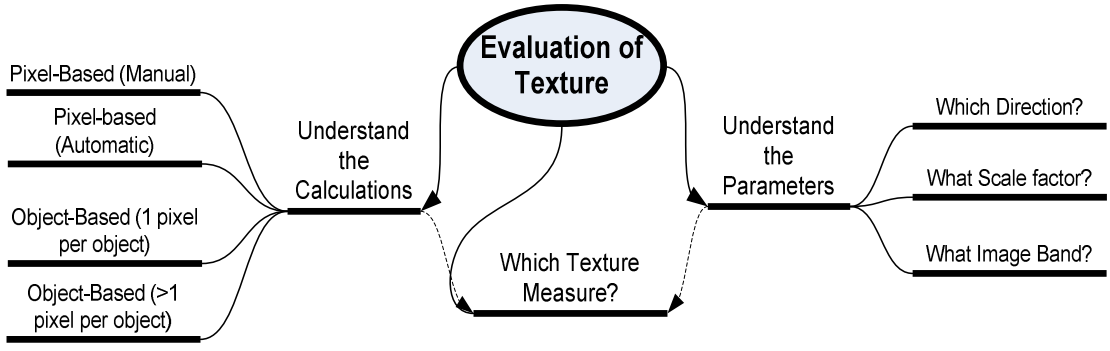

Figure 3-7 Conceptual design of Texture Evaluation process

Process then is to:

- compare actual values of pixel vs. object-based texture calculation (math)
- try to determine how a single texture value is arrived at for each object
- address the factors affecting texture calculation (band, scale factor, directionality)

- determine which texture measure is most useful for landslide mapping and explain what it highlights

For each of these then an experimental design was developed and applied, these results can be seen in the next chapter.

Experimental designs:

Test I. Do the calculations of the GLCM in pixel-based and object-based environments give the same result? Intention is to determine if the resulting texture values would be the same as those of a pixel based texture calculation when an image is segmented to the pixel level (i.e. each pixel is one object).

To compare these calculations a test image was placed in each program (Envi 4.7 for pixel-based and Definiens 7 for object-based) and the texture measures computed then compared. The pixel-based calculation was computed in ENVI 4.7, where according to documentation, the Haralick equations are applied straight. Therefore, a GLC Matrix is computed for the entire image with each pixel receiving a value based on the specific texture algorithm (see Texture Tutorial by Hall-Beyer http://www.fp.ucalgary.ca/mhallbey/tutorial.htm for more details)

In Definiens, for each object the actual Haralick feature is calculated using the GLC Matrix and algorithm of the particular feature. For example, the GLCM contrast feature is calculated using formula:

Pixel-based GLCM calculated in ENVI 4.7	Object-based GLCM calculated in Definiens
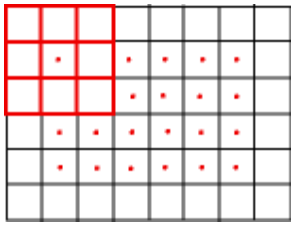	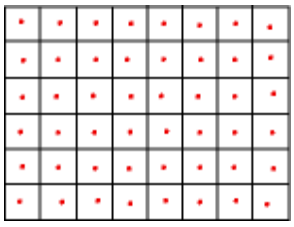
GLCM Contrast calculated using a 3x3 window (red grid) in the direction (1, 1) or 45°. Value obtained for each pixel with a red dot.	Chessboard segmentation to pixel level (each pixel is an object) and GLCM Contrast calculated for each. Value obtained for each object (red dots).

Figure 3-8 Experimental design for comparison of pixel vs. object-based absolute values

Test II. Definiens creates a GLCM for each object by evaluating the pixel pairs making up an object. How is the final single object texture value computed? The intention here is to determine to what extent the two methods are comparable. For example, if the object-based results are an average of the pixel-based textures, what implications will this have as it regards textural 'smoothing' of the image.

Pixel-based GLCM calculated in ENVI 4.7	Object-based GLCM calculated in Definiens
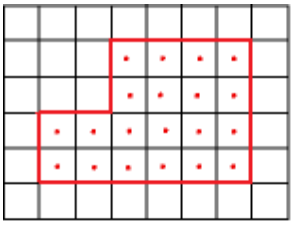	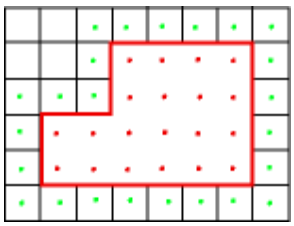
Red dots represent texture values per pixel. If these are summed or averaged will the result be the same as the single object texture value?	Object comprised of multiple pixels. GLCM computed using these pixels and that of the immediate neighbours (green dots) so as to reduce border effects (see Section 2.2.1).

Figure 3-9 Experimental design for determining how a single texture value is computed for each object

The results of these tests can be seen in Section 4.1.

Choosing the parameters

In order to compute texture measures in Definiens, certain parameters need to be chosen by the user; they include scale factor, image band, directionality and the texture measure/s.

Scale factor

Laliberte and Rango (2008) addressed the issue of correlation of object-based texture measures at different scale factors (see Section 2.2.2); therefore in this research, scale factor was examined in terms of its effect on depicting landslide boundaries. This was done by applying segmentations at varying scales and visually examining the result. Additionally, the effect of scale factor on the results of texture computations was also tested. At each segmentation scale sampled, texture measures were calculated and their value ranges were recorded. The idea here was to determine at which scale factor the most significant change occurred.

Image band and texture measure

From the Literature review it was learnt that there are contrasting views on which image band or bands should be used for textural analysis. Thus, to text image band applicability a matrix of the available bands and the eight texture measures was created and visually assessed. This matrix was also used to determine which texture measures appeared most suitable to identifying landslide features. As a way of producing a quantified assessment the feature optimization tool available in Definiens (see Reference Book (2007)) was applied to the various bands and texture measures. Feature optimization identifies the combination of factors (texture measure and Image band) which offers the best class separability, in this case between landslides and its false positives (bare ground, built-up areas and roads).

Directionality

To determine the best direction to use when applying the texture features, a visual assessment of a texture measure applied to representative landslides aligned in the four directions was done. The directionality was assessed in terms of its applicability for recognition of landslide boundaries and maintenance of internal homogeneity in landslide features.

The results of these parameter choice tests can be found in Section 4.2.

3.3.2. Phase 2

The methodology applied in this second phase was developed to test the guide established in Phase 1. Two simple rulesets were created. The first to test the capability of using *only* texture to identify landslides and a second to test how texture can be applied implicitly and in so doing address over-segmentation of landslides with texture-based boundary detection and reconstitution (Figure 2-5).

Explicit identification of landslides

Figure 3-10 is a synopsis of the methodology applied for landslide identification using only texture.

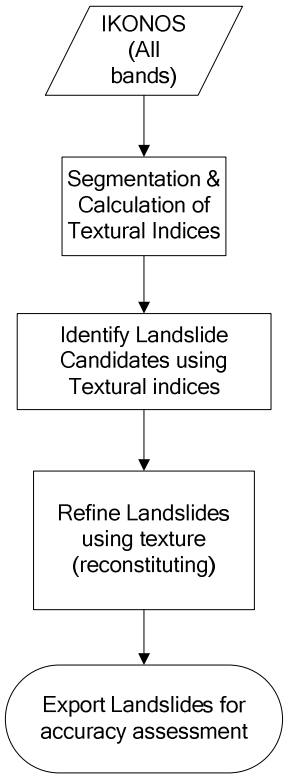

Figure 3-10 Schematic flow-chart of concept for landslide identification using texture only

Step 1: Segmentation
Multi-Resolution Segmentation was done using the Red and NIR Ikonos bands. Table 3-5 shows the segmentation parameters used in the initial segmentation. At this initial stage, the emphasis was on producing compact objects with specific spectral characteristics in order to apply the texture measures.

Table 3-5 Segmentation Parameters

Scale	Shape	Colour	Smoothness	Compactness
50	0.1	0.9	0.1	0.9

Step 2: Determine diagnostic texture indices
GLCM (quick 8/11) temporary feature layers of mean and contrast were calculated for the objects created above. Diagnostic threshold values were determined from the texture measures by manipulating the feature view controls.

Step 3: Classification
A rough classification of landslide candidates was achieved using a GLCM *entropy* threshold. Those objects falling below the threshold were classified as background. This initial classification was then refined by re-segmenting the landslide candidates *only*, to a finer scale (*sf* 50) and applying a GLCM *mean* threshold.

Reconstitution of over-segmented slides: To extract single landslides (Type A), a spectral difference segmentation (*see p. 23 Reference Book* (Definiens 2007)) in which neighbouring objects are merged if the difference between their layer values is below the maximum spectral difference (threshold chosen by user). The layer used was the GLCM Mean temporary feature layer which had to be exported and then imported into the project as a layer for analysis. Landslide candidate objects that were merged into single objects in this way were then assigned to the Type A class based on their boundary relationship to the background class i.e. Type A= '*Landslide candidates' with Relative border to 'Background' = 1*.

At this point, further refinement of the landslide candidate classification was no longer possible with only texture. As such, the remaining classified objects were exported as 'Landslide Candidates' along with the 'Type A' slides for accuracy assessment.

Implicit identification of landslides

Figure 3-11 is a synopsis of the methodology applied for landslide identification using combined textural, spectral and morphological indices.

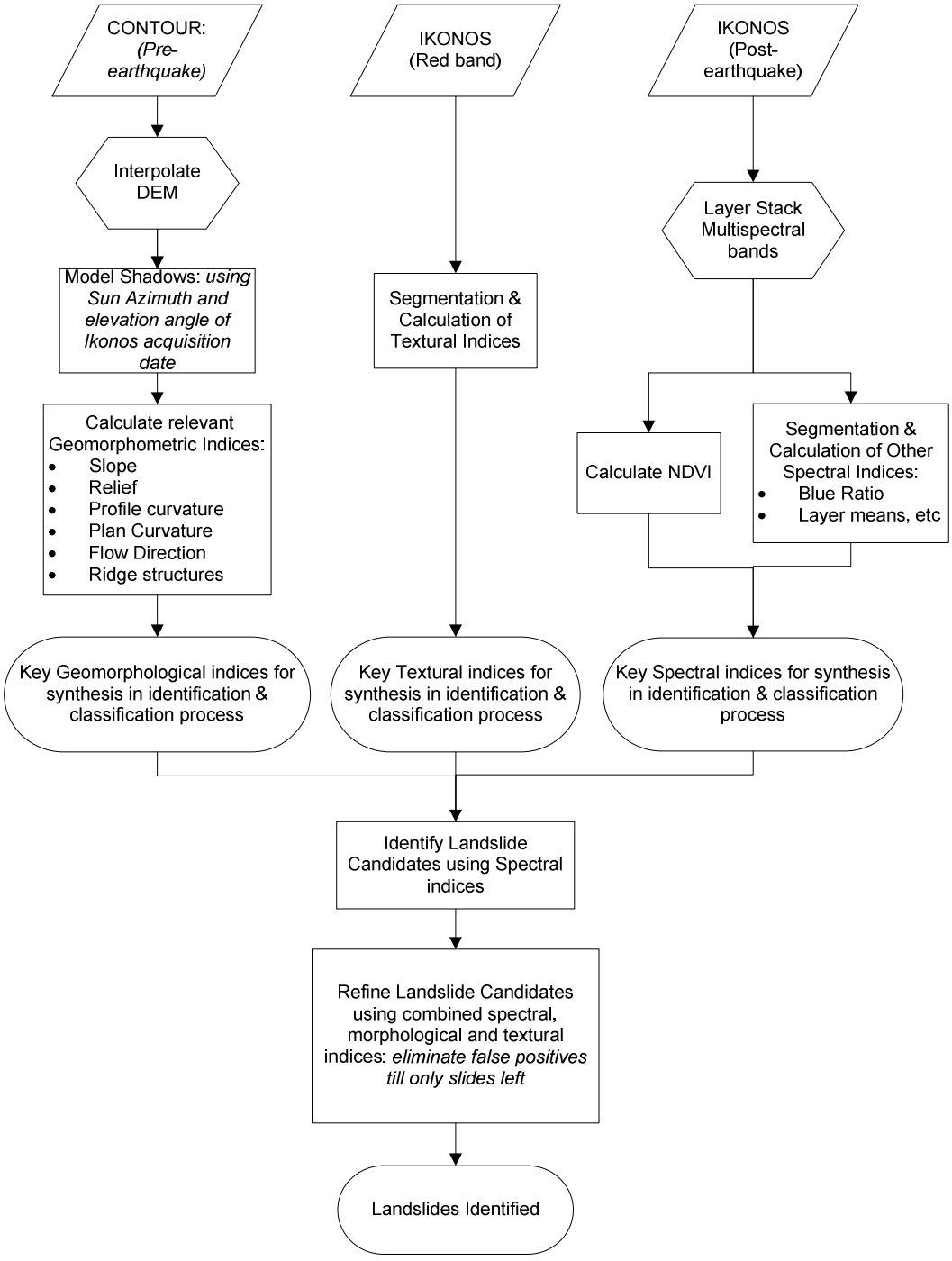

Figure 3-11 Schematic flow-chart of concept for landslide identification using texture, morphological and spectral indices

There are three main processes that were applied before the final analysis procedure for the detection and anatomical classification of landslides is done. First, the DTM was generated and from it all relevant morphometric indices were derived. This was mostly done using ArcGIS. Next, using the Definiens software, segmentation and extraction of i) textural indices from the red band and ii) spectral indices from the multispectral bands, was done.

The procedure applied the same basic steps described for explicit identification above: segmentation, derivation of indices, classification using derived indices. The difference is that the indices used are spectral, morphological and textural (see Figure 3-11). For refinement of landslides (reconstitution of over-segmented slides) the procedure outlined below can be used.

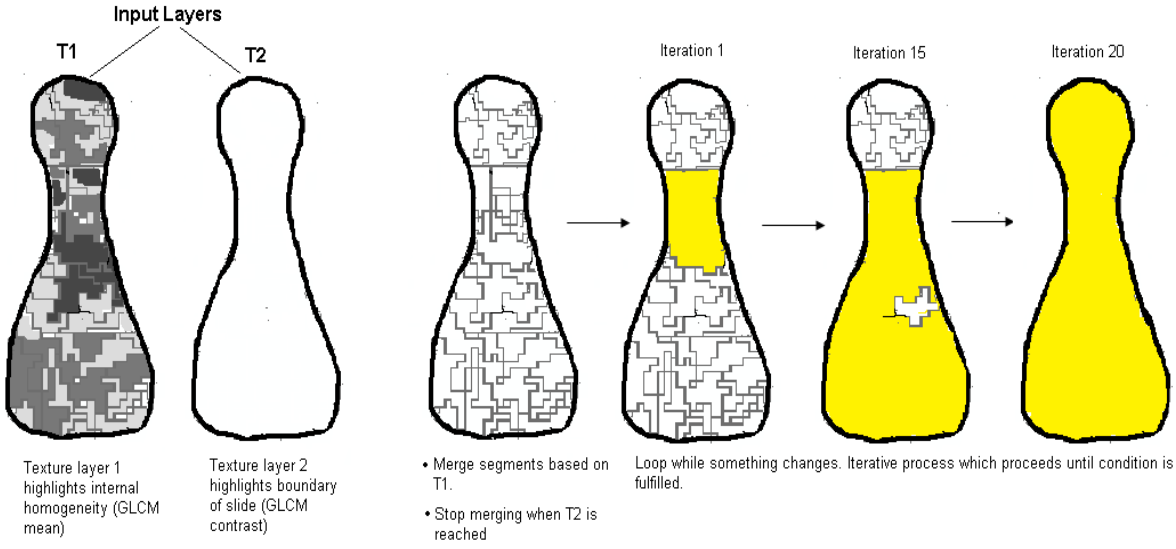

Figure 3-12 Procedure for reconstitution of over-segmented landslides

3.4. Definition of Identification Results

In order to comprehensively assess the results of identification, we look at the landslides in terms of the three main forms prevalent in the study area (Figure 3-13):

Type A These are single landslides in which there is *one source area* leading to *one or more transport and depositional areas*.

Type B These are landslides having *multiple source areas* the debris from which is channelled into a *single transport and depositional area*.

Type C These are landslides with *multiple scarp, transport and depositional areas* which all *overlap*.

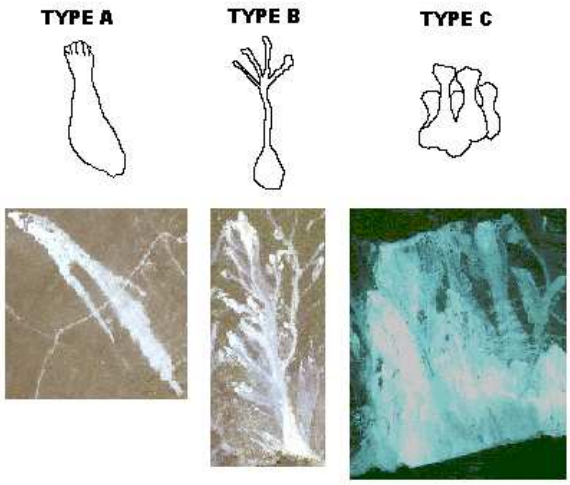

Figure 3-13 Landslide identification output types with imagery examples

Areas of interest (AOIs) with representatives of each of the forms were chosen for validation of the identification and classification results.

3.5. Accuracy Assessment using ROC and Visual Comparison

The results of both automatic procedures in Phase 2 were assessed by visual comparison with a reference dataset of landslides delineated by manual image interpretation (courtesy Tolga Gorum, PhD. Student).

Quantitative assessment was done using ROC (receiver-operating characteristic) plots/curves. This curve plots the *true positive rate* (= TP / (TP-FN)) against the *false positive rate* (= FP / (FP-TN)) as coordinate pairs in a graph. In the graph, the term *Sensitivity* refers to the *true positive rate* and *1-Specificity* represents the *false positive rate*. ROC defines the accuracy of a model (or in this case, OOA procedure) result obtained in relation to the entire range of possible threshold values (Beguería 2006). The AUC (area under curve) describes the ability of the procedure to correctly 'predict' the occurrence or non-occurrence of pre-defined states (in this case, landslide or non-landslide). Significant values range from 0.5 to 1.0. A result of 0.5 indicates that the procedure did not predict the occurrence of a landslide any better than a random approach whilst an AUC of 1.0 shows that the prediction was ideal (Yesilnacar and Topal 2005).

4. Results for Landslide Identification using Texture

4.1. Phase I- Evaluation of Object-based Texture Analysis

Test I. The aim here was to understand the basics of the OOA texture calculations. Are they similar to that of the pixel based calculations? Figure 4-1 shows the test image used as input for this first evaluation. The object of interest here is the landslide but there are also false positives present (road and a bit of bare ground around the slide).

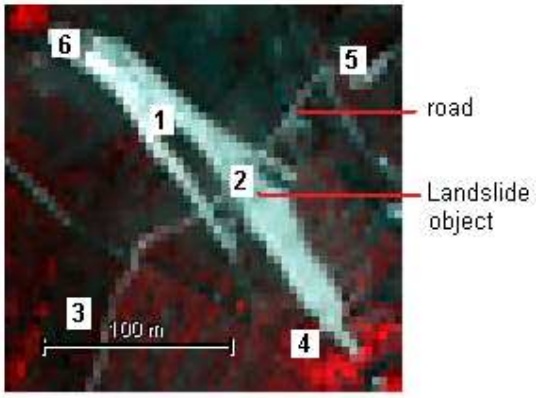

Figure 4-1 Original Image used for texture test input

The texture measures were applied to this image using the parameters specified in Table 4-1 and the absolute values for sample areas (1-6, Figure 4-1) were tabulated for comparison (see Table 4-2).

Table 4-1 Paramaters used for calculating texture measures in pixel and object-based environments

PARAMETER	PIXEL-BASED	OBJECT-BASED
Band	Red	Red
Window size/ Scale factor	3x3	Chessboard pixel level
Direction	45°	45°

Calculations of the measures were done according to the formulas previously outlined in Section 2.2.1. Consider that the only difference between the two methods is that in pixel-based a GLCM is constructed for the entire image whilst for the object-based a GLCM is constructed for each object (in this case each pixel).

Result:

Table 4-2 Pixel- vs. Object-based comparison of absolute texture values

GLCM Measure	Image Result		Calculation Result		
	Pixel-Based	Object-Based	Sample #	Pixel	Object
Contrast	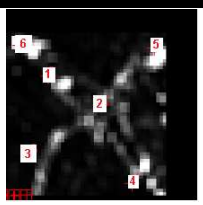		1	32	2242.67
			2	8.55	42.5
			3	3.22	2.66
			4	3.22	0
			5	12.44	13
			6	812.11	2500
Dissimilarity	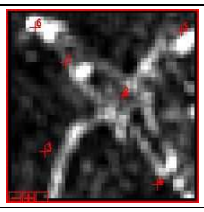	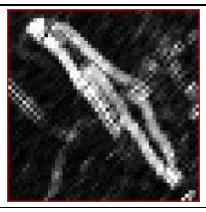	1	4.22	38.67
			2	2.55	6.5
			3	1.66	1.33
			4	1.44	0
			5	2.66	3
			6	22.77	40
Homogeneity	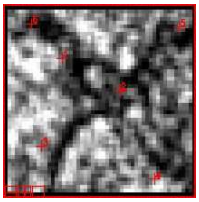	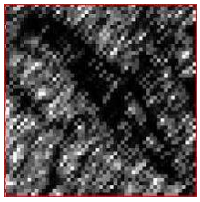	1	0.34	0.33
			2	0.25	0.02
			3	0.32	0.46
			4	0.43	1
			5	0.35	0.27
			6	0.05	0.05
Entropy	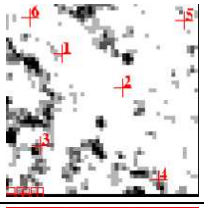	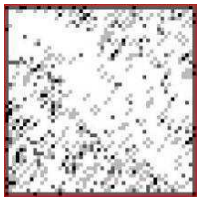	1	2.19	1.09
			2	2.19	1.38
			3	1.83	1.09
			4	1.83	0
			5	2.19	1.38
			6	2.19	1.38
Angular 2nd Moment (ASM)	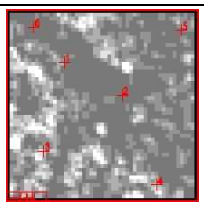	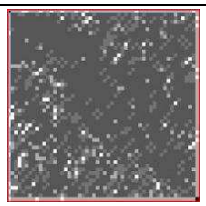	1	0.11	0.33
			2	0.11	0.25
			3	0.18	0.33
			4	0.18	1
			5	0.11	0.25
			6	0.11	0.25
Mean	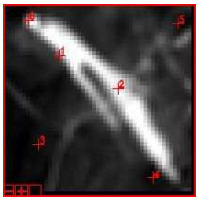	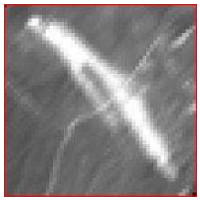	1	22.55	67.33
			2	41.33	91.25
			3	4.44	36.67
			4	4.44	38
			5	4.7	36.5
			6	26.88	96
Variance	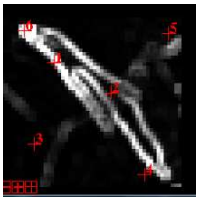		1	218.24	27.34
			2	15.33	4.6
			3	0.46	0.94
			4	1.58	0
			5	5.06	2.06
			6	493.43	29.15

GLCM Measure	Image Result		Calculation Result		
	Pixel-Based	Object-Based	Sample #	Pixel	Object
Correlation	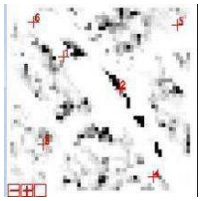	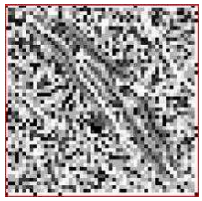	1	-0.06	0.7
			2	-48.47	0.05
			3	-17.13	0.7
			4	-16.07	0
			5	-5.32	0.72
			6	-0.06	0.68

Table 4-2 shows that when an image is segmented into objects at the pixel level (i.e. each object is one pixel), the absolute texture value is not the same as that computed in the pixel-based environment (*see Table 4-2: Calculation Result*). The figures do not appear to be comparable at all as neither the pixel-based or the object-based values are consistently higher or lower than the other. For all measures except GLCM correlation, the emergent patterns are quite similar (*see Table 4-2: Image Result*). Thus, whilst absolute values do differ, both methods essentially display similar 'patterns'.

Test II. The objective of this test was to deduce how the final value of the object-based texture measure is calculated and thereby determine to what extent the two methods (pixel and object-based) for GLCM texture calculations are comparable. In Test 1 (above), it was learnt that even when the objects created contain only one pixel, the resulting texture value still did not match the pixel-based texture value.

Multi-resolution segmentation on the red image band at sf 30 was done to produce objects on which the texture measures were calculated. For the sample object (shown below), the texture value was recorded and for its corresponding pixels, texture values calculated in ENVI were also recorded.

Result:

Selected object with one texture value

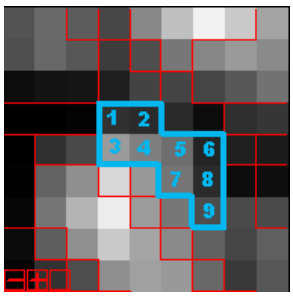

Corresponding pixels with texture values 1-9

Table 4-3 shows the values coming out of this test. Once again the results are not conclusive as no real comparison can be drawn from the limited information given as it regards the calculations in both programs (ENVI and Definiens).

Table 4-3 Texture values pixel vs. object

GLCM Texture	ENVI Pixel texture values											Object Value
	1	2	3	4	5	6	7	8	9	Sum	Average	
Contrast	16.22	27.11	8.55	18.77	18.44	21.44	6.55	9.55	6.55	**133.18**	**14.8**	**842.41**
Dissimilarity	3.55	4.44	2.11	3	3.11	3.88	2.11	2.88	2.33	**27.41**	**3.05**	**23.24**
Homogeneity	0.17	0.15	0.43	0.36	0.32	0.13	0.33	0.15	0.23	**2.27**	**0.25**	**0.12**
Entropy	2.19	2.19	2.19	2.19	2.19	2.19	2.19	2.19	2.19	**19.71**	**2.19**	**3.4**
Angular 2nd Moment	0.11	0.11	0.11	0.11	0.11	0.11	0.11	0.11	0.11	**0.99**	**0.11**	**0.03**
Mean	44.88	43.99	37.78	44	44.44	39.67	44.11	45.55	43.55	**387.97**	**43.11**	**88.44**
Variance	62.32	58.44	202.83	75.11	40.91	110.44	74.76	22.91	75.35	**723.07**	**80.34**	**16.95**
Correlation	-2.97	-5.75	-0.24	-2.43	-15.21	-1.17	-2.4	-41.39	-3.11	**-74.67**	**-8.30**	**0.68**

The final value computed for the object is not equivalent to the sum or average of the corresponding pixels in a pixel-based texture layer for all the texture measures. The values in the table show then that no direct relation can be made between the two methods. Therefore, based on the information given in the Definiens 7 Reference Book, how the final object value is computed still remains unclear.

4.2. Choosing the parameters

This section looks at the logical processes used to determine the most relevant parameters for carrying out object-based texture analysis for landslide detection.

4.2.1. Scale Factor

Landslides of varying sizes occur in the study area therefore the scale factor (*sf*) chosen must adequately represent both small and large slides. Additionally, the delineation of strong versus weak boundaries needed to be considered. To determine an appropriate *sf*, a small test was conducted on a subset of the study area where the above conditions were represented. Scale factors (*sf*) ranging from 10 to 100 in increments of 10 were evaluated visually.

Results (see Figure 4-2 below):

At scales coarser than 50, both large and small landslides with strong boundaries were clearly delineated. However, slides with weak boundaries were being merged into surrounding non-landslide or other landslide objects. At scales smaller than 30, there was gross over-segmentation- too many objects and objects too small- which, in later textural analysis can lead to insignificant values and

decreased computational efficiency (*see Section 2.2.2*). At these smaller scales, the over-segmentation is also unnecessary and the feature of interest can already be delineated at larger scales.

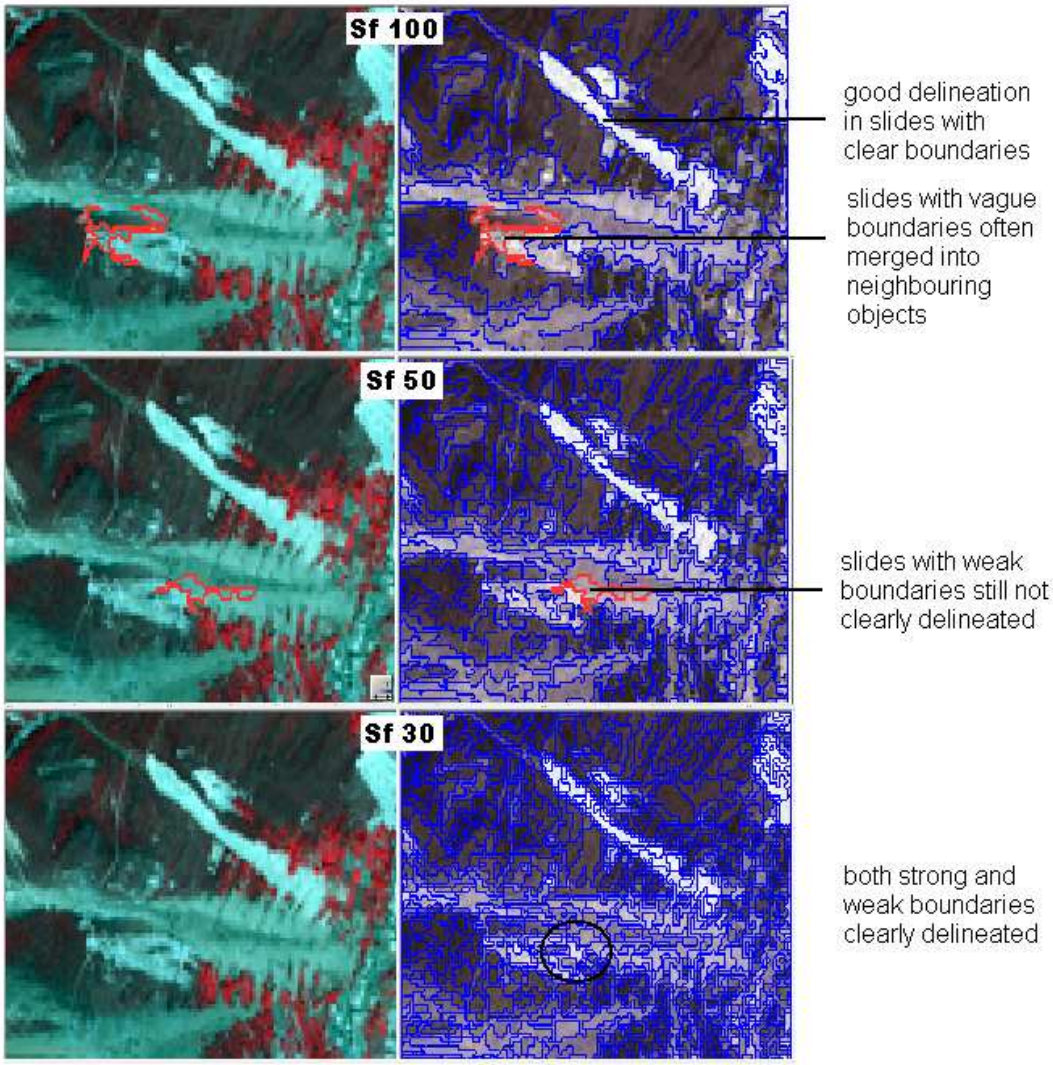

Figure 4-2 Visual analysis of scale factor parameter

This visual consideration was focussed more on finding the most applicable *sf* for delineating clearly the landslide features and the result was within the range of 30 – 50.

As was mentioned in the methodology, some assessment of the effect of scale factor on the computed texture values was also attempted. The results of this assessment can be seen in Table 4-4. In each texture measure calculated, the most significant changes in value range occurred between *sf* 50 and 25 (see values with red oval). In some instances, the value range decreased steadily between 100 and 75 with a dramatic shift to higher values occurring by *sf* 50 which is followed by another increase at *sf* 25. This was observed for Contrast, Dissimilarity and Variance/Std. Dev. The reverse occurs for ASM, with value ranges shifting to lower values but with the same trends described above.

Table 4-4 shows the changes in the range of the different texture measure as scale factor decreases

TEXTURE FEATURE	SCALE FACTOR	VALUE RANGE	
		LOWER BOUNDARY	UPPER BOUNDARY
Contrast	100	0.43	1030
	75	0.3	1028.02
	50	0.18	1052.31
	25	0.15	1317.7
Dissimilarity	100	0.36	20.36
	75	0.2	19.83
	50	0.18	20.74
	25	0.15	20.47
Homogeneity	100	0.47	0.83
	75	0.47	0.87
	50	0.47	0.9
	25	0.48	0.92
Entropy	100	1.3	5.9
	75	0.96	5.42
	50	0.66	4.87
	25	0.54	3.9
ASM	100	0.0077	0.38
	75	0.0085	0.55
	50	0.015	0.67
	25	0.03	0.72
Mean	100	24.54	194.5
	75	24.62	201.4
	50	22.85	201.4
	25	24.6	201.19
Variance/Std.Dev.	100	0.56	26.09
	75	0.39	26.09
	50	0.29	22.92
	25	0.26	23.77
Correlation	100	0.07	0.9
	75	0	0.87
	50	0.0019	0.85
	25	0	0.85

In other instances, the range shifted to lower values at *sf* 50 and then by *sf* 25 returned to the ranges seen at the larger *sf* (75 and 100). This was seen for Mean and Correlation. For Homogeneity, the values ranges fluctuated around similar values at each *sf* (blue ovals). These results suggest in general that some significant change occurs at and after *sf* 50 and as such this may be the optimal sf for calculating the texture measures.

4.2.2. Band and Texture Measure

Varying views exist in literature as to which band or bands to use for landslide texture analysis (see Section 2.2.2) therefore, to test which band or bands were most appropriate for textural analysis, a matrix of the variables was created and assessed visually to determine to what extent the feature of interest (landslides) could be extracted based on i) visibility of the boundary and ii) internal homogeneity. For comparison, a similar matrix was constructed for the pixel-based measures. Figure 4-1 shows the original image used in these tests.

Building on what was learnt from earlier results, a multi-resolution segmentation at *sf* 30 was used on a combination of all multispectral image bands and the direction applied was 45°. For the pixel-based, a 3x3 window was used, also in the 45° direction.

Results:

Figure 4-3 and Figure 4-4 show the resulting matrices for the object-based and pixel-based cases, respectively. The band and texture measures highlighted by a *red box* are the parameters chosen for good representation of *internal homogeneity* and the band and measures highlighted by a *green box* are a good representation of landslide *boundary*.

For the object-based, the texture measure most useful for identifying landslides in terms of *internal homogeneity* is GLCM Mean and the bands most appropriate for its calculation appear to be the green, red and combination of all bands. Both GLCM Contrast and Dissimilarity show clearly the landslide boundaries and they are best calculated using the green, red and all bands.

For the pixel-based, the texture measure most useful for identifying landslides in terms of *internal homogeneity* is GLCM Mean, this is similar to the findings in the object-based case. However, the band most appropriate for its calculation appears to be the panchromatic band and not any of the multispectral bands as seen in the object-based case. This can possibly be because the panchromatic band offers a higher spatial resolution and as such the GLCM Mean calculated appears clearer, but essentially the landslides are still highlighted by the measure in the multispectral bands. Unlike the results in the object-based case, landslide boundaries are best depicted using GLCM variance in the panchromatic, green or red bands (the same spatial resolution issues are apparent). The pixel based does not have an option for all bands.

Figures 4-5 to 4-7 (page 48) show the results of feature space optimization (FSO) assessments done in Definiens in order to determine which combination of image band and texture measure offered the best class separability between landslides and its false positives (bare ground, built-up areas and roads) considered in the test area.

In each of the cases, FSO selected GLCM Mean, Homogeneity and Correlation as the measures offering the best class separability. To distinguish between landslides and roads an additional measure, Standard deviation was also considered suitable. In all cases the red and NIR bands were selected for the texture computations. The green and blue bands were also selected by individual cases.

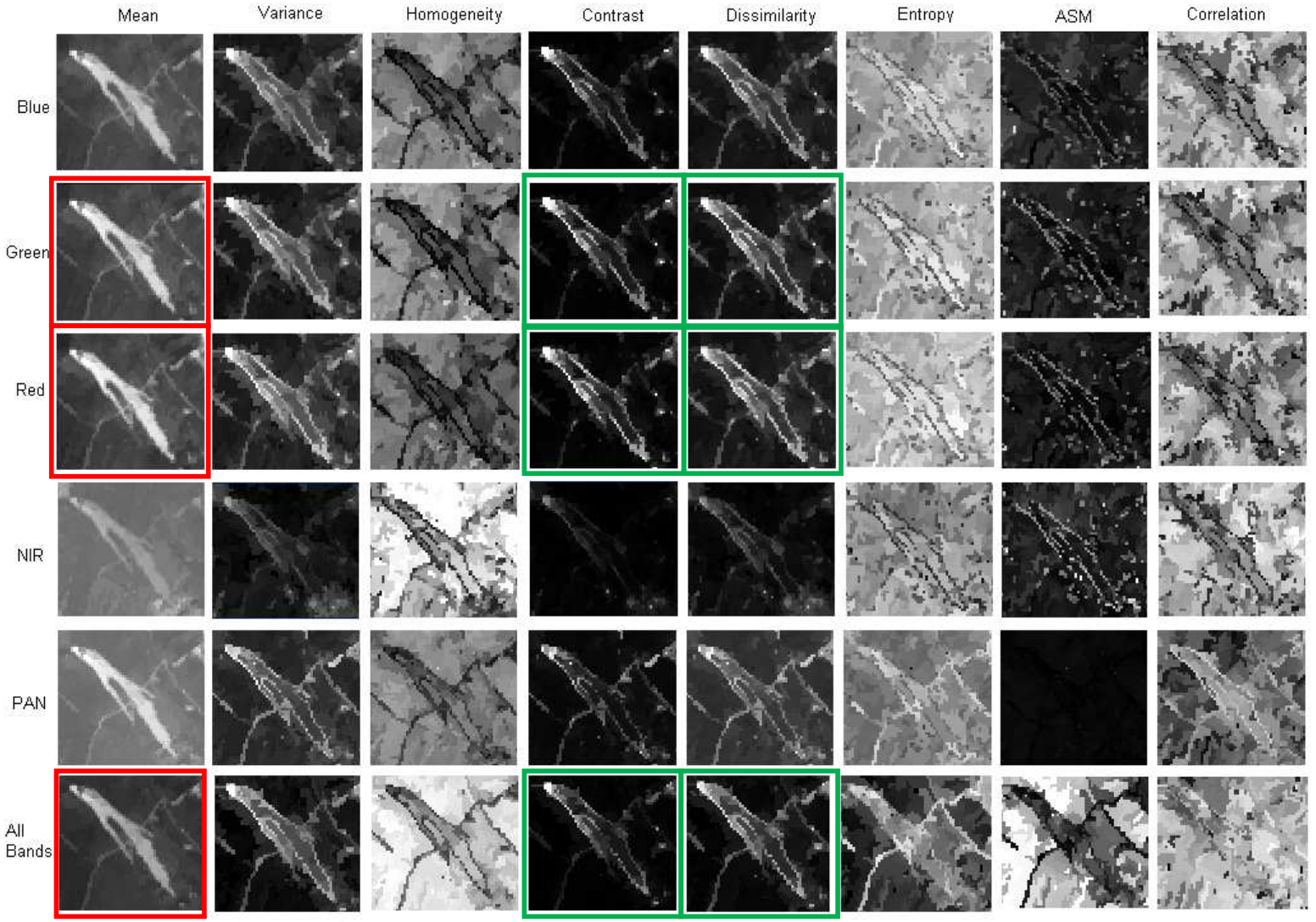

Figure 4-3 Object-Based Band and Texture measure matrix. Red boxes highlight landslides in terms of their internal homogeneity and green boxes in term of visibility of their boundary.

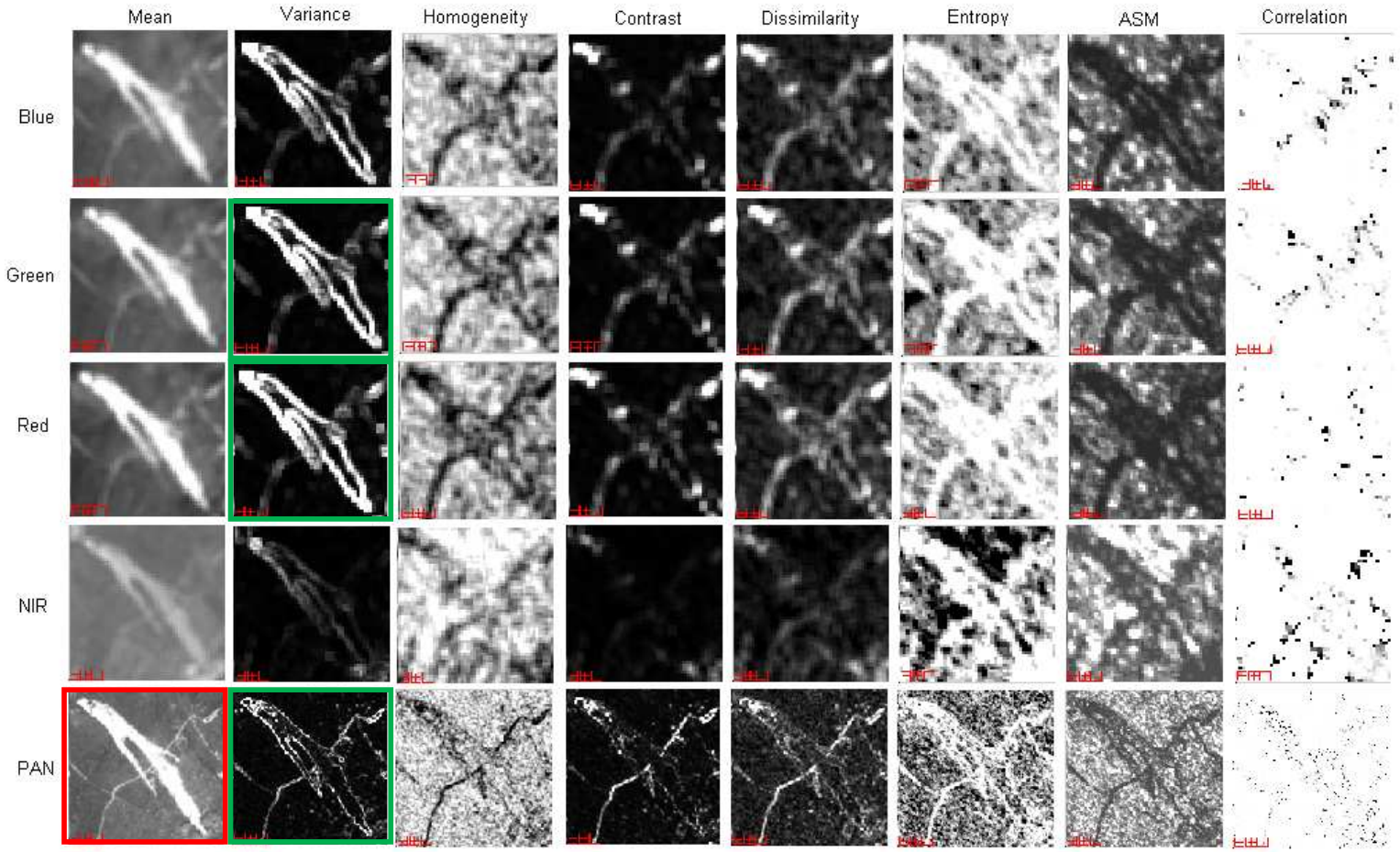

Figure 4-4 Pixel-based Band and Texture measure matrix. Red box highlights landslides in terms of their internal homogeneity and green boxes in terms of visibility of their boundary.

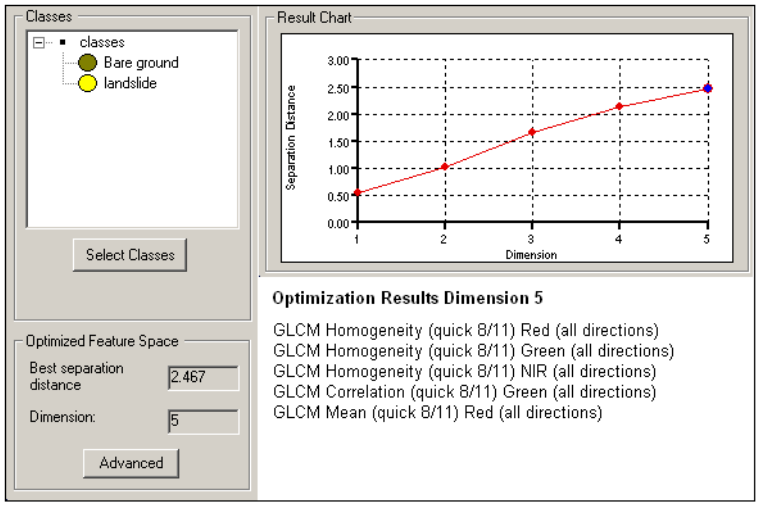

Figure 4-5 Feature Space Optimization- Texture measure and Image Band for distinguishing landslides from bare ground

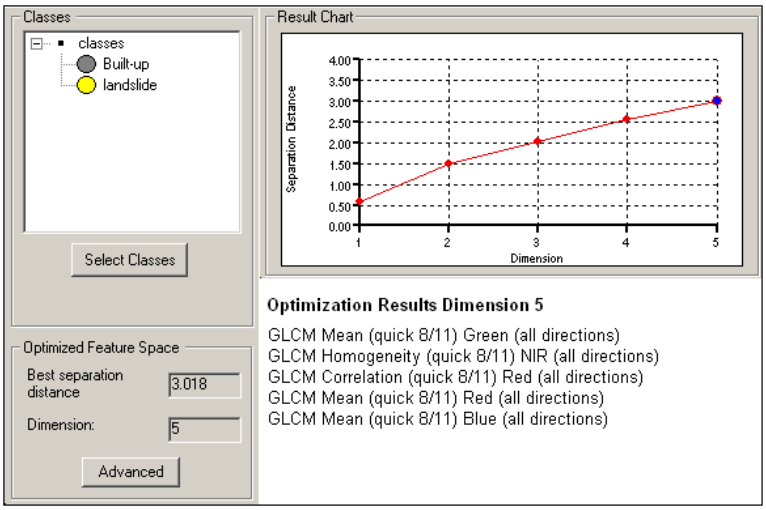

Figure 4-6 Feature Space Optimization- Texture measure and Image Band for distinguishing landslides from built-up areas

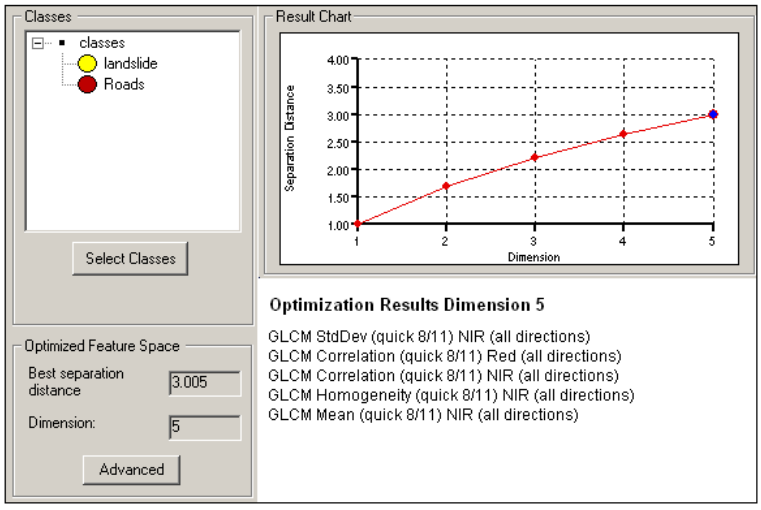

Figure 4-7 Feature Space Optimization- Texture measure and Image Band for distinguishing landslides from roads

The results of FSO assessment do not match that of the object-based visual matrix assessment entirely in terms of suitable bands. FSO selected the NIR band in all cases when from the visual assessment it is clear that landslide features appear blurred or fuzzy when texture measures were calculated on this band (see Figure 4-3). Also, in terms of the texture measure selected, the only one common to both assessments was GLCM mean. The other measures selected by the analysis, homogeneity, correlation and standard deviation/variance, do not reflect well either landslide boundaries or internal homogeneity as is seen in the visual assessment matrix (see Figure 4-3).

The low 'best separation distance' values obtained in the FSO analysis (2.4, 3.01 and 3.005) indicate the difficulty of distinguishing landslides from these classes based on texture alone.

The FSO results fare a little better in comparison with the pixel-based results. Two out of the four measures chosen by FSO were also selected in the pixel-based visual assessment matrix, they are GLCM mean and Standard Deviation. In terms of suitable bands, FSO did not identify the panchromatic band as suitable for analysis whereas in the pixel-based it appeared most appropriate (see Figure 4-4).

4.2.3. Directionality

As was shown in the literature review, authors possess varying views as it regards the application of directions for texture analysis (see Section 2.2.2). Therefore, to test which direction/s were most applicable for textural analysis, a matrix of the variables was created and assessed visually to determine to what extent the feature of interest (landslides) could be extracted based on i) visibility of the boundary and ii) internal homogeneity.

Again, building on lessons learnt in the preceding tests, *sf* 30 and the red and NIR image bands were used for segmentation. GLCM contrast on the red band was computed for highlighting boundary features and GLCM mean was used for highlighting internal homogeneity.

Results:

Figure 4-8 shows a landslide with a N-S alignment in the test area. Landslide boundary features are clearly visible when contrast is calculated in every direction except 0°. For this vertically aligned feature, when contrast is computed with the 0° directionality right boundaries become obscured (see top right of Figure 4-8).

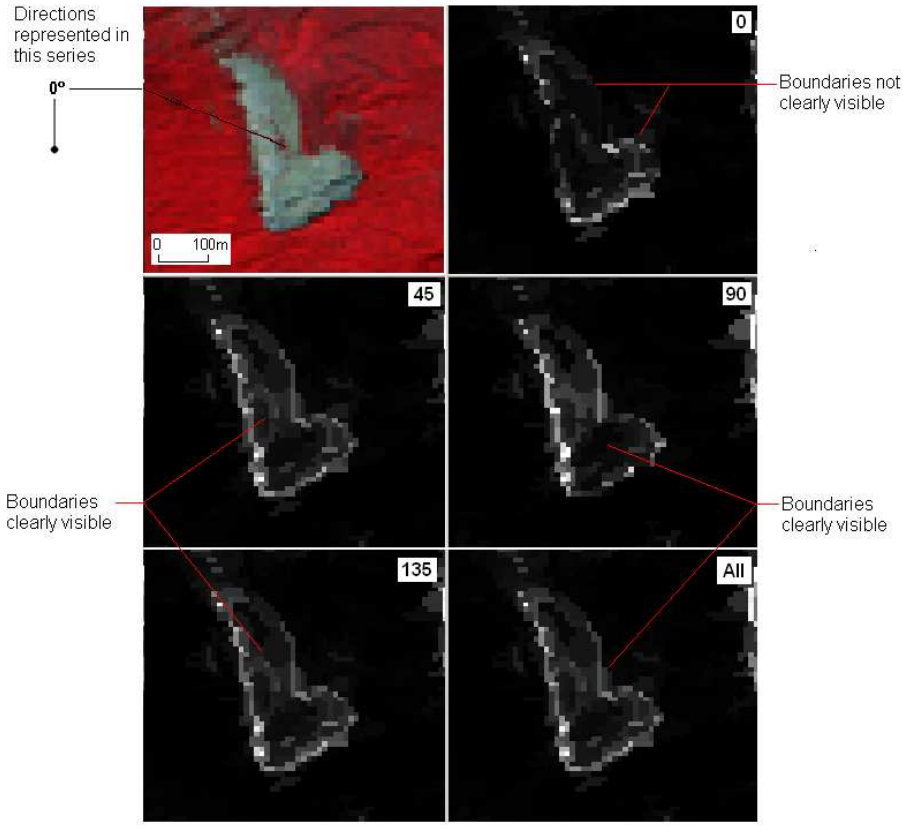

Figure 4-8 Effect of Directionality (*GLCM Contrast- Red band*) on recognition of landslide feature boundaries aligned at 0° degrees

Figure 4-9 shows the effect of directionality on visibility of landslides with a vertical alignment in terms of their internal homogeneity. It is quite clear that regardless of the directionality applied, the landslide feature is always visible – no information is lost.

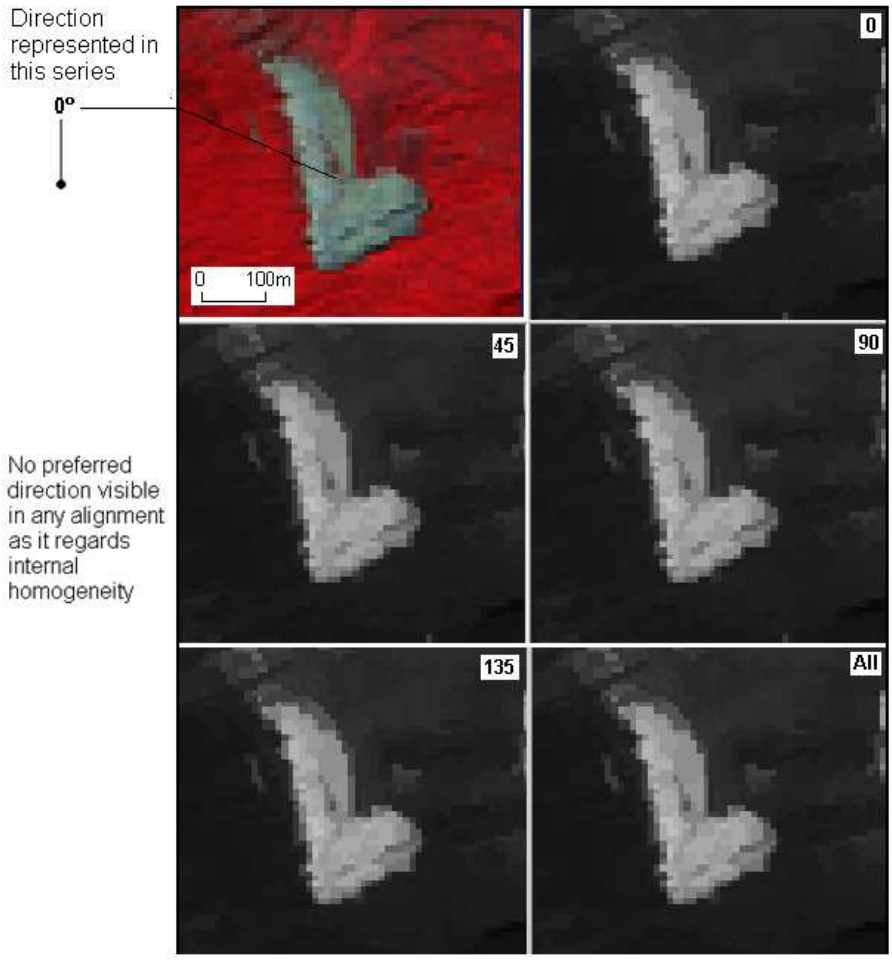

Figure 4-9 Effect of directionality (*GLCM Mean- Red band*) on internal homogeneity of landslide features aligned at 0 degrees

Figure 4-10 shows landslide features with inclined (45° and 135°) and horizontal alignments in the test area. Landslide boundary features are clearly visible when contrast is calculated in 135° and all directions (see figure). At 0, 45 and 90 degrees some boundary features become obscured. In other words, although a particular directionality may highlight the boundary features of a slide aligned in a specific direction, that same directionality will cause a loss of some boundary information for a slide aligned in a different direction. For example, for the feature aligned at 45°, texture computed with 0° directionality causes the boundary of its lower end to become vague (top left, Figure 4-10). In this same directionality (0°), the landslide feature with a horizontal (90°) alignment has very clear boundary representation.

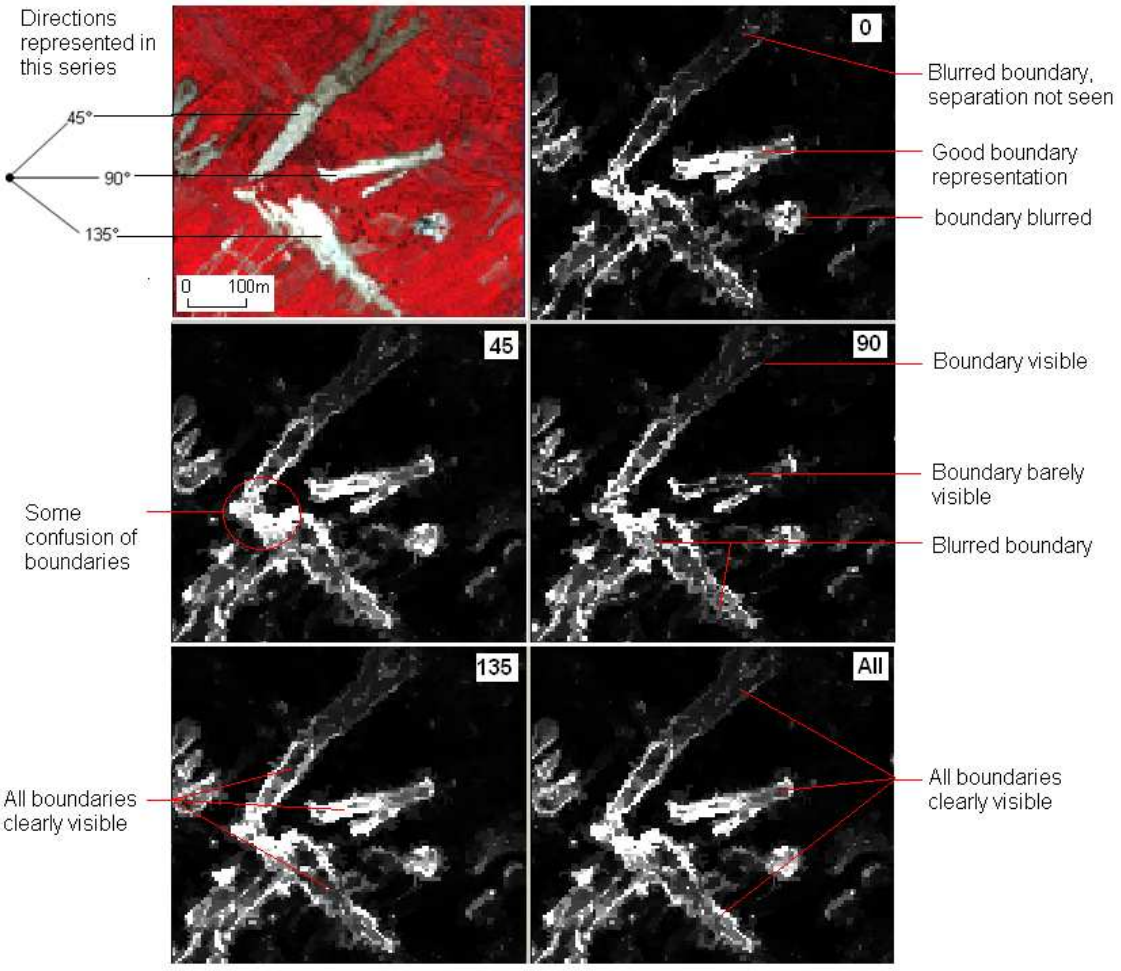

Figure 4-10 Effect of directionality (*GLCM Contrast- Red band*) on recognition of landslide feature boundaries aligned at 45, 90 and 135 degrees

Figure 4-11 shows the effect of directionality on visibility of landslides with inclined (45° and 135°) and horizontal alignments in terms of their internal homogeneity. Just like in the case of vertically aligned landslides (Figure 4-9, above), regardless of the directionality applied, the landslide feature is always visible – no information is lost.

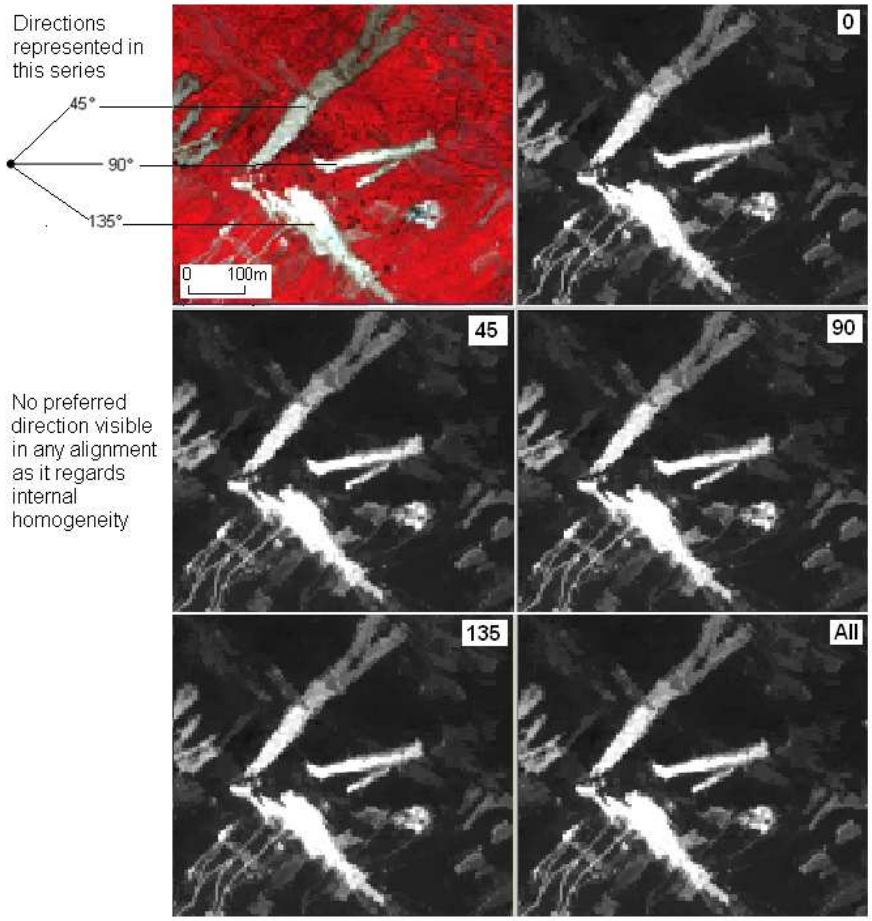

Figure 4-11 Effect of directionality (*GLCM Mean- Red band*) on internal homogeneity of landslide features aligned at 45, 90 and 135 degrees

4.3. Explicit Identification of landslides

This sub-section addresses Objective 1d): Can texture measures be applied explicitly in identifying landslides? The aim here was to determine how far landslides can be identified and extracted using *only* texture measures within the Definiens environment. Authors have proven the utility of texture measures for distinguishing landslide areas from non-landslide areas in a pixel-based environment (see Section 2.2.2). How far this can be achieved using object-based GLCM texture was tested and the results are shown below. The procedure was developed in a test area then applied to the validation AOIs described in Section 3.4.

4.3.1. Visual Assessment

Type A- Individual slides

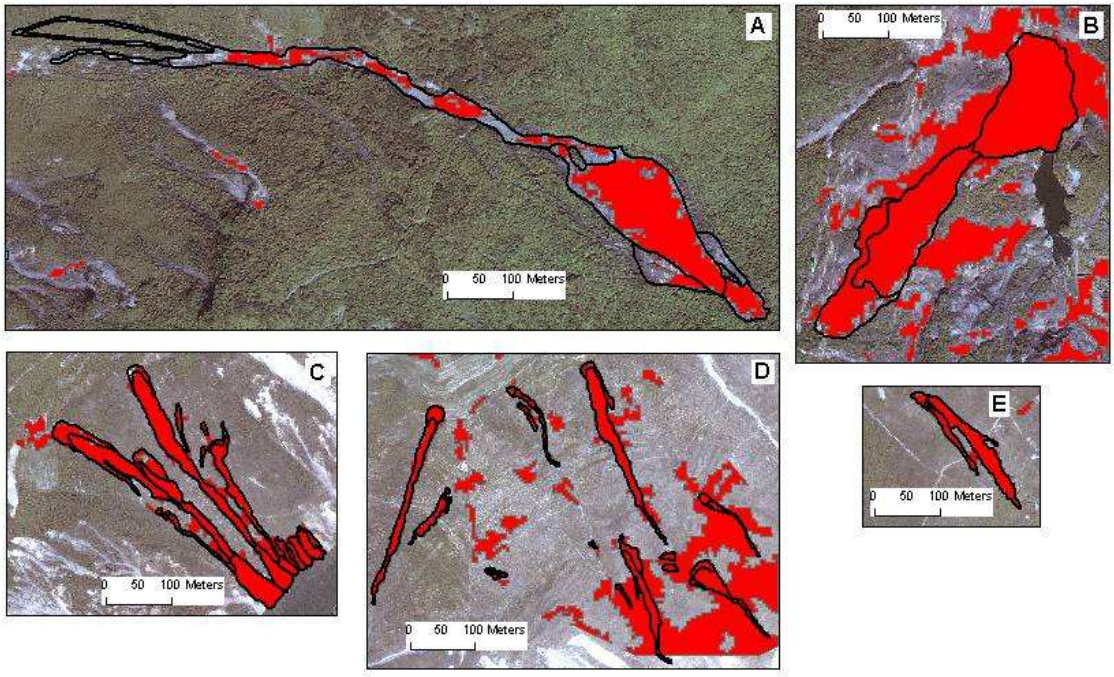

Figure 4-12 Comparison of object-based result (solid red) and manually detected (black outline) landslides for Type A landslides

For Type A landslides, the procedure was able to identify all the slides delineated manually. In some instances, the object-based texture only results identified almost precisely the landslide area delineated manually (C and E, Figure 4-12). In B and D, many of the object-derived slides over-estimated the extent of the actual landslide. In these cases, adjacent bare rocky or terraced land had similar texture values to the landslides and as such could not be differentiated from the landslides. In other instances, the procedure developed underestimated the extent of the landslide as seen in A.

Type B - Multiple source areas, single transport and deposition

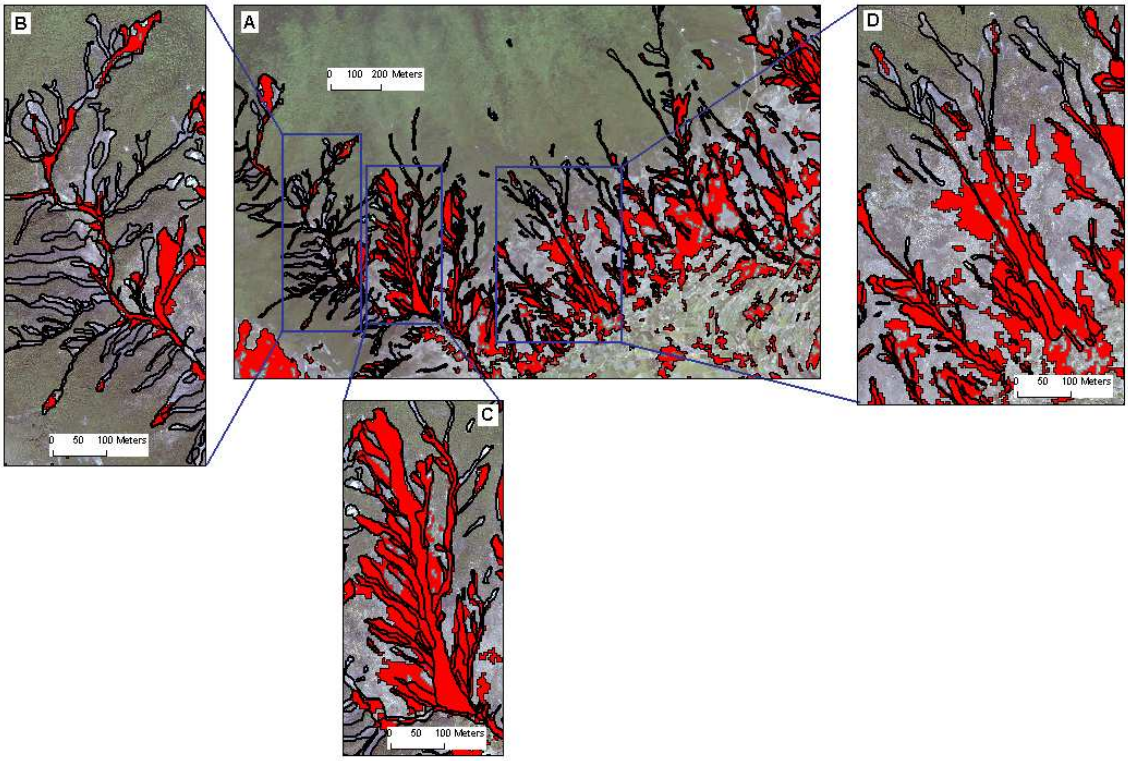

Figure 4-13 Comparison of object-based result (solid red) and manually detected (black outline) landslides for Type B landslides

In general, the procedure developed was not adequate for delineating individual Type B units. For example, C in Figure 4-13 was delineated in the manual classification as a single Type B unit having multiple primary source areas merging to form a single major transport zone. The procedure identified this as one landslide with no differentiation of the multiple source areas. Box B shows that many of the narrower slide areas with more vague boundaries were missed by the procedure. Just like with the Type A landslides, over-estimation of landslide extents also occurred where adjacent non-landslide areas had similar texture values.

Type C- Landslide complex

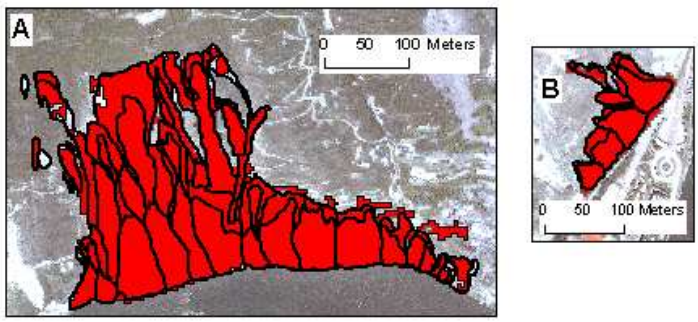

Figure 4-14 Comparison of object-based result (solid red) and manually detected (black outline) landslides for Type C landslides

For Type C landslides, the procedure could only identify the entire complex as one single landslide. The differentiation seen in the manual delineation was not at all possible using texture only. Other than that, the procedure captured the complex in its entirety.

4.3.2. ROC Analysis

The comparison of results from the procedure was also quantified using ROC curves (see description in section 3.5). The accuracy of the OOA procedure result obtained in relation to the entire range of possible values (manually delineated landslides) was good. AUC values for all the types were above 0.75 indicating that the procedure accurately mapped the instances of landslide or non-landslide.

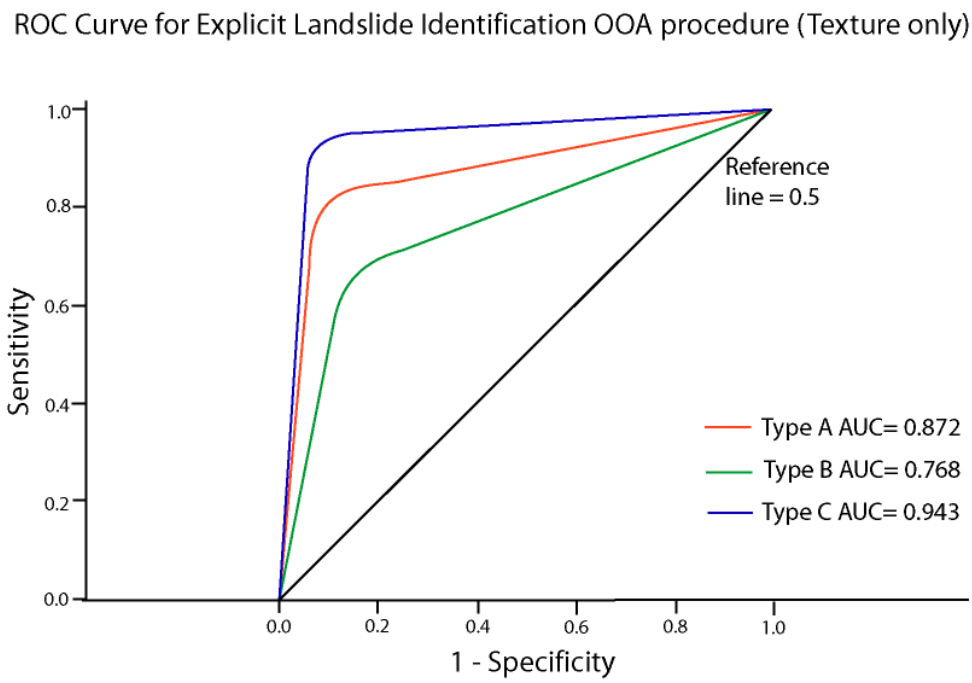

Figure 4-15 ROC and AUC values for explicit landslide identification OOA procedure

The highest AUC (0.943) was recorded for Type C landslides, but from the visual assessment we see that though the entire complex could be identified as being a landslide, the procedure could not map the various individual movements comprising the complex. Type B had the lowest AUC value (0.768) and this is because many landslides were missed with the procedure and several non-landslide areas were mapped as landslides.

4.4. Implicit Identification of Landslides

This sub-section addresses Objective 2): How can the texture measures identified in objective 1 be combined in an OOA-based procedure to identify landslides (inclusive of morphometric and spectral data)? The aim here was to determine how far landslides can be identified and extracted using *combined* spectral, morphological and textural measures within the Definiens environment. Previous work demonstrated that very good identification and classification results were possible using combined indices (see Section 2.2.2). However, since the application of textural indices was not done, it is attempted here and the results are shown below.

The procedure was developed in a test area (Figure 4-16) then applied to the validation AOIs described in Section 3.4. The test area contained numerous false positives that would all need to be eliminated before landslides could be identified.

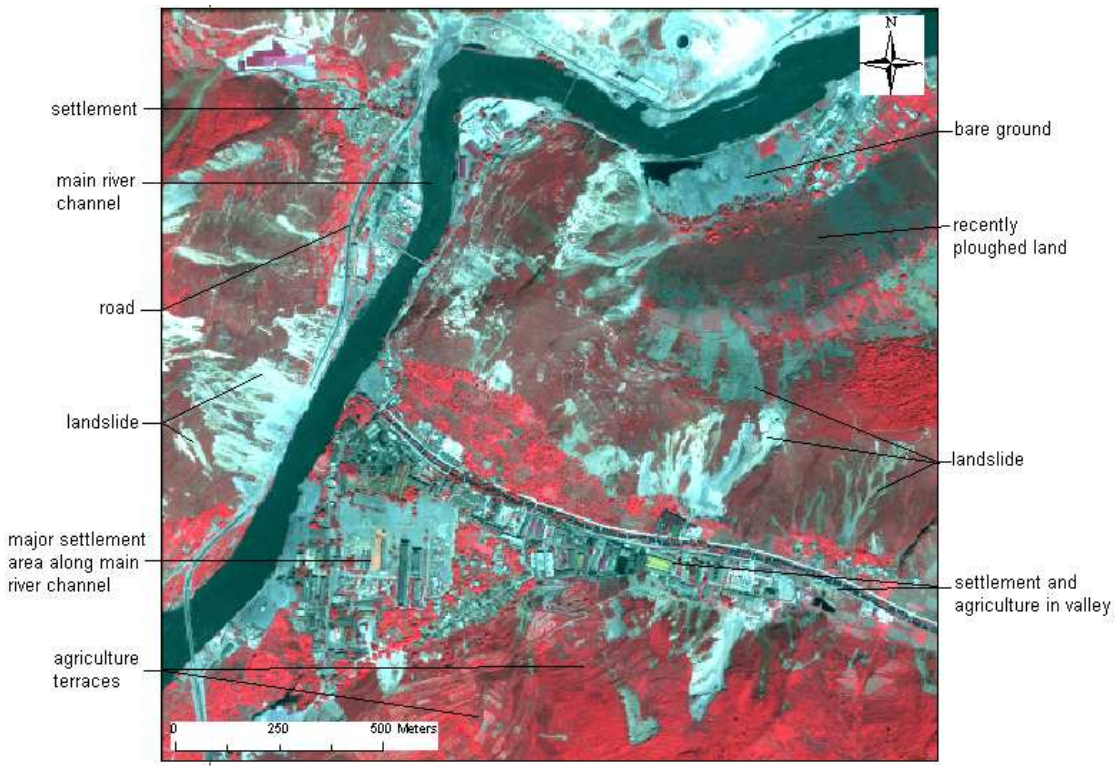

Figure 4-16 Test area used to develop implicit landslide identification procedure

4.4.1. Visual Assessment

Type A- Individual slides

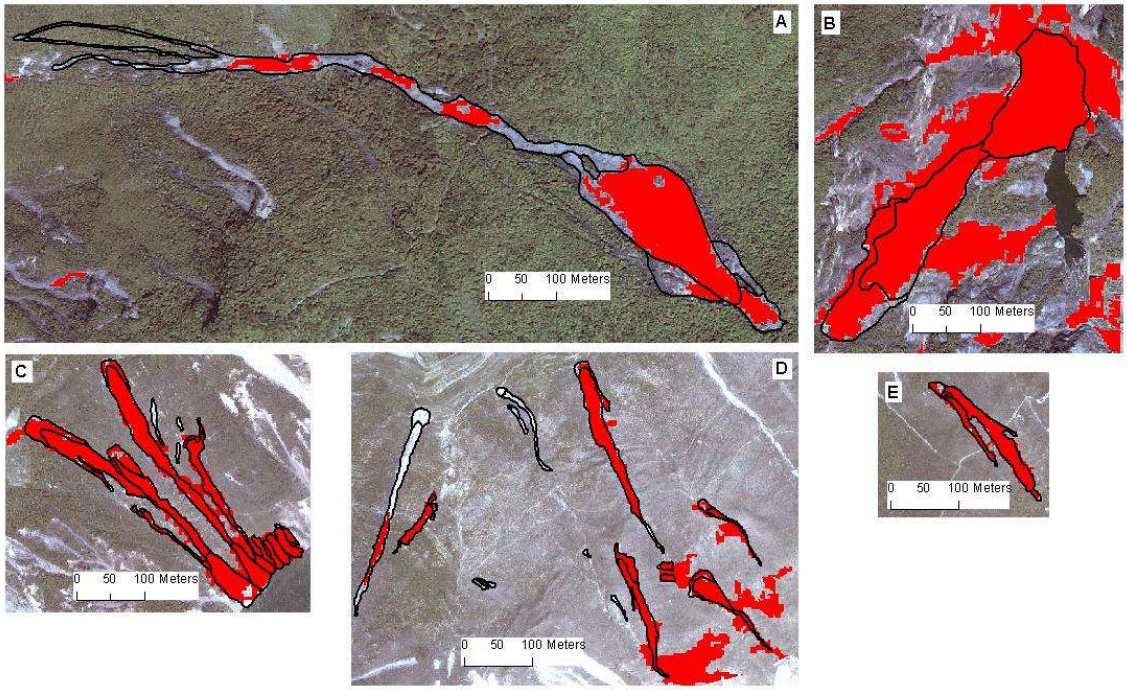

Figure 4-17 Comparison of object-based implicit identification result (solid red) and manually detected (black outline) landslides for Type A landslides

For Type A landslides, the procedure was able to identify most of the slides delineated manually. In some instances, the object-based combined feature results identified almost precisely the landslide area delineated manually (C and E, Figure 4-17). In B, many of the object-based slides over-estimated the extent of the actual landslide. In this case, adjacent bare rocky or terraced land had similar texture values to the landslides and as such, when the criterion for merging of adjacent objects was executed, these areas could not be differentiated from the landslides. In other instances, the procedure developed underestimated the extent of the landslide as seen in A and D, or missed altogether the much smaller slides (C and D).

Type B - Multiple source areas, single transport and deposition

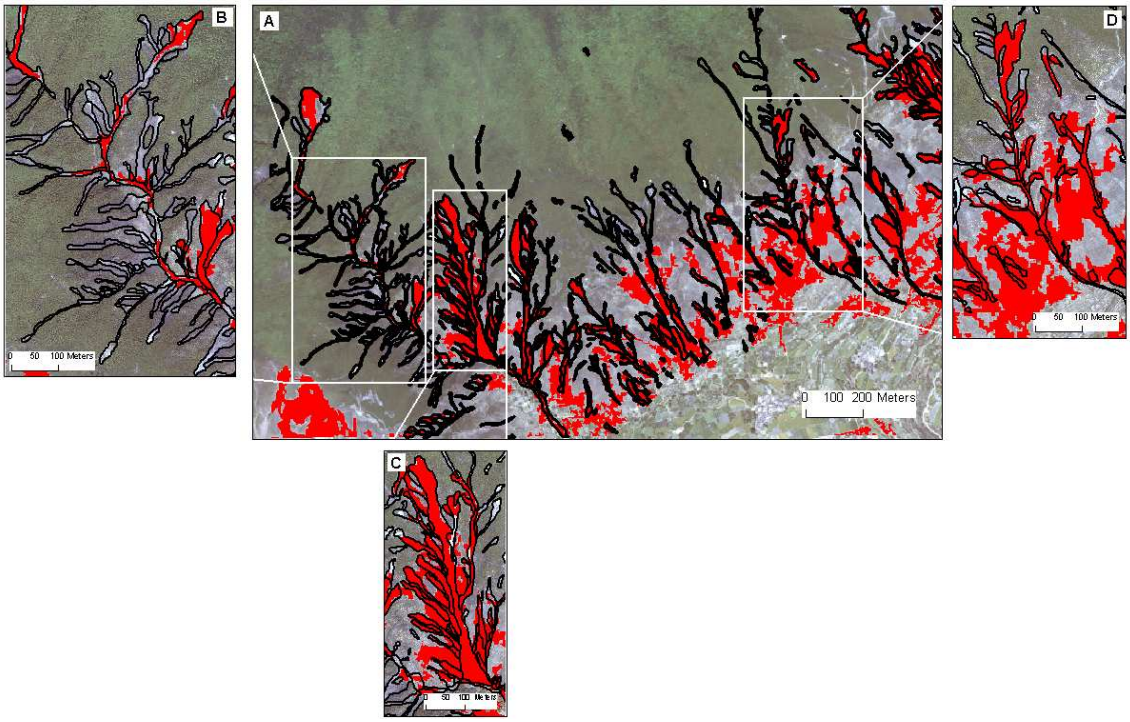

Figure 4-18 Comparison of object-based implicit identification result (solid red) and manually detected (black outline) landslides for Type B landslides

In general, the procedure developed was not adequate for delineating individual Type B units. For example, C in Figure 4-18 was delineated in the manual classification as a single Type B unit having multiple primary source areas merging to form a single major transport zone. The procedure however, identified this as one landslide with no differentiation of the multiple source areas. Box B shows that for many of the narrower slide areas with vague boundaries, the procedure could not register these as landslides. Just like with the Type A landslides, over-estimation of landslide extents also occurred where adjacent non-landslide areas had similar texture values and which could not be removed using other morphological or spectral indices.

Type C- Landslide complex

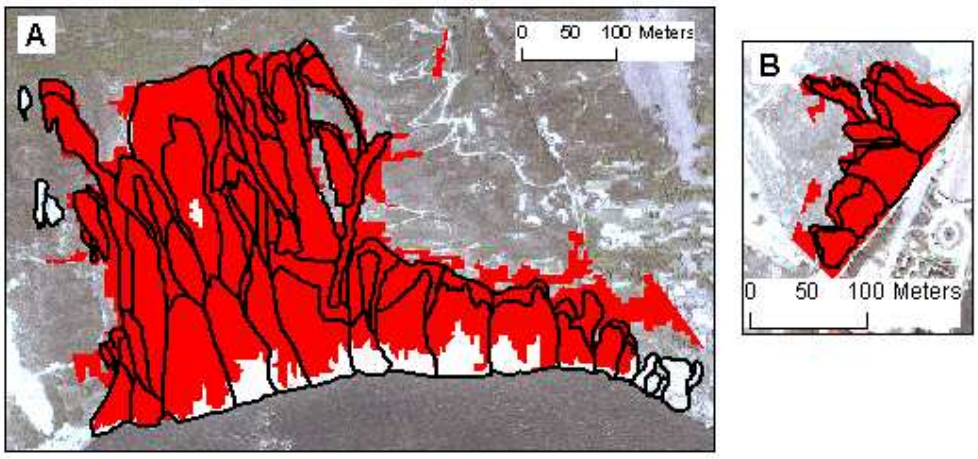

Figure 4-19 Comparison of object-based implicit identification result (solid red) and manually detected (black outline) landslides for Type C landslides

For Type C landslides, even with the use of additional spectral and morphological indices, the procedure could only identify the entire complex as one single landslide. The differentiation seen in the manual delineation was not at all possible using an automated approach. The procedure captured most of the complex, however, along its lower boundary, some information was lost when certain morphological criteria was applied as seen in box A. Here too, many smaller slides were not captured.

4.4.2. ROC Analysis

The accuracy of the OOA procedure result obtained in relation to the entire range of possible values (manually delineated landslides) was good. AUC values for all the types were above 0.75 indicating that the procedure accurately mapped the instances of landslide or non-landslide (see Figure 4-20).

The highest AUC (0.812) was recorded for Type B landslides, but from the visual assessment we see that though some units could be identified as being a landslide, the procedure did not capture the various individual movements contributing to the entire unit. Type A had the lowest AUC value (0.763) and this is because several non-landslide areas were mapped as landslides and existing slides were underestimated or went unmapped. Type C landslides had an AUC value of 0.796 and this could be because the full extents of the complex were not mapped.

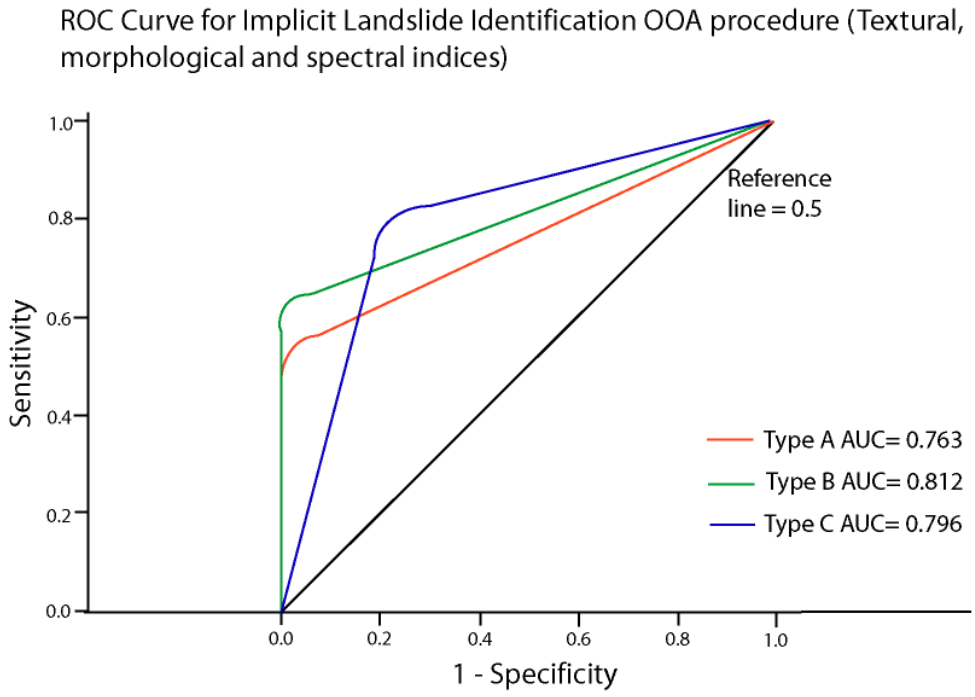

Figure 4-20 ROC and AUC values for implicit landslide identification OOA procedure

The differences between this result and that of the explicit identification results are significant as shown by the AUC values. In general, the ability of this procedure to predict well the occurrence of landslide or non-landslide areas is less than that of its counterpart. The AUC values for type A and C were higher in the explicit procedure than in the implicit. For the type B landslides the situations were reversed

5. Discussion and Review of Procedure Developed

In order to examine the utility of texture for landslide mapping, texture characterization beginning with understanding the basics of object-based versus pixel-based texture calculations was done. It is logical to assume that if an image is segmented to the pixel level, the resulting texture values per 'object' should be equal to that of the corresponding 'pixel' value in a pixel-based texture layer. However, the results shown in Table 4-2 where absolute values are compared prove that this assumption is inaccurate. Even though both software packages (Definiens and ENVI) quote the Haralick texture equations as the source of their algorithms, implementation of the equations clearly differ between the two. From the limited information provided in the user guides, one major difference in calculation could be identified. This difference was in the construction of the GLC matrix which for the pixel-based was done for the entire image but for the object-based was done per object. Thus in terms of processing time and efficiency, calculating the GLCM texture measures in a object-based environment becomes increasingly problematic as image size and number of objects increase. In this regard, newer software versions (Definiens Server Technology 8) offer some solutions for dealing with large datasets such as, automatic tiling and stitching and systematic region-of-interest based processing.

Another issue remains unresolved and this is the method by which the final value for an object is computed within Definiens. The results in Table 4-3 show that neither the sum nor the average of pixel-based textures gives the value obtained for the object-based texture in every measure. This can possibly be explained again by the one known difference in computation; however, such uncertainty makes it difficult to make an informed decision. Whilst the Reference Book does well explain how the GLC matrix is generated for each object, a sort of 'black box' obscures the users' understanding of how the single object value is computed. We understand that for each object a GLC matrix is computed based on the pixel values contained therein, but how we get from that matrix to a single object texture value is not clear. This "black box" also makes evaluation of the output of these texture measures uncertain. This is clearly seen in Table 4-2 where the texture value of some objects greatly exceeds the feature value range (0-90) stipulated in Section 2.2.1 as per the Reference Book. Information garnered from Definiens Support (too late to be usefully integrated in this study) said that for the computation of the single texture value for the object, the actual Haralick feature is calculated using the GLC Matrix and algorithm of the particular feature. For example, the contrast feature is calculated using the formula:

```
for (int i=0; i<mtrx.Rows(); i++)
for (int j=0; j<mtrx.Cols(); j++)
ctrst = mtrx[i][j] * ((i-j)*(i-j))
```

(source Jonathan Sutcliffe, Definiens Support)

He went on to say that using these formulas, values could well exceed 90 and as such the existing documentation is incorrect.

Thus, in terms of understanding the basics of the object-based texture calculations, there are still some unknowns as it relates to algorithm particulars and how they affect the resulting absolute values. Existing documentation on which the user depends for guidance does not contain sufficient information and as was pointed out by technical staff, also contains some errors. This confusion makes it increasingly difficult for users to make informed decisions on how to apply the GLCM texture measures. If however, the user is more interested in the emergent patterns from the texture calculations and absolute values are not essential for the application, the object-based textures correspond well enough with pixel-based counterparts.

On choosing the parameters for textural analysis of landslides

The issue of choosing an optimal segmentation scale for landslide analysis is an ongoing point for research (*In Press*). For now, the general consensus is that the segmentation should accurately depict the landslide boundaries. In some case this might result in large slides being largely over-segmented but this is an unavoidable consequence. Therefore, the optimal scale factor for depicting landslide boundaries will differ based on the study area and imagery used for analysis. Also, as no proven statistical method yet exists for choosing a suitable scale parameter, it is largely left up to the user to visually assess results of segmentation scales, a more or less 'trial and error' process.

The effect of scale factor on the result of texture computations was also considered in this research. Laliberte and Rango (2008) addressed the issue of correlation of object-based texture measures at different scale factors (see Section 2.2.2), however, since then no other work has addressed other scale factor-texture relationships. Results from this analysis showed that between sf 50 and 25 significant changes in the texture values ranges occurred (see Table 4-4). The fact that these changes took place at the same point for all the measures calculated suggests that the optimal *sf* value for calculating texture exists within that range.

Varying views exist in literature as to which band or bands to use for landslide texture analysis (see Section 2.2.2). Some authors are of the opinion that for textural analysis using the panchromatic band is the best option because the high resolution offers the best scale for analysis of textural patterns. However, other authors hold the view that it is more practical to use the band that contains the most information for the particular feature of interest. Results showed that in the object-based environment, the red and NIR multispectral bands gave the best textural responses for landslides (refer to Figures Figure 4-3Figure 4-5, Figure 4-6 andFigure 4-7). These findings support the latter view as the red and NIR bands best discriminate bare ground areas from forested and water classes especially. On the other hand, results from the pixel-based matrix more supported the former view that the high resolution gives a better scale for analysis of textural patterns. This is not to say that any one band will contain the information needed to highlight a particular feature. It is also quite possible that combinations of 2 or more bands may result in an image layer that would give even better results from textural analysis. In this respect, ongoing work is being conducted using prinicipal component analysis (PCA) to create layers with maximum information for a feature.

As it pertains to the choice of direction to apply in the study of a particular landform or feature (roads, agriculture, forest, etc), contrasting views exist in literature. Shaban and Dikshit (1997) claim that

single direction for agricultural land is as good as multi-direction and it is less computationally demanding. Rao *et al.* (2002) have made the point that because of the randomness of orientation of natural features, GLCM computed in all directions is sensible. Furthermore, there are also some claims of redundancy of texture in different orthogonal directions. The results of the directionality test conducted for applicability to identifying landslides in terms of their internal homogeneity supports the latter view of redundancy in different orthogonal directions (see Figure 4-9 and Figure 4-11). However, as it concerns identification of landslide boundaries, texture computed in different directions does have an effect based on the orientation of the feature of interest (see Figure 4-8 and Figure 4-10).

Figure 5-1 Arrows highlight the multiple orientations of landslides in the study area

Because the landslides in the study area all have different orientations (Figure 5-1; arrows point in the direction of downslope movement), it was logical to compute the texture variables using the '*All directions*' option which will allow for directional invariance (*see Section 2.2.1*).

From the literature review, it was learnt that GLCM Entropy has been identified as the most useful for landslide identification in pixel-based analysis (Whitworth et al. 2002; 2005; 2006; Fernández et al. 2008) and it was thus the intention of this research to test that claim for its applicability in an object-based environment. The results of the two tests conducted showed that Entropy could not be used to distinguish slides using object-based textural analysis (refer to FiguresFigure 4-3Figure 4-5,Figure 4-6 andFigure 4-7). These results beg to question to what extent the recommendations coming from pixel-based studies are at all valid in OOA. The pixel-based studies referenced in Section 2.2.2 unanimously point to GLCM entropy as the one texture feature that was ideal for identifying landslides yet neither the texture-band matrix nor the feature space optimization computations (see section 4.2.2) gave results to match the conclusions drawn in pixel-based studies. In fact, even within the texture-band matrix computed for comparison purposes (Figure 4-4), the landslide feature could not be deciphered from the images of entropy calculated on any of the bands. The reciprocal is also true, the measures found useful in object-based analysis were not mentioned in pixel-based studies as being useful for identifying slides. We can say then that the findings and conclusions drawn in pixel-based studies on texture analysis for landslides cannot be extrapolated or applied to object-based landslide texture analysis.

On the procedure developed for identifying landslides in the test area

The first procedure developed was aimed at trying to determine whether or not landslides could be identified using texture only. The results showed that it was possible but a lot of over-estimation of landslides extents and classifying of non-landslide areas as landslides occurred. This procedure was developed in an area that contained very little false positives (only forest, water and a very small urban area were present). Therefore, the texture measures calculated were sufficient to attain good class separability between landslides and its obvious false positives. This was an extremely simplified case and in reality the landscape usually contains much more for analysis.

The second procedure was developed in a more complex area (see Figure 4-16) and it incorporated the use of spectral and morphological information along with texture. The results of this procedure were in some ways less successful than the previous one. This is largely because of the poor quality of the input DTM used to derive the morphological indices. Martha et al. (*In Press*) identified very useful false positive identifiers using DEM-derived products (see Table 3-3). However, these require that a high resolution accurately registered DTM is used. In this study area, this was not readily available and as such these logical criteria could not be applied. The many errors presented by the coarseness and shifting of the DTM used resulted in a large error being propagated to the derivatives and proper quantitative indices could not be applied.

The spectral and textural indices were thus applied as far as possible with only derivatives of slope and relief being used in the procedure. The result was that many false positives still existed so that when a simple spectral difference segmentation was applied using the GLCM mean texture layer, many false positives were classified as landslides. Also as it regards texture and landslides and their false positives, in this test area where false positives were in abundance, the texture measures that were previously good at distinguishing landslide (explicit procedure) were observed to also be common to false positives such as some settlement areas and bare/rocky lands especially. However, if these false positives can be eliminated, the reconstitution procedure (Figure 3-12) could be applied possible with very good results thereby addressing the gap that exists in terms of OOA based landslide mapping and classification..

6. Conclusions & Recommendations

6.1. Conclusions

The main objective of this work was to examine the utility of texture measures for identifying landslide features using object-oriented analysis. The sub-objectives were then divided into a two phase process involving first an evaluation of object-based texture analysis and then the development of procedures to test what was learnt in Phase 1, thereby assessing the usefulness of texture for object-based landslide mapping. The following conclusions were drawn based on the results obtained in this study:

- There is a fundamental difference in the way object-based and pixel-based texture measures are computed and as such they are not directly comparable. This fundamental difference also means that conclusions drawn from studies done using either cannot be extrapolated or assumed to be applicable or correct for the other.

- Texture cannot be used in isolation to distinguish landslides from its false positives such as bare ground and settlement areas. As such object-based texture cannot be applied explicitly to identify landslides. If however it is used in conjunction with spectral and morphological data identification and ultimately classification results can be enhanced.

- The specifics of choosing parameters to apply the texture measures are in some cases essentially site and imagery specific. Scale factor would depend on the available data and the types of landslides prevalent in the area. Scale factor changes also results in fluctuations of the value ranges of the texture measures. Texture computed on the red or NIR bands would be useful but band combinations to create layers emphasizing information for the feature of interest may ultimately prove more useful. Directionality has an effect when the boundaries of the feature of interest are being considered, however there is redundancy measures calculated in different directions when internal homogeneity of the feature is considered. If the feature of interest multiple random alignment in the study area, it is best to use the “all directions” option for computing texture measures.

- GLCM mean and contrast are the most useful measures for use in identifying landslide internal homogeneity and boundaries (respectively).

- Reconstitution of over-segmented landslides using texture is potentially very useful.

- The quality of input data greatly affects the results of the OOA based procedure. Especially because quantitative indices and contextual relationships are being built, input data should at least be accurate so as not to propagate errors in the procedure.

6.2. Limitations

- Existing documentation for the Definiens program was sometimes misleading and questions regarding the implementation of the texture tools available resulted in a referral to online tutorials explaining the *theory* behind GLCM texture measures and which did not address the specifics of the computations going on in the background of the program.

- The quality of the input Dem used in the test study made it difficult to apply logical false positive elimination criteria and as such overall quality of the result was diminished and the intended test for application of the textural indices for reconstitution could not be completed in its entirety.

6.3. Recommendations

Points for further research:

- With better DEM data it would be possible to develop a proper procedure which eliminates false positives and thus the reconstitution process can truly be tested and refined accordingly.

- Statistical methods for assessing the optimal image band for object-based texture analysis. Aim is to quantify the choice of the most suitable band on which to compute texture measures for any specific application.

- Statistical measures for determining the effect of scale factor on computation of texture measures.

Other possible applications of object-based texture analysis for landslide mapping

1. The applicability of Definiens contextual textures for landslide detection.
2. Event-based change detection where texture is used to identify whether or not reactivations have occurred in slides from T_1 to T_2.
3. Texture to distinguish between landslide types
4. Texture to determine the dominant material involved in a failure (bedrock vs soil; sandstone vs clay).
5. Texture as a site specific monitoring tool to track deformation changes within a failed mass over time.
6. Texture analysis to map old/relict slides in areas covered by vegetation using radar interferometry or Lidar data.
7. Texture analysis for site specific mapping of the different parts of a landslide.

8. Applicability of texture as a tool for identifying zones of potential failure by detecting landslide precursors such as deformation cracks and vegetation anomalies (caused by soil moisture changes)

References

Ait-Kheddache, A. and S. A. Rajala (1988). Texture classification based on higher-order fractals. Acoustics, Speech, and Signal Processing, 1988. ICASSP-88., 1988 International Conference on.

Arai, K. (1993). "A classification method with a spatial-spectral variability." International Journal of Remote Sensing **14**(4): 699 - 709.

Atkinson, P. M. and P. Lewis (2000). "Geostatistical classification for remote sensing: an introduction." Computers & Geosciences **26**(4): 361-371.

Balaguer, A., L. A. Ruiz, T. Hermosilla and J. A. Recio (*In Press*). "Definition of a comprehensive set of texture semivariogram features and their evaluation for object-oriented image classification." Computers & Geosciences **In Press, Corrected Proof**.

Baltsavias, E. P. (2004). "Object extraction and revision by image analysis using existing geodata and knowledge: current status and steps towards operational systems." ISPRS Journal of Photogrammetry and Remote Sensing **58**(3-4): 129-151.

Baraldi, A. and F. Parmiggiani (1995). "An investigation of the textural characteristics associated with gray level cooccurrence matrix statistical parameters." Geoscience and Remote Sensing, IEEE Transactions on **33**(2): 293-304.

Barlow, J., S. Franklin and Y. Martin (2006). "High spatial resolution satellite imagery, DEM derivatives, and image segmentation for the detection of mass wasting processes." Photogrammetric Engineering and Remote Sensing **72**(6): 687-692.

Barlow, J. and S. E. Franklin (2008). "Mapping snow avalanche chutes in the Canadian Rockies using Landsat TM and DEM data." Canadian Journal of Remote Sensing **34**(6): 516-525.

Barlow, J., Y. Martin and S. E. Franklin (2003). "Detecting translational landslide scars using segmentation of Landsat ETM+ and DEM data in the northern Cascade Mountains, British Columbia." Canadian Journal of Remote Sensing **29**(4): 510-517.

Beguería, S. (2006). "Validation and Evaluation of Predictive Models in Hazard Assessment and Risk Management." Natural Hazards **37**(3): 315-329.

Berberoglu, S. and P. J. Curran (2004). Merging Spectral and Textural information for Classifying Remotely Sensed Images. Remote sensing image analysis : including the spatial domain. S. M. de Jong and F. D. van der Meer. Dordrecht Kluwer Academic**:** 113-136.

Blaschke, T., C. Burnett and A. Pekkarinen (2004). Image segmentation methods for object-based analysis and classification. Remote sensing image analysis : including the spatial domain. S. M. de Jong and F. D. van der Meer. Dordrecht Kluwer Academic**:** 211-236.

Booth, A. M., J. J. Roering and J. T. Perron (2009). "Automated landslide mapping using spectral analysis and high-resolution topographic data: Puget Sound lowlands, Washington, and Portland Hills, Oregon." Geomorphology **109**(3-4): 132-147.

Borghuis, A. M., K. Chang and H. Y. Lee (2007). "Comparison between automated and manual mapping of typhoon-triggered landslides from SPOT-5 imagery." International Journal of Remote Sensing **28**(8): 1843 - 1856.

Brabb, E. E. and B. L. Harrod, Eds. (1989). Landslides : extent and economic significance : proceedings of the 28th international geological congress : symposium on landslides, Washington, D.C. 17 July 1989. Rotterdam etc., Balkema.

Brunsden, D. (1999). "Some geomorphological considerations for the future development of landslide models." Geomorphology **30**(1-2): 13-24.

Canuti, P., N. Casagli, L. Ermini, R. Fanti and P. Farina (2004). "Landslide activity as a geoindicator in Italy: significance and new perspectives from remote sensing." Environmental Geology **45**(7): 907-919.

Carr, L. and E. Rathje (2008). The Use of Remote Sensing to Identify Landslides Caused by the 2004 Niigata-ken Chuetsu Earthquake in Japan. 6th International Workshop on Remote Sensing for Disaster Management Applications. University of Pavia, Italy.

Castellanos Abella, E. A. and C. J. Van Westen (2008). "Qualitative landslide susceptibility assessment by multicriteria analysis: A case study from San Antonio del Sur, Guantánamo, Cuba." Geomorphology **94**(3-4): 453-466.

Catani, F., N. Casagli, L. Ermini, G. Righini and G. Menduni (2005). "Landslide hazard and risk mapping at catchment scale in the Arno River basin." Landslides **2**(4): 329-342.

Chacón, J., C. Irigaray, T. Fernández and R. El Hamdouni (2006). "Engineering geology maps: landslides and geographical information systems." Bulletin of Engineering Geology and the Environment **65**(4): 341-411.

Cheng, K. S., C. Wei and S. C. Chang (2004). "Locating landslides using multi-temporal satellite images." Advances in Space Research **33**(3): 296-301.

Chica-Olmo, M. and F. Abarca-Hernández (2000). "Computing geostatistical image texture for remotely sensed data classification." Computers & Geosciences **26**(4): 373-383.

Clague, J. J. (2009). Climate Change and Slope Instability. Landslides – Disaster Risk Reduction**:** 557-572.

Crozier, M. J. and T. Glade (2005). Landslide Hazard and Risk: Issues, Concepts and Approaches. Landslide Hazard and Risk. T. Glade, M. Anderson and M. J. Crozier. Chichester, Wiley & Sons.

Definiens (2007). Developer 7: Reference Book. Germany, Definiens AG.

Dikau, R. and European Commission. (1996). Landslide recognition : identification, movement, and causes. Chichester ; New York, Wiley.

Dikshit, O. (1996). "Textural classification for ecological research using ATM images." International Journal of Remote Sensing **17**(5): 887 - 915.

Eeckhaut, M. V. D., J. Poesen, G. Verstraeten, V. Vanacker, J. Nyssen, J. Moeyersons, L. P. H. v. Beek and L. Vandekerckhove (2007). "Use of LIDAR-derived images for mapping old landslides under forest." Earth Surface Processes and Landforms **32**(5): 754-769.

Eyers, R., J. Moore, J. Hervás and J. G. Lui (1998). Integrated use of Landsat TM and SPOT panchromatic imagery for landslide mapping: case histories from southeast Spain. Geohazards in Engineering Geology. J. G. Maund and M. Eddleston. London, Geological Society. **15:** 133-140.

Fernández, T., J. Jiménez, P. Fernández, R. El Hamdouni, F. J. Cardenal, J. Delgado, C. Irigaray and J. Chacón (2008). Automatic Detection of Landslide Features with Remote Sensing Techniques in the Betic Cordilleras (Granada, Southern Spain) 21st ISPRS Congress: Silk Road for Information from Imagery, Beijing, International Society for Photogrammetry and Remote Sensing.

Forsythe, K. W. and R. D. Wheate (2003). "Utilization of Landsat TM and digital elevation data for the delineation of avalanche slopes in Yoho National Park (Canada)." Geoscience and Remote Sensing, IEEE Transactions on **41**(11): 2678-2682.

Galli, M., F. Ardizzone, M. Cardinali, F. Guzzetti and P. Reichenbach (2008). "Comparing landslide inventory maps." Geomorphology **94**(3-4): 268-289.

Gao, J. (2009). Digital Analysis of Remotely Sensed Imagery New York, McGraw-Hill.

Geertsema, M., L. Highland and L. Vaugeouis (2009). Environmental Impact of Landslides. Landslides – Disaster Risk Reduction**:** 589-607.

Glenn, N. F., D. R. Streutker, D. J. Chadwick, G. D. Thackray and S. J. Dorsch (2006). "Analysis of LiDAR-derived topographic information for characterizing and differentiating landslide morphology and activity." Geomorphology **73**(1-2): 131-148.

Gong, P., D. J. Marceau and P. J. Howarth (1992). "A comparison of spatial feature extraction algorithms for land-use classification with SPOT HRV data." Remote Sensing of Environment **40**(2): 137-151.

Guzzetti, F., M. Cardinali, P. Reichenbach and A. Carrara (2000). "Comparing Landslide Maps: A Case Study in the Upper Tiber River Basin, Central Italy." Environmental Management **25**(3): 247-263.

Guzzetti, F., A. Carrara, M. Cardinali and P. Reichenbach (1999). "Landslide hazard evaluation: a review of current techniques and their application in a multi-scale study, Central Italy." Geomorphology **31**(1-4): 181-216.

Hall-Beyer, M. (2007). "The GLCM Tutorial Home Page." from http://www.fp.ucalgary.ca/mhallbey/tutorial.htm.

Haralick, R. M. (1979). "Statistical and structural approaches to texture." Proceedings of the IEEE **67**(5): 786-804.

Haralick, R. M., K. Shanmugam and I. H. Dinstein (1973). "Textural Features for Image Classification." IEEE Transactions on Systems, Man and Cybernetics **3**(6): 610-621.

Haugerud, R. A., D. J. Harding, S. Y. Johnson, J. L. Harless, C. S. Weaver and B. L. Sherrod (2003). "High-resolution lidar topography of the Puget Lowland, Washington - A bonanza for earth science." GSA Today **13**(6): 4-10.

Hay, G. J., D. J. Marceau, P. Dube and A. Bouchard (2001). "A multiscale framework for landscape analysis: Object-specific analysis and upscaling." Landscape Ecology **16**: 471-490.

Hervás, J., J. I. Barredo, P. L. Rosin, A. Pasuto, F. Mantovani and S. Silvano (2003). "Monitoring landslides from optical remotely sensed imagery: the case history of Tessina landslide, Italy." Geomorphology **54**(1-2): 63-75.

Hervás, J. and P. Bobrowsky (2009). Mapping: Inventories, Susceptibility, Hazard and Risk. Landslides – Disaster Risk Reduction**:** 321-349.

Hervás, J. and P. L. Rosin (1996). Landslide mapping by textural analysis of ATM data. Proceedings Eleventh Thematic Conference Applied Geologic Remote Sensing.

Highland, L. M. and P. T. Bobrowsky (2008). The Landslide handbook : a guide to understanding landslides. Reston, United States Geological Survey (USGS).

Huggel, C., A. Kääb, W. Haeberli and B. Krummenacher (2003). "Regional-scale GIS-models for assessment of hazards from glacial lake outburst: evaluation and application in the Swiss Alps." Natural Hazards and Earth System Sciences(3): 647-662.

Hungr, O. (1995). "A model for the runout analysis of rapid flow slides, debris flows, and avalanches." Canadian Geotechnical Journal **32**(4): 610-623.

IGOS (2007) "2nd Geohazards Theme Report."

Iverson, R. M., S. P. Schilling and J. W. Vallance (1998). "Objective delineation of lahar-inundation hazard zones." Bulletin of the Geological Society of America **110**(8): 972-984.

Kamagata, N., K. Hara, M. Mori, Y. Akamatsu, Y. Li and Y. Hoshino (2008). Object-based classification of IKONOS data for vegetation mapping in Central Japan. Object-Based Image Analysis: Spatial Concepts for Knowledge-Driven Remote Sensing Applications. T. Blaschke, S. Lang and G. J. Hay, Springer**:** 459-475.

Kawabata, D. and J. Bandibas (2009). "Landslide susceptibility mapping using geological data, a DEM from ASTER images and an Artificial Neural Network (ANN)." Geomorphology **113**(1-2): 97-109.

Kayitakire, F., C. Hamel and P. Defourny (2006). "Retrieving forest structure variables based on image texture analysis and IKONOS-2 imagery." Remote Sensing of Environment **102**(3-4): 390-401.

Keefer, D. K. (1999). "Earthquake-induced landslides and their effects on alluvial fans." Journal of Sedimentary Research **69**(1): 84-104

Kerle, N. (2002). "Volume estimation of the 1998 flank collapse at Casita volcano, Nicaragua : a comparison of photogrammetric and conventional techniques." Earth surface processes and landforms : the journal of the British geomorphological research group **27**(7).

Kjekstad, O. and L. Highland (2009). Economic and Social Impacts of Landslides. Landslides – Disaster Risk Reduction**:** 573-587.

Laliberte, A. S. and A. Rango (2008). Correlation of Object-Based texture Measures at Multiple Scales in Sub-Decimeter Resolution Aerial Photography. GEOBIA 2008 – Pixels, Objects, Intelligence. GEOgraphic Object Based Image Analysis for the 21st Century., Calgary, Alberta, University of Calgary.

Lineback Gritzner, M., W. A. Marcus, R. Aspinall and S. G. Custer (2001). "Assessing landslide potential using GIS, soil wetness modeling and topographic attributes, Payette River, Idaho." Geomorphology **37**(1-2): 149-165.

Liu, Y., M. Li, L. Mao, F. Xu and S. Huang (2006). "Review of remotely sensed imagery classification patterns based on object oriented image analysis." In: Chinese Geographical Science, 16(2006)3, pp. 282-288.

Luckman, A. J., A. C. Frery, C. C. F. Yanasse and G. B. Groom (1997). "Texture in airborne SAR imagery of tropical forest and its relationship to forest regeneration stage." International Journal of Remote Sensing **18**(6): 1333 - 1349.

Marceau, D. J., P. J. Howarth, J. M. Dubois and D. J. Gratton (1990). "Evaluation Of The Grey-level Co-occurrence Matrix Method For Land-cover Classification Using Spot Imagery." Geoscience and Remote Sensing, IEEE Transactions on **28**(4): 513-519.

Martha, T. R., N. Kerle, V. G. Jetten, C. J. van Westen and K. V. Kumar (2009). "Characterising spectral, spatial and morphometric properties of landslides for automatic detection using object-oriented methods." *In press*.

Martha, T. R., N. Kerle, V. G. Jetten, C. J. van Westen and K. V. Kumar (2010). "Landslide Volumetric Analysis Using Cartosat-1-Derived DEMs." *IEEE Geoscience and Remote Sensing Letters*.

Martha, T. R., N. Kerle, V. G. Jetten, C. J. van Westen and K. V. Kumar (*"In press"*). "Characterising spectral, spatial and morphometric properties of landslides for automatic detection using object-oriented methods."

Martha, T. R., N. Kerle, V. G. Jetten, C. J. van Westen and K. V. Kumar (*In Press*). "Characterising spectral, spatial and morphometric properties of landslides for automatic detection using object-oriented methods." *In press*.

Martin, Y. E. and S. E. Franklin (2005). "Classification of soil- and bedrock-dominated landslides in British Columbia using segmentation of satellite imagery and DEM data." International Journal of Remote Sensing **26**(7): 1505-1509.

Marui, H. and F. Nadim (2009). Landslides and Multi-Hazards. Landslides – Disaster Risk Reduction**:** 435-450.

Mason, P. J., M. S. Rosenbaum and J. M. Moore (1995). Texture Analysis using multi-temporal digital data for landslide hazard mapping. Proceedings 31st Annual Conference Geohazards and Engineering Geology, Coventry University, Coventry, UK.

Mason, P. J., M. S. Rosenbaum and J. M. Moore (1998). Digital texture Analysis for landslide hazard mapping. Geohazards in Engineering Geology. J. G. Maund and M. Eddleston. London, Geological Society**:** 297-305.

McKean, J. and J. Roering (2004). "Objective landslide detection and surface morphology mapping using high-resolution airborne laser altimetry." Geomorphology **57**(3-4): 331-351.

Miliaresis, G., N. Sabatakakis and G. Koukis (2005). "Terrain Pattern Recognition and Spatial Decision Making for Regional Slope Stability Studies." Natural Resources Research **14**(2): 91-100.

Moine, M., A. Puissant and J.-P. Malet (2009). Detection of landslides from aerial and satellite images with a semi-automatic method. Application to the Barcelonnette basin (Alpes-de-Haute-Provence, France). Landslide Processes: from geomorphological mapping to dynamic modelling. J.-P. Malet, A. Remaitre and T. Bogaard. Strasbourg, France, CERG**:** pp. 63-68.

Moore, I. D., R. B. Grayson and A. R. Ladson (1991). "Digital terrain modelling: A review of hydrological, geomorphological, and biological applications." Hydrological Processes **5**(1): 3-30.

Nadim, F. and O. Kjekstad (2009). Assessment of Global High-Risk Landslide Disaster Hotspots. Landslides – Disaster Risk Reduction**:** 213-221.

Narasimha Rao, P. V., M. V. R. Sesha Sai, K. Sreenivas, M. V. Krishna Rao, B. R. M. Rao, R. S. Dwivedi and L. Venkataratnam (2002). "Textural analysis of IRS-1D panchromatic data for land cover classification." International Journal of Remote Sensing **23**(17): 3327 - 3345.

Nichol, J. and M. S. Wong (2005). "Satellite remote sensing for detailed landslide inventories using change detection and image fusion." International Journal of Remote Sensing **26**(9): 1913 - 1926.

Nikolakopoulos, K. G., D. A. Vaiopoulos, G. A. Skianis, P. Sarantinos and A. Tsitsikas (2005). Combined use of remote sensing, GIS and GPS data for landslide mapping. Geoscience and Remote Sensing Symposium, 2005. IGARSS '05. Proceedings. 2005 IEEE International.

Ozdemir, I., D. Norton, U. Ozkan, A. Mert and O. Senturk (2008). "Estimation of Tree Size Diversity Using Object Oriented Texture Analysis and Aster Imagery." Sensors **8**(8): 4709-4724.

Pacifici, F., M. Chini and W. J. Emery (2009). "A neural network approach using multi-scale textural metrics from very high-resolution panchromatic imagery for urban land-use classification." Remote Sensing of Environment **113**(6): 1276-1292.

Pack, R. T., D. G. Tarboton and C. N. Goodwin (1998). Terrain Stability Mapping with SINMAP: Technical description and User Guide for version 1.00. Salmon Arm, BC, Canada**:** 68.

Petley, D. (2009). "On the occurrence of fatal landslides in 2008." Geophysical Research Abstracts **11**(EGU2009-9030).

Petley, D. and N. Rosser (2007). The Impact of Landslides - 2007, Durham University.

Petley, D. N., W. D. O. Crick and A. B. Hart (2002). The use of satellite imagery in landslide studies in high mountain areas. Proceedings of the 23rd Asian Conference on Remote Sensing (ACRS 2002), Kathmandu.

Pike, R. J. (1988). "geometric signature : quantifying landslide terrain types from digital elevation models." In: Mathematical Geology, 20(1988)5, pp. 491-511.

Pike, R. J., G. R.W., S. Roberts, N. B. Kalman and S. Sobieszczyk (2001). Map and Map Database of susceptibility to slope failure by sliding and earthflow in Oakland area, California. pamphlet to accompany Miscellaneous Field Studies Map MF-2385 version 1.0, USGS.

Rib, H. T. and T. Liang (1978). Recognition and Identification. Landslides: Analysis and Control. R. L. Schuster and R. J. Krizek. Washington, D.C., National Academy of Sciences. **Special Report 176**.

Rodriguez, J., F. Vos, R. Below and D. Guha-Sapir (2009). Annual Disaster Statistical Review 2008 :The numbers and trends

Rosin, P. L. and J. Hervás (2005). "Remote sensing image thresholding methods for determining landslide activity." International Journal of Remote Sensing **26**(6): 1075 - 1092.

Schulz, W. H. (2007). "Landslide susceptibility revealed by LIDAR imagery and historical records, Seattle, Washington." Engineering Geology **89**(1-2): 67-87.

Schuster, R. L. and L. M. Highland (2001). Socio-economic costs of landslides for selected countries in the Western hemisphere.

Shaban, M. A. and O. Dikshit (1997). Textural classification of high resolution digital satellite data of urban environment. Nat. Sym. on Remote Sensing for Natural Resources with Special Emphasis on Infrastructure Development, Hyderabad, India.

Shikada, M., Y. Suzuki, T. Kusaka, S. Goto and Y. Kawata (1997). An application of GIS information and remotely sensed data for extraction of landslide. Geoscience and Remote Sensing, 1997. IGARSS '97. Remote Sensing - A Scientific Vision for Sustainable Development., 1997 IEEE International.

Sidle, R. C. and H. Ochiai (2006). Landslides : processes, prediction, and land use. Washington, DC, American Geophysical Union (AGU).

Singhroy, V. (2009). Satellite Remote Sensing Applications for Landslide Detection and Monitoring. Landslides – Disaster Risk Reduction**:** 143-158.

Singhroy, V., K. E. Mattar and A. L. Gray (1998). "Landslide characterisation in Canada using interferometric SAR and combined SAR and TM images." Advances in Space Research **21**(3): 465-476.

Singhroy, V. and K. Molch (2004). "Characterizing and monitoring rockslides from SAR techniques." Advances in Space Research **33**(3): 290-295.

Singhroy, V. H., J. E. Loehr and A. C. Correa (2000). Landslide risk assessment with high spatial resolution remote sensing satellite data. Geoscience and Remote Sensing Symposium, 2000. Proceedings. IGARSS 2000. IEEE 2000 International.

Soeters, R. and C. J. van Westen (1996). Slope Instability Recognition, Analysis and Zonation. Landslides : investigation and mitigation. A. K. Turner and R. L. Schuster. Washington, D.C., National Academy Press**:** 673.

Tuominen, S. and A. Pekkarinen (2005). "Performance of different spectral and textural aerial photograph features in multi-source forest inventory." Remote Sensing of Environment **94**(2): 256-268.

Turner, A. K. and R. L. Schuster, Eds. (1996). Landslides : investigation and mitigation. Washington, D.C., National Academy Press.

van Westen, C. (2004). Geo-information tools for landslide risk assessment: an overview of recent developments. Landslides: evaluation and stabilization. W. Lacerda, M. Ehrlich, S. Fontoura and A. Sayao. London, Balkema. **1:** 39-56.

van Westen, C. (2009). "Multi-Hazard Risk Assessment."

van Westen, C. J. (2007). "Mapping landslides : recent developments in the use of digital spatial information : keynote." In: Landslides and society : keynote and invited presentations of the 1st North American landslide conference : landslides and society, integrated science, engineering, management, and mitigation Vail, Colorado June 3-8, 2007. / ed. by A.K. Turner and R.L. Schuster. Madison : Omnipress, 2007. ISBN 978-0-9754295-2-5 (AEG special publication ; 22), pp. 221-238.

van Westen, C. J. and F. Lulie Getahun (2003). "Analyzing the evolution of the Tessina landslide using aerial photographs and digital elevation models." Geomorphology **54**(1-2): 77-89.

van Westen, C. J., T. W. J. van Asch and R. Soeters (2006). "Landslide hazard and risk zonation—why is it still so difficult?" Bulletin of Engineering Geology and the Environment **65**(2): 167-184.

Varnes, D. J. (1974). Logic of geological maps : with reference to their interpretation and use for engineering purposes. Washington, D.C., United States Government Printing Office.

Varnes, D. J. (1978). Slope Movement Types and Processes. Landslides: Analysis and Control. R. L. Schuster and R. J. Krizek. Washington, D.C., National Academy of Sciences.

Varnes, D. J. (1984). Landslide hazard zonation: a review of principles and practice. Paris, UNESCO.

Wang, F., Q. Cheng, L. Highland, M. Miyajima, H. Wang and C. Yan (2009). "Preliminary investigation of some large landslides triggered by the 2008 Wenchuan earthquake, Sichuan Province, China." Landslides **6**: 47-54.

Whitworth, M., D. Giles and W. Murphy (2002). Identification of landslides in clay terrains using Airborne Thematic Mapper (ATM) multispectral imagery, SPIE.

Whitworth, M. C. Z., D. P. Giles and W. Murphy (2005). "Airborne remote sensing for landslide hazard assessment: a case study on the Jurassic escarpment slopes of Worcestershire, UK." Quarterly Journal of Engineering Geology and Hydrogeology **38**: 285-300.

Whitworth, M. Z., D. Giles and I. Anderson (2006). Landslide imaging techniques for urban geoscience reconnaissance. IAEG2006.

Wieczorek, G. F. (1984). "Preparing a detailed landslide - inventory map for hazard evaluation and reduction." In : Bulletin of the Association of Engeneering Geologists, 21(1984)3, pp. 337-342.

Woodcock, C. E. and A. H. Strahler (1987). "The factor of scale in remote sensing." Remote Sensing of Environment **21**(3): 311-332.

Wulder, M. A., E. F. LeDrew, S. E. Franklin and M. B. Lavigne (1998). "Aerial Image Texture Information in the Estimation of Northern Deciduous and Mixed Wood Forest Leaf Area Index (LAI)." Remote Sensing of Environment **64**(1): 64-76.

Yang, Y. and P. Hsu (2006). Application of Remote Sensing and GIS in Landslide Detection. Proceedings of the 27th Asian Conference on Remote Sensing (ACRS), Ulaanbaatar, Mongolia, Curran Associates Inc.

Yesilnacar, E. and T. Topal (2005). "Landslide susceptibility mapping: A comparison of logistic regression and neural networks methods in a medium scale study, Hendek region (Turkey)." Engineering Geology **79**(3-4): 251-266.

Yin, Y., F. Wang and P. Sun (2009). "Landslide hazards triggered by the 2008 Wenchuan earthquake, Sichuan, China." Landslides **6**(2): 139-152.

Záruba, Q. and V. Mencl (1961). Ingenieurgeologie. Berlin, Prague.

Záruba, Q. and V. Mencl (1969). Landslides and their control. Amsterdam, Elsevier Academia.

Zillman, J. (1999). The physical impact of disaster. Natural disaster management : a presentation to commemorate the international decade for natural disaster reduction IDNDR 1990 - 2000. J. Inglegton. Leicester, Tudor Rose**:** 320.

Appendices

Appendix 1: Landslide Inventory form

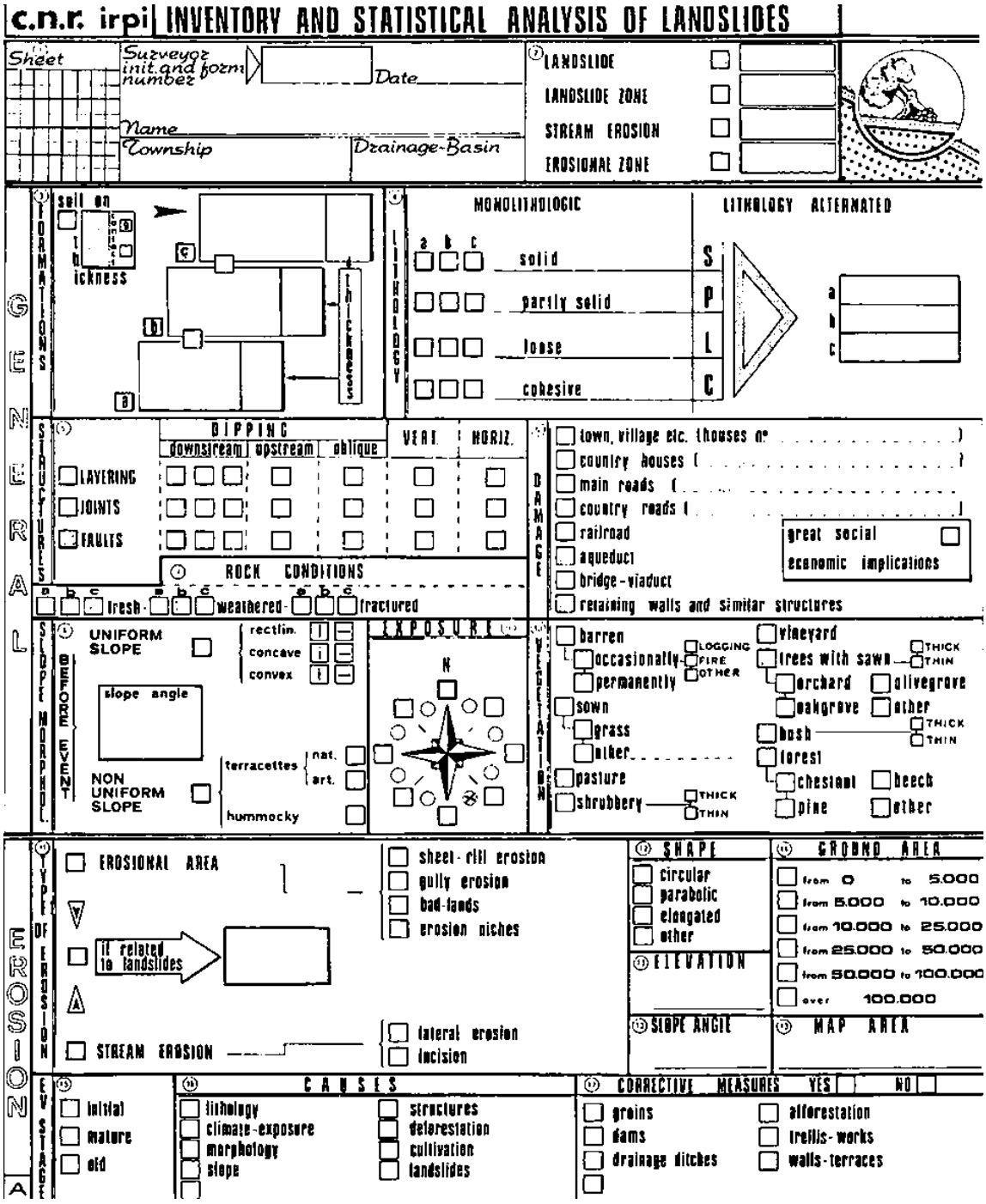

Appendix 2: Landslide Anatomy

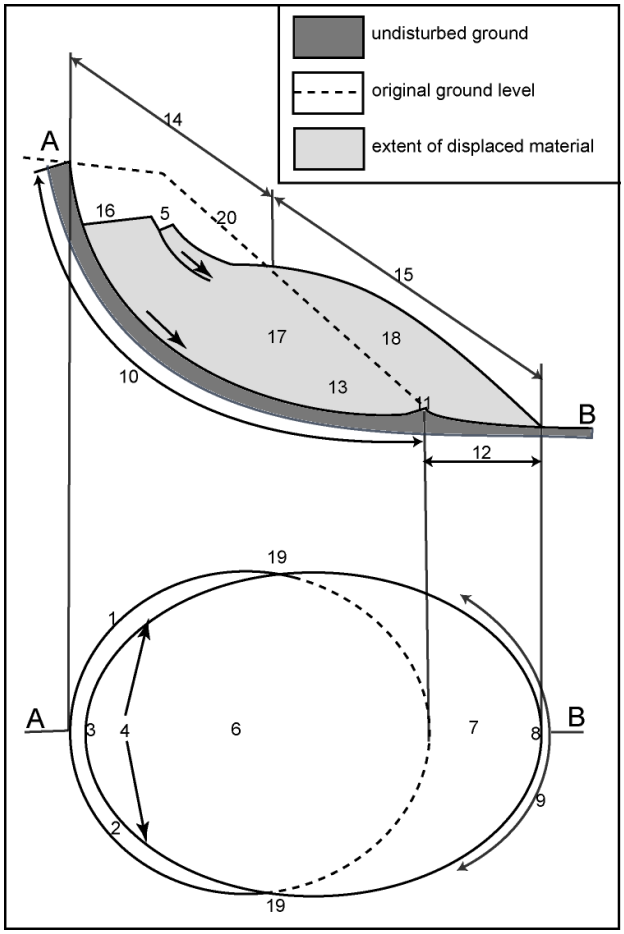

1. Crown: The practically undisplaced material still in place and adjacent to the highest parts of the main scarp (**2**).

2. Main Scarp: A steep surface on the undisturbed ground at the upper edge of the landslide, caused by movement of the displaced material (**13**) away from the undisturbed ground. It is the visible part of the surface of rupture (**10**).

3. Top: The highest point of contact between the displaced material (**13**) and the main scarp (**2**).

4. Head: The upper parts of the landslide along the contact between the displaced material and the main scarp (**2**).

5. Minor Scarp: A steep surface on the displaced material (**13**) of the landslide produced by differential movements within the displaced material.

6. Main Body: The part of the displaced material (**13**) of the landslide that overlies the surface of rupture (**10**) between the main scarp (**2**) and the toe of the surface of rupture (**11**).

7. Foot: The portion of the landslide that has moved beyond the toe of the surface of rupture (**11**) and overlies the original ground surface (**20**).

8. Tip: The point of the toe (**9**) farthest from the top (**3**) of the landslide.

9. Toe: The lower, usually curved margin of the displaced material of a landslide, it is the most distant from the main scarp (**2**).

10. Surface of Rupture: The surface which forms (or which has formed) the lower boundary of the displaced material (**13**) below the original ground surface (**20**).

11. Toe of the Surface of Rupture: The intersection (usually buried) between the lower part of the surface of rupture (**10**) of a landslide and the original ground surface (**20**).

12. Surface of Separation: The part of the original ground surface (**20**) overlain by the foot (**7**) of the landslide.

13. Displaced Material: Material displaced from its original position on the slope by movement in the landslide. It forms both the depleted mass (**17**) and the accumulation (**18**).

14. Zone of Depletion: The area of the landslide within which the displaced material (**13**) lies below the original ground surface (**20**).

15. Zone of Accumulation: The area of the landslide within which the displaced material (**13**) lies above the original ground surface (**20**).

16. Depletion: The volume bounded by the main scarp (**2**), the depleted mass (**17**) and the original ground surface (**20**).

17. Depleted Mass: The volume of the displaced material (**13**), which overlies the rupture surface (**10**) but underlies the original ground surface (**20**).

18. Accumulation: The volume of the displaced material (**13**), which lies above the original ground surface (**20**).

19. Flank: The undisplaced material adjacent to the sides of the rupture surface (**10**). Compass directions are preferable in describing the flanks but if left and right are used, they refer to the flanks as viewed from the crown (**1**).

20. Original Ground Surface: The surface of the slope that existed before the landslide took place.

Appendix 3: OOA procedure for identification of landslides using texture only

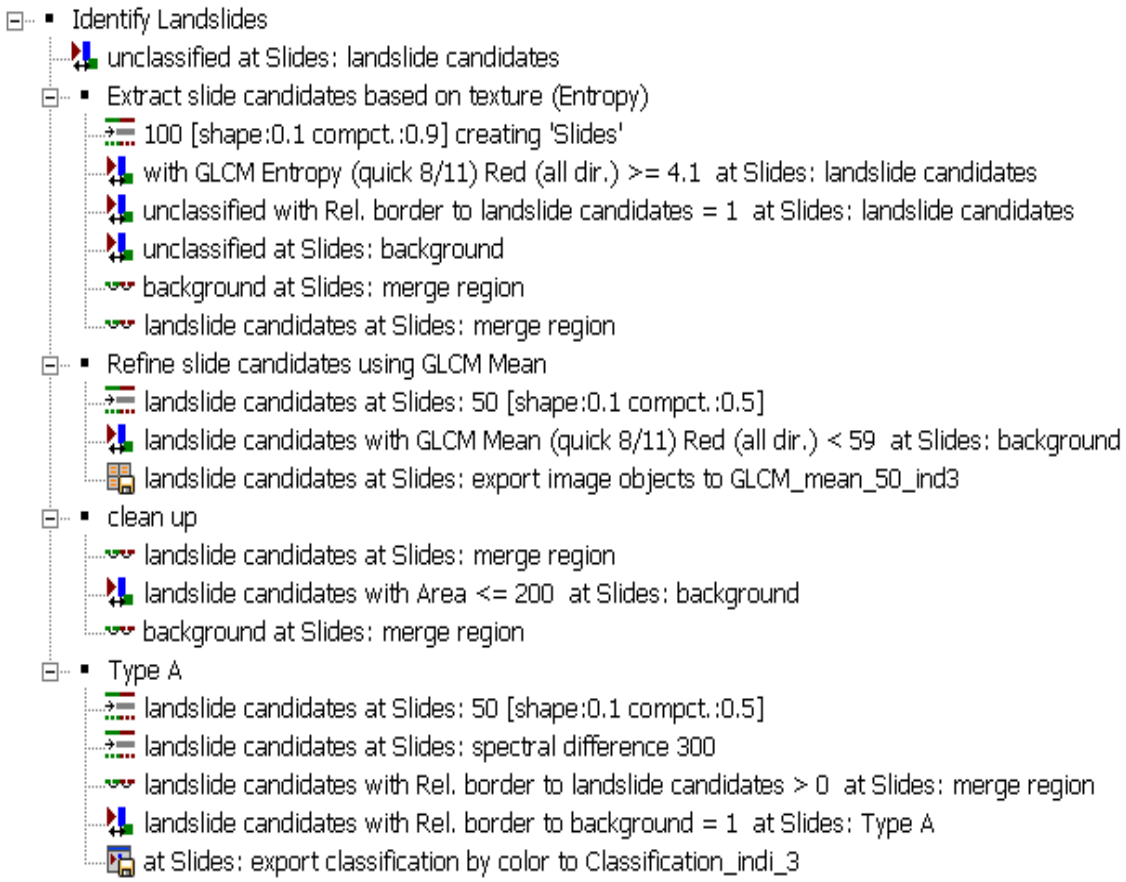

Appendix 4: OOA procedure for identification of landslides using texture, morphological and spectral indices

- Identify Landslides
  - Classify vegetation using NDVI
    - NDVI temp layer
      - layer arithmetics (val (NIR-Red)/(NIR+Red), layer NDVI[float] range [0.000000,255.000000])
    - Set vegetation threshold
      - Veg_Thres_NDVI = 0.25
    - segment and classify vegetation
      - edge ratio split NDVI (not assigned)[0] :100-> [creating 'Vegetation', Vegetation,unclassified]
    - Merge
      - unclassified at Vegetation: merge region
      - Vegetation at Vegetation: merge region
    - Clean up
      - with Area <= 50 Pxl at Vegetation: remove objects
  - Classify water using Blue ratio
    - Segment and classify
      - unclassified at Vegetation: 50 [shape:0.1 compct.:0.5]
      - unclassified at Vegetation: Water *
    - clean up
      - Water at Vegetation: merge region
      - unclassified at Vegetation: merge region
      - unclassified with Rel. border to Water = 1 at Vegetation: Water
  - Landslide candidates and false positives
    - unclassified at Vegetation: 50 [shape:0.1 compct.:0.5]
    - unclassified with Mean NDVI < 0.18 at Vegetation: landslide candidates
    - landslide candidates with GLCM Mean (quick 8/11) Red (all dir.) <= 59 at Vegetation: unclassified
    - landslide candidates with Mean Slope < 15 at Vegetation: _temp1
    - landslide candidates at Vegetation: merge region
    - landslide candidates at Vegetation: 60 [shape:0.1 compct.:0.5]
    - landslide candidates with GLCM Mean (quick 8/11) Red (all dir.) > 60 at Vegetation: <- _temp1 Rel. border to landslide candidates > 0
    - landslide candidates with Length/Width > 7 at Vegetation: background
    - _temp1, bare ground, urban, unclassified at Vegetation: background
    - landslide candidates at Vegetation: merge region
    - landslide candidates at Vegetation: 50 [shape:0.1 compct.:0.5]
    - landslide candidates at Vegetation: export image objects to GLCM_Mean_LTO_indi
  - Landslides
    - landslide candidates at Vegetation: 50 [shape:0.1 compct.:0.5]
    - landslide candidates at Vegetation: spectral difference 100
    - landslide candidates with Relief < 60 at Vegetation: background
    - Vegetation, Water at Vegetation: background
    - landslide candidates with Rel. border to background = 1 at Vegetation: Type A
    - at Vegetation: export classification by color to Classification_indi_3

Appendix 5: ROC complete calculation reports from SPSS 16

Texture Only: Type A

Case Processing Summary

Inv_LS	Valid N (listwise)
Positivea	138274
Negative	1716544

Larger values of the test result variable(s) indicate stronger evidence for a positive actual state.
a. The positive actual state is 1.

Chart title : ROC Curve
Chart file exported to : "g:\mscthesis\data_processed\validation\roc\roc_type_a_texture_only0.bmp"

Area Under the Curve
Test Result Variable(s):OOA_LS

Area	Std. Errora	Asymptotic Sig.b	Asymptotic 95% Confidence Interval	
			Lower Bound	Upper Bound
.872	.001	.000	.870	.873

The test result variable(s): OOA_LS has at least one tie between the positive actual state group and the negative actual state group. Statistics may be biased.
a. Under the nonparametric assumption
b. Null hypothesis: true area = 0.5

Coordinates of the Curve
Test Result Variable(s):OOA_LS

Positive if Greater Than or Equal Toa	Sensitivity	1 - Specificity
-1.00	1.000	1.000
.50	.818	.075
2.00	.000	.000

The test result variable(s): OOA_LS has at least one tie between the positive actual state group and the negative actual state group.
a. The smallest cutoff value is the minimum observed test value minus 1, and the largest cutoff value is the maximum observed test value plus 1. All the other cutoff values are the averages of two consecutive ordered observed test values.

Texture Only: Type B

[DataSet3]

Case Processing Summary

Inv_LS	Valid N (listwise)
Positivea	413969
Negative	3136199

Larger values of the test result variable(s) indicate stronger evidence for a positive actual state.
a. The positive actual state is 1.

Chart title : ROC Curve
Chart file exported to : "g:\mscthesis\data_processed\validation\roc\roc_type_b_texture_only0.bmp"

Area Under the Curve
Test Result Variable(s):OOA_LS

Area	Std. Errora	Asymptotic Sig.b	Asymptotic 95% Confidence Interval	
			Lower Bound	Upper Bound
.768	.000	.000	.768	.769

The test result variable(s): OOA_LS has at least one tie between the positive actual state group and the negative actual state group. Statistics may be biased.
a. Under the nonparametric assumption
b. Null hypothesis: true area = 0.5

Coordinates of the Curve
Test Result Variable(s):OOA_LS

Positive if Greater Than or Equal Toa	Sensitivity	1 - Specificity
-1.00	1.000	1.000
.50	.661	.124
2.00	.000	.000

The test result variable(s): OOA_LS has at least one tie between the positive actual state group and the negative actual state group.
a. The smallest cutoff value is the minimum observed test value minus 1, and the largest cutoff value is the maximum observed test value plus 1. All the other cutoff values are the averages of two consecutive ordered observed test values.

Texture Only: Type C

Case Processing Summary

Inv_LS	Valid N (listwise)
Positivea	81975
Negative	196977

Larger values of the test result variable(s) indicate stronger evidence for a positive actual state.
a. The positive actual state is 1.

Chart title : ROC Curve
Chart file exported to : "g:\mscthesis\data_processed\validation\roc\roc_type_c_texture_only0.bmp"

Area Under the Curve
Test Result Variable(s):OOA_LS

Area	Std. Errora	Asymptotic Sig.b	Asymptotic 95% Confidence Interval	
			Lower Bound	Upper Bound
.943	.001	.000	.942	.944

The test result variable(s): OOA_LS has at least one tie between the positive actual state group and the negative actual state group. Statistics may be biased.
a. Under the nonparametric assumption
b. Null hypothesis: true area = 0.5

Coordinates of the Curve
Test Result Variable(s):OOA_LS

Positive if Greater Than or Equal Toa	Sensitivity	1 - Specificity
-1.00	1.000	1.000
.50	.946	.060
2.00	.000	.000

The test result variable(s): OOA_LS has at least one tie between the positive actual state group and the negative actual state group.
a. The smallest cutoff value is the minimum observed test value minus 1, and the largest cutoff value is the maximum observed test value plus 1. All the other cutoff values are the averages of two consecutive ordered observed test values.

Combined Indices: Type A

Case Processing Summary

Inv_ls	valid N (listwise)
Positivea	4900
Negative	60635

Larger values of the test result variable(s) indicate stronger evidence for a positive actual state.
a. The positive actual state is 1.

Chart title : ROC Curve
Chart file exported to : "g:\mscthesis\data_processed\validation\validation_lto\exports\roc_type_a0.bmp"

Area Under the Curve
Test Result Variable(s):OOA

Area	Std. Errora	Asymptotic Sig.b	Asymptotic 95% Confidence Interval	
			Lower Bound	Upper Bound
.763	.005	.000	.754	.772

The test result variable(s): OOA has at least one tie between the positive actual state group and the negative actual state group. Statistics may be biased.
a. Under the nonparametric assumption
b. Null hypothesis: true area = 0.5

Coordinates of the Curve
Test Result Variable(s):OOA

Positive if Greater Than or Equal Toa	Sensitivity	1 - Specificity
-1.00	1.000	1.000
.50	.532	.006
2.00	.000	.000

The test result variable(s): OOA has at least one tie between the positive actual state group and the negative actual state group.
a. The smallest cutoff value is the minimum observed test value minus 1, and the largest cutoff value is the maximum observed test value plus 1.
All the other cutoff values are the averages of two consecutive ordered observed test values.

Combined Indices: Type B

Case Processing Summary

Inv_ls	Valid N (listwise)
Positivea	2222
Negative	63313

Larger values of the test result variable(s) indicate stronger evidence for a positive actual state.
a. The positive actual state is 1.

Chart title : ROC Curve
Chart file exported to : "g:\mscthesis\data_processed\validation\validation_lto\exports\roc_type_b0.bmp"

Area Under the Curve
Test Result Variable(s):OOA

Area	Std. Errora	Asymptotic Sig.b	Asymptotic 95% Confidence Interval	
			Lower Bound	Upper Bound
.812	.006	.000	.799	.824

The test result variable(s): OOA has at least one tie between the positive actual state group and the negative actual state group.
Statistics may be biased.
a. Under the nonparametric assumption
b. Null hypothesis: true area = 0.5

Coordinates of the Curve
Test Result Variable(s):OOA

Positive if Greater Than or Equal Toa	Sensitivity	1 - Specificity
-1.00	1.000	1.000
.50	.626	.003
2.00	.000	.000

The test result variable(s): OOA has at least one tie between the positive actual state group and the negative actual state group.
a. The smallest cutoff value is the minimum observed test value minus 1, and the largest cutoff value is the maximum observed test value plus 1.
All the other cutoff values are the averages of two consecutive ordered observed test values.

Combined Indices: Type C

Case Processing Summary

Inv_ls	Valid N (listwise)
Positivea	26244
Negative	39291

Larger values of the test result variable(s) indicate stronger evidence for a positive actual state.
a. The positive actual state is 1.

Chart title : ROC Curve
Chart file exported to : "g:\mscthesis\data_processed\validation\validation_lto\exports\roc_type_c0.bmp"

Area Under the Curve
Test Result Variable(s):OOA

Area	Std. Errora	Asymptotic Sig.b	Asymptotic 95% Confidence Interval	
			Lower Bound	Upper Bound
.796	.002	.000	.792	.800

The test result variable(s): OOA has at least one tie between the positive actual state group and the negative actual state group.
Statistics may be biased.
a. Under the nonparametric assumption
b. Null hypothesis: true area = 0.5

Coordinates of the Curve
Test Result Variable(s):OOA

Positive if Greater Than or Equal Toa	Sensitivity	1 - Specificity
-1.00	1.000	1.000
.50	.806	.214
2.00	.000	.000

The test result variable(s): OOA has at least one tie between the positive actual state group and the negative actual state group.
a. The smallest cutoff value is the minimum observed test value minus 1, and the largest cutoff value is the maximum observed test value plus 1.
All the other cutoff values are the averages of two consecutive ordered observed test values.